

# **Development and Application of Passive Samplers for Determining the Fate of Toxic Metals in Wetlands Polluted by Mining Activities**

Report to the  
**Water Research Commission**

by

**Nthabiseng Motsoane, Xolisiwe Maputsoe, Heidi Richards, Hlanganani Tutu,  
Izak Kotze, Ewa Cukrowska, Luke Chimuka**

Molecular Sciences Institute, School of Chemistry  
University of Witwatersrand

**WRC Report No. 2551/1/21  
ISBN 978-0-6392-0269-3**

**August 2021**

**Obtainable from**

Water Research Commission  
Private Bag X03  
Gezina  
Pretoria, 0031

[orders@wrc.org.za](mailto:orders@wrc.org.za) or download from [www.wrc.org.za](http://www.wrc.org.za)

**DISCLAIMER**

This report has been reviewed by the Water Research Commission (WRC) and approved for publication. Approval does not signify that the contents necessarily reflect the views and policies of the WRC nor does mention of trade names or commercial products constitute endorsement or recommendation for use.

## EXECUTIVE SUMMARY

In this project, two types of passive samplers for water monitoring of metals were modified, optimised and applied to study the transport and behaviour of metals in wetlands polluted by acid mine drainage. The first passive involved a polymer inclusion membrane (PIM)-based passive sampler. Here a new design was machined. The other work involved modifying the diffusive gradient in thin films (DGT) passive sampler. Current DGT is used once and thrown away but here a new cap was designed making the sampler holder to be reusable.

The constructed PIMs components were machined in our workshop from PTFE cylindrical rod. The final assembled PIMs passive sampler consists of 10 ml acceptor solution separated by the polymer inclusion membrane from sample solution. Target compounds diffuse from sample solution through the membrane into acceptor solution. The membrane is incorporated by a mobile carrier that transports the target metal specie from the sample into the acceptor solution. The driving force in this case is the proton in the acceptor solution that is transported across to the sample solution too. The membrane consists of PVC incorporated with dihexyl phosphoric acid (D2EHPA). The characterized PIMs from atomic force microscopy and scanning electron microscopy showed that it had some rough surfaces. Fourier transform infra-red revealed the presence of carrier molecules. The contact angle ( $\sim 78.80^\circ\text{C}$ ) showed that the polymer had hydrophilic surfaces due to the carrier functional groups.  $1\text{ mol L}^{-1}\text{ HNO}_3$  was used as receiving solution. The effect of variables such as the carrier composition, pH, membrane thickness, receiver phase concentration and the stability of PIM were optimised to measure the time-weighted average concentration of first and second row transition metal elements which are Ni(II), Co(II), Cu(II), and Cd(II). The PIM optimum conditions were composed of 40% D2EHPA as a carrier and 60% PVC poly (vinyl chloride) (PVC) as a base polymer. Sample pH of 3-7, 1 M  $\text{HNO}_3$  as acceptor solution and membrane thickness of 150  $\mu\text{m}$  were found to be optimum. The stability of PIM as passive was tested up to three cycles and showed remarkable stability. The stability was further followed using thermal gravimetric analysis and Phosphorus-31 NMR spectroscopy. The developed passive sampler showed a large time lag up to five days for all the metals and then uptake became linear up to 15 days. Thus slow release of the metals from the PIM into the bulk acceptor solution was the rate limiting factor. Thus the passive sampler is best suited to be deployed for two weeks instead short period of time ranging of few days.

The modified DGT-based passive sampler was also machined in our workshop. Key was to design a cap that can be screwed on and off instead of the one that has to be broken when opening the passive sampler after deployment. This was followed by synthesising the resin gel. For this reason, cross-linked polyethylenimine (CPEI) is a polymeric adsorbent that was used. It was functionalised in two ways; the first functionalisation was phosphonation of CPEI by reacting it with phosphorous acid and formaldehyde to form phosphonated cross-linked polyethylenimine (PCPEI). In the second functionalisation reaction it was sulfonated by a reaction with 3-chloropropanesulfonyl chloride to form sulfonated cross-linked polyethylenimine (SCPEI). Various amounts of the two functionalised polymer were mixed and used as an adsorbent in the passive sampler for the removal of mercury, arsenic and selenium from spiked water solution. For optimisation based on previous preliminary results, a total mass of 1.9 g was used made of 80% sulphonated crossed linked polyethylenimine (SCPEI) and 20% phosphonated crossed linked polyethylenimine (PCPEI) as trapping sorbent a maximum amount of 0.8 g on the passive sampler piston was used. This was the maximum

sorbent mass sampler could take. An elution solvent of 1 M sulphuric acid from the sorbent for arsenic, selenium and mercury was found to be best. The diffusive gel was found to play an important role in controlling the rate of transport across to the receiving sorbent. It also helps to mimic the biological uptake of the metal species. Without the diffusive gel, the trapping sorbent reached saturation within three days of exposure. With a diffusive gel, exposure time could go on up to 12 days or more depending on whether the system is stirred and on exposure concentration. From exposure, concentration of 0.5 mg L<sup>-1</sup> and below, the sampling rates seemed to be independent of the sample concentration. Stirring the sample solution was found to increase the sampling rates and thus sampler was best suited on near stagnant water systems such as wetlands and dams.

The passive samplers were deployment in dam water and AMD in the lab and in the field to study the transport and fate of these metals. Overall, the PIM-based passive sampler performed much better than the DGT, as it seemed to tolerate high metal content in AMD. The release of H<sup>+</sup> on the source feed from the acceptor solution also prevented any biofouling. Linear uptake of the metals was observed in PIM sampler but lab-based uptake in AMD failed because of precipitation that reduced the amount of the bioavailable fraction. Metals like Fe and Al were found to control these reactions along with redox potential. The DGT passive sampler also showed linear uptake of As in both dam and AMD water but in the lab, precipitation reactions reduced the amount of bioavailable fraction. The resin in DGT also adsorbed high amounts of Fe, which was seen precipitation on the surface. The PIM-based sampler showed high versatile as it could tolerate AMD matrix while the DGT-based sampler could not. The major limiting factor of the DGT passive was the capacity of the sorbent especially that it was not very selective.

## **DISSEMINATION ACTIVITIES**

### **International Conferences**

Euromembrane 2018, Valencia, 9-13 July 2018. Poster presentation. Development of polymer inclusion membrane for metal ion monitoring.

### **Local conferences**

Analytical 2018 conference, 22-25 July 2018, Legend Golf and Safari Resort, Limpopo, South Africa. Keynote lecture: Technical development and optimisation of passive sampler for metal ions in polluted water bodies.

### **PG training**

Ms Nthabiseng Motsoane, PhD student, writing final dissertation

Ms Xolisiwe Maptsoe, PhD student, writing final dissertation

Mr Kgomotso Maiphetho, MSc student, writing final MSc dissertation and continuing for PhD.

## **Publications in international journal**

Nthabiseng Motsoane , Kgomotso Maiphetlho, Somandla Ncube, Heidi Richards , Izak Kotze, Hlanganani Tutu , Ewa Cukrowska , Luke Chimuka, Technical development of a passive sampler for determination of trace metals in natural dam waters using polymer inclusion membrane, manuscript

Nthabiseng Motsoane, Heidi Richards, Izak Kotze, Hlanganani Tutu, Ewa Cukrowska, Luke Chimuka, Studying the behaviour and bioavailability of trace metals in dam water using a polymer inclusion membrane passive sampler, manuscript

Nthabiseng Motsoane, Heidi Richards, Izak Kotze, Hlanganani Tutu, Ewa Cukrowska, Luke Chimuka, Determination of trace metals in AMD using polymer inclusion membrane passive sampler, manuscript

Xolisiwe Maptsoe , Heidi Richards , Hlanganani Tutu , Ewa Cukrowska, Luke Chimuka, Development of a passive sampler for selenium, arsenic and mercury in polluted wetland using diffusive gradient in thin films passive sampler with modified crossed linked polyethylenimine as resin, manuscript

## ACKNOWLEDGEMENTS

The financial support from the Water Research Commission is gratefully acknowledged, for both this work and the associated project (WRC K5/7025)

The authors would like to thank the following for their guidance and/or contribution towards this research project.

Dr B Petja	WRC (Manager and Chairperson)
Gerda Kruger	WRC (Coordinator)
Prof Luke Chimuka	Project leader, University of the Witwatersrand
Prof Ewa Cukrowska	Project team member, University of the Witwatersrand
Prof. Hlanganani Tutu	Project team member, University of the Witwatersrand
Dr Heidi Richards	Project team member, University of the Witwatersrand
Dr Izak Kotze	Project team member, University of the Witwatersrand
Ms Nthabiseng Motsoane	Project team member, University of the Witwatersrand
Ms Xolisiwe Maputsoe	Project team member, University of the Witwatersrand
Prof NS Mokgalaka	Reference group member, Tshwane University of Technology
Prof Patricia Forbes	Reference group member, University of Pretoria
Dr Orpah Ozinyemba	Reference group member, University of Johannesburg
Dr Cornelius Rimayi	Reference group member, Department of Water Affairs and Sanitation

## TABLE OF CONTENTS

<b>CHAPTER ONE: INTRODUCTION</b>	<b>1</b>
1.1 Heavy metals and their monitoring in the environment	1
<b>CHAPTER TWO: LITERATURE REVIEW</b>	<b>5</b>
2.1 Theory of passive samplers	5
2.2 Technical development and their optimisation	7
2.3 Types of passive samplers for metals	7
2.3.1 Diffusive gradients in thin film technique (DGT)	7
2.3.2 Polymer inclusion membrane passive sampler	9
2.3.3 Biological-based passive sampler	10
2.4 Trends in passive samplers for metals	11
2.4.1 New sorbents in DGT	11
2.4.2 Combining biomonitoring with passive samplers	13
2.5 Applications of passive samplers	14
2.5.1 Risk assessment	14
2.5.2 Fate and transport	15
2.5.3 Temporal trends	16
<b>CHAPTER THREE: RESEARCH METHODOLOGY</b>	<b>17</b>
3.1 Part A: PIM-Based passive sampler	17
3.1.1 Materials and chemicals	17
3.1.2 Instrumentation	17
3.1.3 Experimental	18
3.1.3.1 Preparation of the membrane	18
3.1.3.2 Sampler holder components design	18
3.1.3.3 Assembly of PIM components	20
3.1.3.4 Passive sampler exposure area design	21
3.1.3.5 PIM set up	22
3.1.4 Transport mechanism in PIM sampler	24
3.1.5 Metal flux determination	25
3.1.6 Sampling rates determination	26
3.1.7 Optimisation of the PIM sampler	26
3.1.7.1 Effect of carrier on PIMs passive sampler	26
3.1.7.2 Effect of source phase pH	26
3.1.7.3 Effect of Membrane thickness	26
3.1.7.4 Effects receiver solution composition	27
3.1.7.5 Effects of turbulence	27
3.1.7.6 Effects of membrane stability	27
3.1.8 Application of the developed PIM-based sampler	27
3.1.8.1 Study site	27
3.1.8.2 Construction of cage	28
3.1.8.3 Deployment	29
3.1.9 Collection of samplers and metal analysis	29
3.2 Part B: DGT-based passive sampler	30

3.2.1	Materials and chemicals	30
3.2.2	Instrumentation	30
3.2.2.1	Metal analysis	30
3.2.2.2	FTIR analysis	30
3.2.2.3	Solid state NMR analysis	30
3.2.2.4	CHNS analysis	30
3.2.2.5	Ion chromatography analysis	31
3.2.2.6	Field measurements	31
3.2.3	Methodologies	31
3.2.3.1	Polymer sorbent synthesis and characterisation	31
3.2.3.2	Batch studies	32
3.2.4	Elution factor calculations	33
3.2.5	Construction of sampler samples	33
3.2.5.1	Sampler holders	33
3.2.5.2	Preparation of the resin embedded in agarose	33
3.2.5.3	Preparation of diffusive gel	34
3.2.6	Experimental set of DGT-based sampler	34
3.2.7	Optimisation of DGT-based sampler	35
3.2.7.1	Performance of SCPEI-based DGT sampler	35
3.2.7.2	Performance of SCPEI-PCPEI-based DGT sampler	35
3.2.7.3	Effect of resin mass study	35
3.2.7.4	Effect of resin gel	36
3.2.7.5	Effect of diffusive gel thickness	36
3.2.7.6	Effect of turbulence	36
3.2.7.7	Effect of sample concentration	36
3.2.7.8	Effect of sample pH	36
3.2.8	Calculation of diffusion coefficient and diffusive gel boundary layer	37
3.2.8.1	Diffusion coefficient	37
3.2.8.2	Diffusive gel boundary layer	37
3.2.9	Blank and method detection limit determination	37
3.2.10	Field application of DGT-based sampler	37
3.2.10.1	Construction of sampler holder	37
3.2.10.2	Deployment in Fleurhof dam	40
3.2.10.3	Deployment in AMD efflorescent dissolved crust	40
3.2.10.4	Deployment in AMD	41
3.2.11	Modelling of results	42
<b>CHAPTER FOUR: RESULTS AND DISCUSSION</b>		<b>43</b>
4.1	Part A: Polymer inclusion membrane-based passive sampler	43
4.1.1	Optimisation polymer inclusion membrane sampler	43
4.1.1.1	Effect of the carrier composition	43
4.1.1.2	Effect of receiver solution	44
4.1.1.3	Effect of sample pH	45
4.1.1.4	Effect of membrane thickness	46
4.1.1.5	Effect of receiver phase concentration	47
4.1.1.6	Effect of stirring rate	48
4.1.1.7	Effect of exposure area	49

4.1.1.8	Effect of deployment time	50
4.1.1.9	PIM stability and reuse	50
4.1.2	Membrane characterisation	52
4.1.2.1	Scanning electron microscopy analysis	52
4.1.2.2	Thermal gravimetric analysis	52
4.1.2.3	Nuclear magnetic resonance analysis	53
4.1.2.4	Contact angle analysis	54
4.1.3	Optimisation of PIM sampler in field water samples	54
4.1.3.1	Effect of stirring rate	54
4.1.3.2	Effect of contact time	56
4.1.3.3	Receiver pH behaviour	60
4.1.4	Deployment in Fleurhof dam water	62
4.1.4.1	Field parameters	62
4.1.4.2	Total metal ion concentration	65
4.1.4.3	pH changes in the acceptor phase	66
4.1.4.4	State of the sampler after deployment	67
4.1.4.5	Comparison of the bioavailable fraction	68
4.1.4.6	Uptake of other metals	69
4.1.4.7	Sampling rates determination in PIM sampler	70
4.1.5	Deployment in AMD	72
4.1.5.1	Field parameters	72
4.1.5.2	Total metal concentration	73
4.1.5.3	pH changes in the acceptor pH	76
4.1.5.4	State of the sampler after deployment	76
4.1.5.5	Bioavailable fraction	77
4.1.5.6	Other metals taken	78
4.1.5.7	Characterisation PIM before and after deployment	79
4.2	Part B: Diffusive gradient in thin films-based sampler	82
4.2.1	Polymer sorbent characterisation	82
4.2.1.1	FTIR analysis	82
4.2.1.2	Solid state NMR analysis	84
4.2.1.3	CHNS analysis	85
4.2.2	Batch analysis	86
4.2.2.1	Combination of two resins	86
4.2.2.2	Elution efficiency	88
4.2.3	Design and construction of DGT sampler	91
4.2.4	Optimisation of DGT-based sampler	92
4.2.4.1	Performance of SCPEI-based sampler	92
4.2.4.2	Performance of SCPEI-PCPEI resin-based sampler	93
4.2.4.3	Effect of resin mass	95
4.2.4.4	Effect of diffusive gel	96
4.2.4.5	Effect of diffusive gel thickness	98
4.2.4.6	Effect of turbulence	98
4.2.4.7	Effect of sample concentration	100
4.2.4.8	Effect of sample pH	101
4.2.5	Calculations of diffusion coefficient and diffusive boundary layer	104
4.2.5.1	The diffusion coefficient	104

4.2.5.2	The DBL	106
4.2.6	Resin blank and method detection limit	107
4.2.7	Comparison with other DGT samplers	108
4.2.8	Application of the optimised DGT sampler	100
4.2.8.1	Uptake by DGT in lab-based experiments using water from Fleurhof Dam	110
4.2.8.2	Deployment in Fleurhof dam	114
4.2.8.3	Arsenic, selenium and mercury uptake from dissolved efflorescent crust	118
4.2.8.4	Uptake in laboratory-based experiments using AMD drainage water	125
4.3	Comparison of PIM and DGT samplers	129
<b>CHAPTER FIVE: CONCLUSION AND RECOMMENDATIONS</b>		<b>130</b>
5.1	Conclusion	130
5.2	Recommendations	131
<b>REFERENCES</b>		<b>133</b>

## LIST OF FIGURES

Figure 1: Publications on passive samplers for water monitoring	3
Figure 2: Citations on publications on passive samplers for water monitoring	4
Figure 3: An illustration of passive sampler uptake of analyte	4
Figure 4: Regimes of passive sampler uptake	5
Figure 5: Analyte concentration gradient in passive sampler uptake	8
Figure 6: Simplified illustration of DGT sampler	9
Figure 7: Transport mechanisms in PIM sampler	10
Figure 8: Casting of membrane instrument	18
Figure 9: PTFE rod used to machine PIM sampler	19
Figure 10: Components of machined PIM sampler	19
Figure 11: Fully assembled PIM sampler	20
Figure 12: Unassembled components of PIM sampler	20
Figure 13: Exposure surface areas of PIM sampler	20
Figure 14: Different dimensions of exposure areas of PIM sampler	21
Figure 15: Passive sampler holder	23
Figure 16: Lab set up PIM-based sampler	23
Figure 17: Transport in PIM showing H <sup>+</sup> as driving force	25
Figure 18: Study site PIM sampler applications	28
Figure 19: Design of cages and set up for field applications	29
Figure 20: PTFE used to machine DGT samplers	33
Figure 21: DGT components and assembled units	34
Figure 22: Lab set of DGT samplers	35
Figure 23: Cages and set up for field application of DGT samplers	38
Figure 24: Sampling sites for DGT samplers	39
Figure 25: DGT exposure in AMD crust solution in the lab	41
Figure 26: DGT exposure in AMD in the lab	42
Figure 27: Effect of carrier concentration in PIM sampler	43
Figure 28: Effect of receiver solution type at sample pH 3	44
Figure 29: Effect of receiver solution type at sample pH 6	45
Figure 30: Effect of sample pH on PIM sampler	45
Figure 31: Effect of membrane thickness	47
Figure 32: Effect of stripping solution concentration	48
Figure 33: Effect of stirring speed	48
Figure 34: Effect exposure area	49
Figure 35: Effect of deployment time	50
Figure 36: Stability study of PIM-based sampler	51
Figure 37: Comparison of membrane surface before and after exposure	51
Figure 38: SEM membrane images before and after exposure	52
Figure 39: TGA graphs before and after exposure of membrane	53
Figure 40: NMR results of membrane before and after exposure	54
Figure 41: Effect of stirring rate of PIM uptake in dam water	55
Figure 42: Effect of stirring rate of PIM uptake in AMD	56
Figure 43: Effect of contact time of spiked dam water	57
Figure 44: Effect of contact time in unspiked dam water	58
Figure 45: Comparison of metal uptake in AMD in the lab	59
Figure 46: Iron precipitation in AMD in the lab	59

Figure 47: Changes in redox and pH in the receiver solution	61
Figure 48: Changes in pH receiver solution PIM sampler deployed in dam water	61
Figure 49: Changes in pH receiver solution PIM sampler deployed in AMD	62
Figure 50: Uptake of metals in PIM in dam water	66
Figure 51: pH changes in receiver solution in field deployment in dam water	67
Figure 52: Cages appearance before and after exposure in field dam water	68
Figure 53: Membrane appearance in during exposure in field dam water	68
Figure 54: Metal ion bioavailability in the lab and in the field in dam water	69
Figure 55: Uptake of other metals in PIM sampler in the field in dam water	70
Figure 56: Sampling rates of metal ions in PIM sampler	72
Figure 57: Uptake of metals in PIM in AMD in the field	76
Figure 58: pH changes in the receiver solution in PIM sampler	76
Figure 59: Surface changes in the cages and membrane during exposure in AMD	77
Figure 60: Metal bioavailability in the lab and field in AMD in PIM sampler	78
Figure 61: Other metal uptake in PIM sampler deployed in the field	79
Figure 62: FTIR results from PIM sampler before and after deployment	80
Figure 63: ATM results from PIM sampler before and after deployment	82
Figure 64: Pictures of crossed linked polyethylenimine (CPEI) polymer	82
Figure 65: FTIR results of CPEI polymers	83
Figure 66: Solid-state NMR results	85
Figure 67: Metal uptake in mixed CPEI polymers	87
Figure 68: Effect of elution solvent concentration from CPEI polymer	89
Figure 69: Effect of different elution solvents from CPEI polymer	89
Figure 70: Effect of elution solvents concentration from CPEI polymer	90
Figure 71: DGT passive sampler design and construction	91
Figure 72: Preliminary uptake of DGT passive sampler with SCPEI resin	93
Figure 73: Uptake of mixed resin DGT sampler	94
Figure 74: Effect of sorbent mass in DGT sampler	96
Figure 75: Effect of diffusive gel thickness on metal transport in DGT	98
Figure 76: Effect of turbulence in DGT sampler	99
Figure 77: Effect of sample concentration in DGT sampler	101
Figure 78: Influence of sample pH in DGT sampler	103
Figure 79: Effect of exposure time on diffusion coefficient	104
Figure 80: Reciprocal of mass accumulated vs diffusive gel thickness	107
Figure 81: Uptake of target metals in DGT in dam water in the lab	113
Figure 82: Uptake of other metals in DGT in dam water in the lab	114
Figure 83: Uptake of target metals in DGT in the field dam water	116
Figure 84: Uptake of other metals in DGT in the field dam water	117
Figure 85: Uptake of target metals in DGT in AMD crust solution	122
Figure 86: Uptake of other metals in DGT in AMD crust solution	124
Figure 87: Biofouling of DGT sampler in AMD	126
Figure 88: Uptake of DGT sampler of target metals in AMD	127
Figure 89: Uptake of other metals in DGT sampler in AMD	128

## LIST OF TABLES

Table 1: Polymer inclusion membrane composition	23
Table 2: Metal ion concentration in AMD	60
Table 3: The source solution parameters and anions	64
Table 4: Maximum permissible water concentrations of metal ions and the concentration found in dam water	65
Table 5: Maximum allowed limits of metals in AMD	73
Table 6: Roughness of the membrane before and after exposure	81
Table 7: Description of the absorption band observed in Figure 65	83
Table 8: Element analysis of the polymers	86
Table 9: Comparison of metal flux in stirred and non-stirred in DGT sampler	100
Table 10: Diffusion coefficients of the metals	105
Table 11: Comparison of diffusion coefficients of the metals in DGT sampler	105
Table 12: Literature comparison of the diffusion gel thickness used	109
Table 13: Metal and ion concentration in Fleurhof dam water	111
Table 14: Changes in physical properties of Fleurhof dam water during exposure	118
Table 15: Metal ion concentration in AMD crust solution	120
Table 16: Metal ion concentration AMD	125

This page was intentionally left blank

## CHAPTER 1: INTRODUCTION

### 1.1 Heavy metals and their monitoring in the environment

Monitoring pollutant levels such as metal ions in the aquatic environment is a crucial step in ensuring that good water quality is maintained. Monitoring is through regular sampling and analysis in order to detect levels of pollutants, particularly those considered high risk to life (Vrana *et al.*, 2005). In order to ascertain the quality of the water, the information obtained must be comparable either on a national or international level (Allan *et al.*, 2008). One of the major pollutants in the aquatic environment is heavy metals. Heavy metals are naturally occurring in the environment and aquatic systems, however, anthropogenic activities have led to an increase in the concentration of heavy metals in these systems. For example, industries such as mining and metallurgy discharge effluents that have high levels of uranium, mercury, and copper are responsible for pollution of aquatic water bodies with these metals (Gavrilescu, 2004). South Africa income partly relies on mining of metals such as gold, copper, platinum group metals, uranium, manganese and iron. This means that mining related pollution is a major problem.

The problem with heavy metals is their persistence in the environment. For example, sediments act as sinks in aquatic systems. The concentration of heavy metals in sediments can be between three and five times the magnitude found in the aqueous medium. Within the sediments, heavy metals can bind to iron oxides and organics; thereby decreasing the bioavailable fraction in the aqueous medium (Bryan and Langston, 1992). However, during heavy downpour, adsorbed heavy metals in the sediments have the potential to re-desorb in the liquid fraction, thus causing continued pollution.

Living organisms may be exposed to non-essential heavy metals such as mercury, lead and arsenic and trace essential nutrients like manganese, copper, chromium, nickel, zinc and others. Since these metals are not required for either growth or function of the organism or are required in small quantities, they disrupt normal physiological processes at the cellular and even at the molecular level by inactivating enzymes, blocking functional groups and even disrupting the membrane (Rascio and Navari-Izzo, 2011). Toxicity due to these metals is dependent on a number of factors such as exposure rate. Exposure rate is in turn dependent on metal speciation. Metal speciation determines how much of the total metal present will actually interact, and be absorbed across a physiological membrane (Reeder *et al.*, 2006). The concentration of the metal capable of cross across the biological membrane is referred to as bioavailable fraction. The bioavailable metal fraction is capable of being bioconcentrated in living organisms and can up the food chain where can under biomagnification (Mountouris

*et al.*, 2002). Bioavailability has different definitions depending on discipline and context (Reeder *et al.*, 2006). A simplified definition coined by Semple *et al.* (2004) is more relevant to these studies. They describe bioavailability as the ability of a compound to cross an organism's cell membrane from the medium inhabited by the organism. On the other hand, chemical speciation is defined as the chemical form of a metal, therefore oxidation state, stoichiometry, coordination, the number and type of ligands, as well as the physical state all influence speciation, according to the International Union of Pure and Applied Chemistry (IUPAC). This, in turn, influences the chemical behaviour and mobility of the metal within the environment and most importantly ingestion by organisms and toxicity (Reeder *et al.*, 2006). Total metal concentration therefore, is not necessarily the bioavailable concentration that can pose a potential health threat in an environmental setting (Davies *et al.*, 2005; Reeder *et al.*, 2006). Absorption of metal through a cell membrane can be through passive, active or facilitated transport depending on the cell type, metal specie being transported and its chemical form (Dawson and Ballatori, 1995; Foulkes, 2000 cited in Reeder *et al.*, 2006). The importance of metal speciation and uptake is depicted in the transport of the following metals: Chromium (VI) uptake is through facilitated transport whereas chromium (III) is through passive diffusion. Methylmercury has high lipid solubility than inorganic ionic mercury; this means it has greater chance of crossing the plasma membrane than chromium (III) (Reeder *et al.*, 2006). It is therefore important to consider metal speciation during monitoring.

In most aquatic monitoring, it is common practice to collect grab, spot or bottle water samples at specific sites and a given time. There are a few concerns regarding these monitoring methods. Firstly, in situations where pollutants are found in trace amounts, large volume samples have to be collected in order to make better assumptions on the levels that are present. Secondly, there is a possibility of contamination and changes in metal speciation during storage and transport of samples (Horowitz, 1997). Furthermore, laboratory analysis of these samples only provides information on the levels of pollutant taken at a specific time rather than the average concentration levels. In addition, analysis of data obtained through spot sampling produces different results for the apparent pollutant concentration, depending on the pre-treatment method used (Vrana *et al.*, 2005). Spot sampling provides information on the total amount of pollutant present and not the dissolved, bioavailable fraction. In order to overcome some of these sampling issues, various methods were developed and passive sampling proved to be the one with the greatest potential.

Passive sampling techniques have been applied in order to monitor pollutants in the environment (Figure 1). The figure indicate that the area is getting more popular and recognized as alternative approach for environmental monitoring. Figure 2 shows the citations

of passive samplers papers published for water monitoring. The citations have also been increasing especially from 2005. In passive samplers, analyte molecules are progressively accumulated within the passive sampler against a concentration gradient (Vrana *et al.*, 2005). Passive samplers have advantages over other sampling and sample pre-treatment techniques in that they measure the average concentration as they are deployed for longer periods such as two weeks or more (Figure 3). They combine sampling and sample pre-concentration thus allowing detecting even trace amounts of pollutants in water. They require no energy input during deployment and thus can be deployed over a wide area. They measure the bioavailable fraction and thus very important in assessment of the potential health risk assessment of the concerned aquatic water bodies. Diffusive gradients in thin-films (DGT) is one of the most commercially successful passive samplers for the monitoring of labile species of metal pollutants in the environment. DGT can be used to establish the bioavailable concentrations of metals in the environment being tested (Davison and Zhang, 1994).

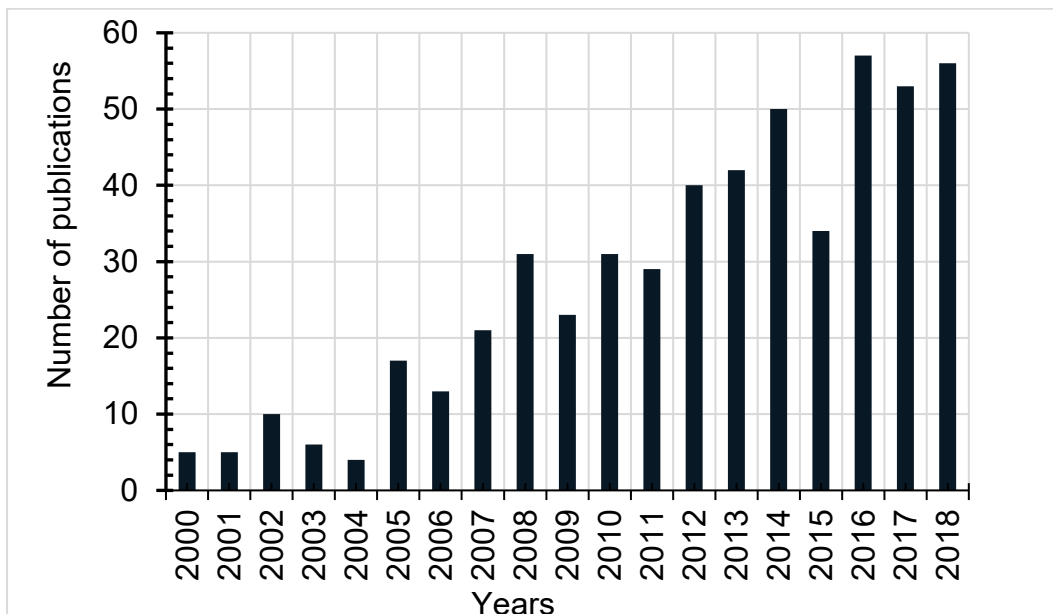


**Figure 1:** The number of publications on passive samplers for water monitoring

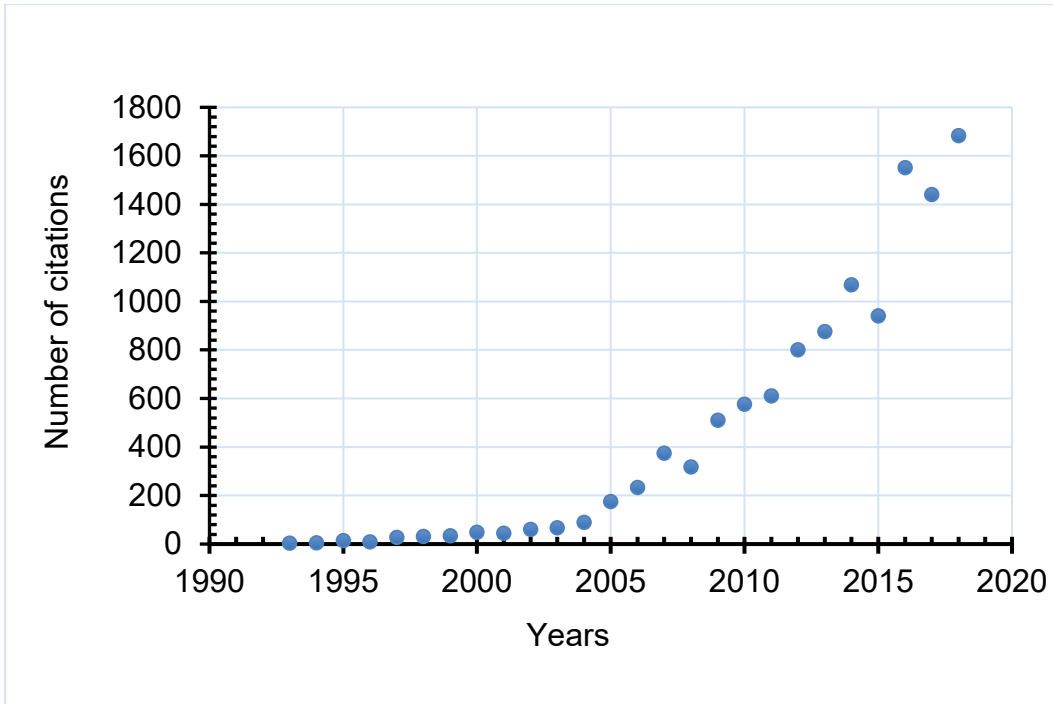


**Figure 2:** The number of citations per year of passive samplers for water monitoring.

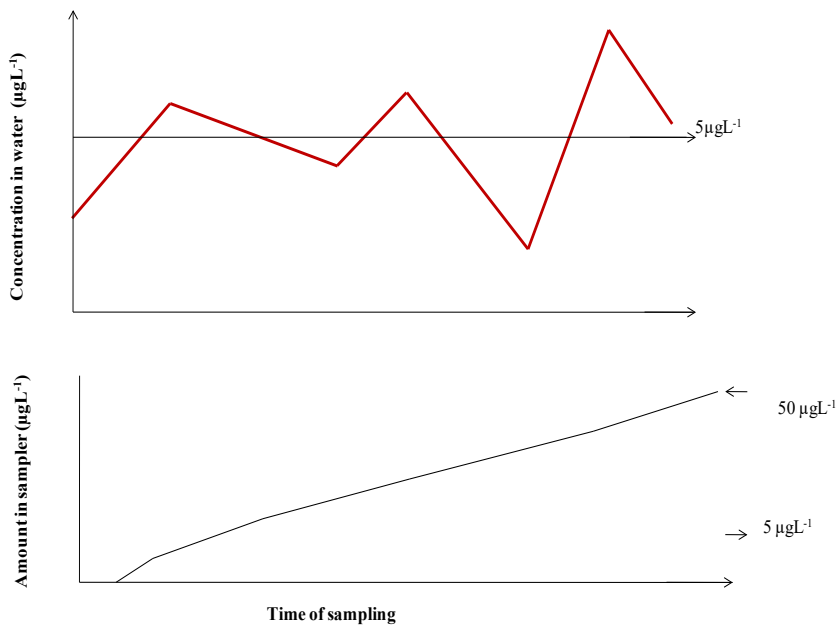


**Figure 3:** An illustration of the uptake of the passive sampler in the water body where the concentration changes all the time. Passive sampler measures the integrative average concentration since sampling is performed continuously.

## CHAPTER TWO: LITERATURE REVIEW

### 2.1 Theory of passive samplers

Passive sampling is a technique based on the principle of free-flow. Analyte molecules travel from the sampled medium to the receiving phase within the passive sampler due to the difference in chemical potential between the two media. Sampling can proceed without the need of an external energy source besides the chemical potential (Vrana *et al.*, 2005).

As analyte molecules continue to travel through the passive sampler, they are retained within a reference or receiving phase. This can be a solvent, chemical reagent or a porous adsorbent. The reference phase is in contact with the water phase. The exchange kinetics between water and the sampler follow first order kinetics according to the following equation:

$$C_s(t) = C_w \frac{k_1}{k_2} (1 - e^{-k_2 t})$$

Where  $C_s(t)$  is analyte concentration within the sampler at exposure time  $t$ ,  $C_w$  is the analyte concentration in the water phase,  $k_1$  and  $k_2$  represent the uptake and offload rate constants respectively. The manner in which analytes are adsorbed from water onto the receiving phase of the passive sampler is illustrated in Figure 4. Molecule uptake is controlled either kinetically or through equilibrium.

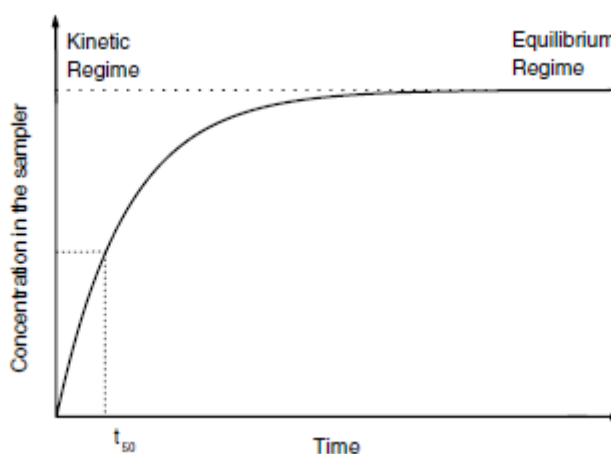


**Figure 4:** Passive sampler uptake can be described in term of either the kinetic or the equilibrium regime.

In kinetically controlled passive samplers, it is assumed that the rate of uptake is linearly proportional to the chemical potential between the water and reference phase. During the

initial phase after exposure, the rate of desorption becomes negligible in comparison to the rate of uptake, and equation above is simplified to:

$$C_s(t) = C_w k_1 t$$

The above equation can further be rearranged to an equation with a similar relationship:

$$M_s(t) = C_w R_s t$$

Where  $M_s(t)$  is the mass of analyte accumulated in the receiving phase after time (t) and  $R_s$  is the proportionality constant. This proportionality constant is a product of the first-order rate constant  $k_1$  and the volume of water that gives the same chemical activity as the volume of the receiving phase. If the value of  $R_s$  is known then  $C_w$ , which is the time weighted average (TWA) of pollutant in water, may be calculated from  $M_s(t)$ , (t) and  $R_s$ . The value of  $R_s$  does not vary with  $C_w$  for samplers operating in the kinetic region. This value is however, affected by turbulences, temperature and biofouling. Kinetic passive samplers are able to sequester contaminants from episodic events which are commonly not detected with spot sampling, and can therefore be used where water concentrations are variable. They allow measurement of ultra-trace, yet toxicologically relevant, contaminant concentrations over extended periods (Vrana *et al.*, 2005).

Equilibrium passive samplers require a longer period of incubation in order to allow the establishment of thermodynamic equilibrium to take place between the water and reference phase. First equation re-arranges to:

$$C_s(t) = C_w \frac{k_1}{k_2} = C_w K$$

The concentration of dissolved analyte can be estimated from the phase-water partition coefficient (K). One fundamental requirement of equilibrium-passive sampling is that stable concentrations are obtained after a known, specific time (Vrana *et al.*, 2005).

A barrier between the sampled medium and the receiving phase is a common characteristic shared by most passive samplers. The barrier is an important aspect of the passive sampler because it determines the rate at which the analyte can be sequestered into the receiving phase at a given concentration. The barrier also ensures the selectivity of the sampling device where certain groups of analyte will be selected more than others. The rate of analyte uptake depends on the sampler design, physicochemical properties of the analytes as well as environmental variables such as water turbulence, water, temperature and biofouling (Vrana *et al.*, 2005).

## **2.2 Technical developments and optimisation in passive samplers**

Passive samplers are designed to mimic living organisms in the transport of chemicals to the receiving or trapping medium (Pesavento et al., 2009). It is one of the analytical methods that measure the free and labile fractions of the chemical within the water bodies just like aquatic living organism. Typical compartments of the passive sampler for metals consists of a hydrophilic membrane that allows the passing of water and metals through its pores. Thus any bigger particulates are excluded from going through. Next is the diffusion gel allows metals to diffuse through just like in cell membranes. After this is a trapping media embedded in agarose or same gel used as diffusion media. The embedding of trapping particles in a gel helps to make sure that chemicals can diffuse all-round the particles and get trapped. The polarity of the membrane can influence transport across of the metals thus should be polar enough not limit the transport across into the diffusion gel. The diffusion gel thickness has to be controlled as this allows the passive sampler to mimic living organisms.

The actual trapping of the metals is determined by the type of sorbent used. Because of diverse metal ions and in different chemical forms, this is an area that is very active currently. The sorbent must be tailored towards the target metals. Critical is also the possible interferences from other metals or chemicals within the sample. Metals like Ca, Na, Mg and K are found in very high amounts and if are also trapped, that could reduce the capacity of the sorbent and thus the deployment time. Thus calibration of the passive sampler in the laboratory before final deployment is very critical. Calibration typically allows one to study the most important parameters that will influence passive sampler performance such as exposure time, sample pH, turbulence, elution solvent and its volume and possible interfering matrices (Turner et al., 2012; Dabrin et al., 2016). When finally, the passive sampler is applied is common to take few grab samples to compare the total versus free and labile fraction obtained in passive samplers.

## **2.3 Types of passive samplers**

### **2.3.1 Diffusive Gradients in Thin-films Technique (DGT)**

The technique of diffusive gradients in thin-films technique (DGT) was developed by the Zhang group (Davison and Zhang, 1994) at Lancaster University as a means of *in situ* measurement of labile trace metal species in natural water. *In situ* measurements mean that contamination problems normally encountered during sampling and transport are eliminated (Davison and Zhang, 1994; Zhang and Davison, 1995). During the deployment of DGT, metal ions are gradually accumulated according to a diffusion gradient. Metal ion accumulation in DGT is based on Fick's first law of diffusion as shown in Figure 5. The total mass of metal accumulated

after a specific period can then be calculated (Davison and Zhang, 1994; Zhang and Davison, 1995). The fact that DGT operates on the fundamentals of a concentration gradient means that it is kinetically controlled. This is advantageous because it can be deployed for extended periods unlike equilibrium techniques (Li *et al.*, 2002).

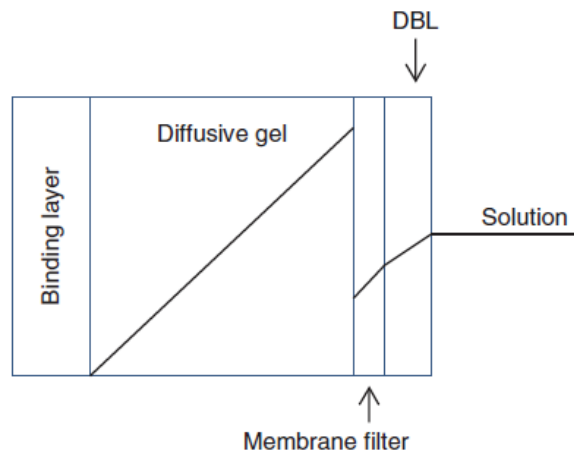


**Figure 5:** A representation of the free ionic species in a gel assembly that's in contact with natural water. The DBL is the diffusive boundary layer (Davison and Zhang, 2012).

DGT is a 25 mm diameter plastic device that looks like a small piston as shown in Figure 6. The top cap has a 20 mm diameter window (Allen *et al.*, 2008; Mengistu, 2009). The functional part is made up of three layers: a cellulose acetate filter membrane with a pore size of 0.45  $\mu\text{m}$ , a layer of polyacrylamide hydrogel, on top of a Chelex 100 cation-exchange resin layer. The layers within the device are compact and sealed such that only the filter membrane interacts directly with the external environment; it helps protect the hydrogel from external particles. Both the filter membrane and the hydrogel make up the diffusive layer (Zhang and Davison, 1995; Li *et al.*, 2002; Mengistu, 2009).

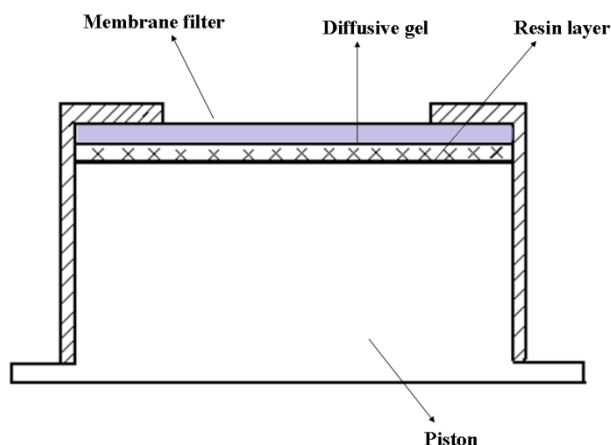


**Figure 6:** A simple representation of the DGT device with the functional components as indicated (adapted from Mengistu, 2009).

DGT can operate under varying ionic strengths and temperature; however, ideally, for more comprehensive data, the temperature should remain constant, within  $\pm 2^\circ\text{C}$ . The Chelex 100 resin in the binding layer is the limiting factor in DGT. The cation-exchange resin is affected by pH below 5 (Zhang and Davison, 1995). Therefore, sampling at a pH below 5 is not recommended.

### 2.3.2 Polymer inclusion membrane passive sampler

DGT despite being the most popular for metal ions it has its own limitations. The major limitation is that target metals bound onto the sorbent have to be re-desorbed using a suitable solution mostly acids are used. This has led to the development of other passive samplers with aqueous receiving phase. One such that is getting a lot of attention is polymer inclusion membranes (PIMs). PIMs are a type of liquid membranes, where a suitable carrier or ion-exchanger is immobilized within the chains of a plasticized thermoplastic polymer often referred to as base polymer. The polymer is synthesized in the presence of a carrier that is physically trapped in the polymer matrix. The carrier is essentially a complexing or ion-exchange reagent, responsible for binding the species of interest (i.e. analyte) at the membrane/source phase interface and transporting it across the PIM. The analyte is back-extracted into the receiving aqueous solution by a suitable stripping reagent thus releasing the carrier that diffuses back to the membrane/source phase interface where it can bind another analyte ion/molecule. The transport of the analyte across the membrane continues even when the total analyte concentration in the receiving phase becomes higher than that in the source phase. This transport process is known as facilitated transport (Figure 7). The analyte concentration in the receiving phase of the passive sampler can be measured by a suitable analytical method either directly or after derivatization. Due to the facilitated membrane transport outlined above PIM-based passive samplers are expected to provide a high level of

pre-concentration of the analyte in the receiving phase, thus allowing the use of less sensitive analytical methods.

Almeida et al. (2014) is reported to have developed a passive sampler for Zinc (II) in urban pond waters using a polymer inclusion membrane. The passive sampler consists of a compartment containing an acidic receiving solution which is separated from the external source solution by PIM consisting of 40 wt% di-2-(ethylhexyl) phosphoric acid as the extractant and 60 wt% poly-(vinyl chloride) as the base polymer. Two approaches of the passive sampler exposure were tested that is dip in approach vs sample flow through approach. The latter approach was found to be more suitable for the calibration of the passive sampler under the laboratory conditions. A proof of concept application was performed using a dip in approach (Almeida et al., 2014). In PIMs, the transport of analytes mimics biological membranes and thus there is no need of a diffusion gel like in DGT. Passive sampler based on PIMs thus measures the bioavailable fraction just like DGT and in all passive samplers. This is because uptake of analytes in passive sampler mimics biological membranes.

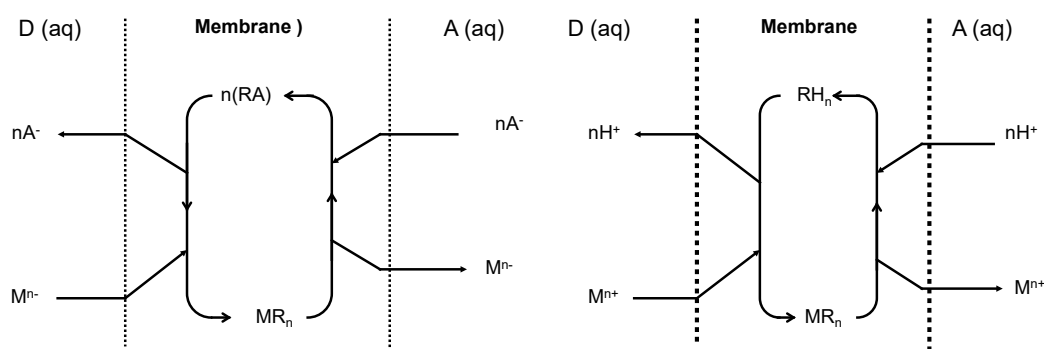


**Figure 7:** Facilitated transport mechanisms in polymer inclusion membranes passive sampler adapted from Djane et al., 1997. Where  $Mn^+$  and  $Mn^-$  are target metal species, RH and RA are acidic and basic extractant, respectively.  $H^+$  and  $A^-$  are the driving forces.

### 2.3.3 Biological-based passive samplers

By a simplified definition, a passive sampler is any device that is able to accumulate gas or vapour pollutants from the atmosphere through diffusion, without the active movement of the air through the sampler (Brown *et al.*, 1984). Of course this definition can be applied to all environmental compartments. For this reason, a number of species can be used to monitor pollution in the marine environment. The species of interest need to be abundant, stationary, easy to identify, long-lived and unaffected by any changes in environmental conditions. Most importantly, they need to be able to concentrate the pollutant of interest in their tissues

(Søndergaard *et al.*, 2014). The main drawbacks of using monitoring species exclusively is effects of metabolism, depuration rates, excretion, stress, viability and the condition of specie (Vrana *et al.*, 2005; Søndergaard *et al.*, 2014). The use of monitoring specie is often paired with the use of passive sampling as a comparative tool

## 2.4 Trends in passive samplers

### 2.4.1 New sorbents in DGT

The method by which passive samplers sequester and accumulate target analytes is already well established. This is why the basic characteristics of passive samplers remain the same. In DGT for example, the basic layout has not changed. The outer layer is a protective polyethersulphone (PES) membrane. Below this, is the diffusive gel layer, which may be made from either a polyacrylamide-agarose gel or exclusively an agarose gel. Underneath the diffusive gel layer is the resin gel layer, onto which the analyte will be accumulated (Davison *et al.*, 1994).

The original DGT sampler has a Chelex-polyacrylamide resin gel. It was designed to measure concentrations of nickel, copper, iron, manganese, zinc and cadmium in pore waters (Zhang *et al.*, 1995). The resin layer has been adapted in various studies for the measurement of specific analytes. This has also led to the development of new sorbents, as well as the exploration of already existing materials as passive sampler components. This is a fast growing area of research and only a few examples will be discussed. Research is focused on using different sorbents that can trap other metals such inorganic and organic forms of the metals as toxicity is depended on the metal specie form (Price *et al.*, 2013). Some are focused on developing resins that trap negatively charged forms of the metal like uranium since has a negative charge in its oxygen complex (Turner *et al.*, 2015).

A new zinc ferrite, ( $\text{ZnFe}_2\text{O}_4$ ) binding gel was synthesised and used as part of the DGT passive sampler by the Madé group (Gorny *et al.*, 2015). This binding gel is selective for total arsenic, including inorganic arsenic (III) and arsenic (V), mono-methyl arsenic acid as well as dimethyl arsenic acid. Compared to binding gels that have been used previously, this zinc ferrite binding gel is easy and cheap to synthesise. 3-mercaptopropyl functionalized silica for example is only selective for arsenic (III) and it tends to be brittle and has a complex synthesis procedure (Gorny *et al.*, 2015). Total arsenic concentrations could be determined using ferrihydrite, Metsorbs® HMRP 50 or zirconium oxide. However, these binding gels have limitations with regards to elution and optimum pH ranges. The Zn-ferrite binding gel underwent several tests in order to validate its application in DGT. The effects of pH, ionic strength, and competitive anions on arsenic uptake were assessed, as well as the reproducibility of the results. An

environmental study was carried out and it proved that this new binding gel can be used for field studies (Gorny *et al.*, 2015). In another example, a thiol functionalised silica binding layer was used as a DGT binding layer. The objective of this study was to determine how the performance of DGT might be affected by nanoparticulate species of mercury and zinc. The DGT samplers were deployed in solutions with known concentrations of mercury (II) and nanoparticulate mercury sulphate, dissolved zinc (II) along with nanoparticulate zinc sulphate. The amount of mercury and zinc accumulated by the passive samplers was then analysed as well as the rate of diffusion (Pharm *et al.*, 2015). The results suggested that the nanoparticles deposited on the surface of the DGT passive samplers, acting as additional sorbents. This has negative implications since the DGT sampler underestimated the concentration of dissolved metal in solution. Price *et al.* (2013) studied the measurements of oxyanion species (As, Se, V, P) using a new ferrihydrite and Metsorb™ DGT techniques. Various parameters were studied such as effective capacity and diffusion coefficients. Because other possible competitors in binding these oxyanions, it was suggested that in sea water deployment time should be less than two days while in freshwater longer deployment times are feasible. The study also found out that ferrihydrite-DGT out performed Metsorb™- DGT contrary to previous reports. Variation in masses used for binding was cited as major cause of this and thus preparation of the binding layer need to be optimised so that there is no variation. A resin based on Diphonix® resin in DGT technique has been reported for trapping uranium in natural waters (Turner *et al.*, 2015). The resin was bought commercially and showed the potential for monitoring uranium in aquatic environment. However, in sea water the uptake was not linear and the resin seems to suffer from matrix interference due to limited capacity. In a recent study by Tafurt-Cardona *et al.* (2015), baker yeast has been reported as trapping sorbent for methyl mercury in DGT passive sampler. The baker yeast was immobilized in agarose gel as binding phase and polyacrylamide as diffusive layer in the DGT. Parameters such as sample pH, ionic strength and potential interfering metals (Cu, Fe, Mn, and Zn) were investigated. Selectivity study between methyl mercury and Hg<sup>2+</sup> was also tested and the sampler showed much preference towards methyl mercury. In another study, multiple DGT with different sorbents were studied for measuring manganese in treated acid mine drainage water. DGT devices with different binding phases were (Chelex-100, P81 and DE81 membranes) were used to perform the in situ speciation of Mn. Chelex-100 was found to perform much better while P81 too both Mn<sup>2+</sup> and MnSO<sub>4</sub>. The DE81 sorbent was affected by high concentration of Ca<sup>2+</sup> in the sample.

In another development, Whatman P81 cation exchange membrane has been used as a binding layer (Li *et al.*, 2002). In this study, they found that there were few advantages over the original DGT, including simplicity in the preparation and handling of the DGT device, as

well as reusability. They also found that this new binding phase binds transition metals better than it does to matrix ions such as potassium, sodium, calcium and magnesium, which are normally competitive ions in natural water (Li *et al.*, 2002). There have also been adaptations on DGT to specifically select for mercury (Diviš *et al.*, 2005; Dočekalová and Diviš, 2005). Silica gels with 3 mercaptopropyl functional groups have been used as binding phases in order to monitor levels of methylmercury (Clarisse and Hintelmann, 2006; Clarisse *et al.*, 2009, 2011).

A new mercury passive sampler that uses organosilica sol-gel has been developed (Zhou *et al.*, 2013). The binding layer consists of thiol groups that bind sequestered mercury compounds. Although in its initial stages of development, this mercury passive sampler shows great promise since the binding of mercury is independent of the type of mercury-chloride complex, implying that it can be used in different types of aquatic systems (Zhou *et al.*, 2013).

The above examples do show that new sorbents will continue to be explored for some time in DGT because no single sorbent can bind all the potential metal ions at one go. Also depending on possible sample matrix, some sorbents are suited only in certain water samples and may fail to give same results in other water types like sea water or acid drainage waters with high concentration of both heavy metals and major elements like calcium and magnesium.

#### **2.4.2 Combination of biomonitoring with passive samplers**

In order to have a comprehensive study of possible risk assessment of potential metal or organic pollutants to living organisms, often passive samplers are deployed along with a study of analytes in living organisms within the water body. Biomonitoring alone can be misleading because of cited disadvantages mentioned earlier on like decomposition of potential chemicals within the organisms and/or its excretion. Thus one of the trends is to combine both biomonitoring and using passive samplers. A multitude of studies have been conducted using various organisms to monitor environmental conditions. For simplicity we will look at two case studies. In the first, DGT samplers were deployed alongside transplanted seaweeds (*Fucus vesiculosus*), blue mussels (*Mytilus edulis*) and sea snails (*Littorina saxatilis*) near a former lead-zinc mine in West Greenland. The three species are representative of seaweeds, suspensions feeders and herbivores (Søndergaard *et al.*, 2014).

After deployment for nine days, the concentration of zinc, lead and iron were determined. High concentrations of each metal were obtained at sites closer to the mine. Lead concentration obtained from the three species and DGT shows a linear correlation, implying simple uptake with no internal regulation by either specie. Zinc and iron concentrations were less correlated and therefore accumulating of these two metals follows a more complex mechanism in these

living organisms. It can be concluded however, that significant pollution still arises from the zinc-lead mine (Søndergaard *et al.*, 2014).

In the second case study the extent of water toxicity in the Great Barrier Reef (GBR) was examined. Once again, passive sampling was paired with the use of specific monitoring species. Instead of looking at one toxicant at a time, this risk assessment looked at the combined effect of all the pollutants involved.

Passive samplers with SDB-RPS Empore™ disks were used. These discs are able to accumulate a wide range of organic pollutants, specifically; pesticides in the logK<sub>OW</sub> range 1.8-4.7 (Shaw *et al.*, 2009). After deployment, pollutants were extracted from the passive samplers using bioassays relevant for coral reefs. In order to predict the effect of these various pollutants, four groups of coral reef organism's representative of the coral reef ecosystem were selected and exposed to the passive sampler extracts. The selected coral reef organisms were scleractinian coral (*Acropora millepora*), a grazing sea urchin (*Heliocidaris tuberculata*), a primary producing microalga (*Phaeodactylum tricornutum*) and a marine bacterium (*Vibrio fischeri*) (Shaw *et al.*, 2009). Exposure from the extracts showed detrimental effects on the coral organisms; photosynthesis in the microalga was inhibited. Luminescence in the marine bacterium was also inhibited. In scleractinian coral, settlement was inhibited by concentrations of 50 times the sampled environmental levels of organic pollutants and 100-fold environmental enrichment led to 100% inhibition of the sea urchin larval development (Shaw *et al.*, 2009). This study shows the benefits of pairing passive sampling with bioassays can serve as an important tool in the risk assessment of pollutants.

## **2.5 Applications of passive samplers**

### **2.5.1 Risk assessment**

Passive sampling can be used to determine the exact state and quality of specific environmental compartments such as the atmosphere, indoor air, water basins, soil and biota. Since measurement of analyte is given as a time weighted average (TWA), episodic incidents of pollution can be determined without resulting in overall extreme variations in the measured concentration. This provides a long-term overview of pollutant levels (Namieśnik *et al.*, 2005, Vrana *et al.*, 2005).

A recent risk assessment study was done on the Witwatersrand Goldfields using DGT, by Mengistu *et al.*, 2012. After a century or more of mining in this area, the aftermath of mining activities was observed in the form of pollution in surface and ground water, soil as well as effects on biota. It was therefore essential to conduct an assessment on the geochemistry as

well as the rate and amount of acid mine drainage resulting from the mine waste dumps. The assessment was done using two methods, DGT as a sampling device, as well as conventional grab sampling method. Total concentrations that were obtained using the conventional grab sampling method were not representative of bioavailable fractions. From this study, it was concluded that DGT is a better option at monitoring the fate and transport of metal species along a polluted stream. Most importantly, it will be useful in locating the exact sources of pollution where contamination may result from different sources (Mengistu *et al.*, 2012).

### **2.5.2 Fate and transport**

The evolution of pollutants is an important aspect of monitoring. Understanding fate and transport is important in predicting potential contamination into aquatic systems (Bennett *et al.*, 2012). In this respect, the speciation of the target analyte plays a crucial role. It is well known that speciation controls reactivity, solubility and the eventual toxicity of an element. Transformation in speciation can occur as a result of the various interactions with the immediate environment (Reeder *et al.*, 2006).

A good example highlighting the application of passive sampling in elucidating fate and transport of a pollutant is a study conducted by the Jolley group (Bennett *et al.*, 2012). The study was aimed at understanding the mobilisation of arsenic under the influence of iron. Diffusive equilibration in thin films (DET) and DGT were used as the sampling methods of choice. DET is made up of similar components as DGT. It is used for the measurement of pore waters and relies on establishing equilibrium between the surrounding solution and the device (Davison *et al.*, 1991; Davison *et al.*, 1994).

DET was used to measure the concentration of iron (II) in pore water and DGT was for the measurement of inorganic arsenic. The reason for measuring the two elements at the same time is because the mobility of arsenic has been linked to the biogeochemistry of iron. Iron hydroxide minerals are capable of strongly adsorbing dissolved inorganic arsenic through complexation. It is suggested that arsenic (III) in particular, has a stronger affinity for iron (III) (hydro) oxide minerals. Under sub-oxic conditions, iron (III) (hydro) oxide minerals are reduced to iron (II), leading to the dissolution of the complexed arsenic, releasing it into the overlying water (Bennett *et al.*, 2012); Kocar *et al.*, 2006; Tufano *et al.*, 2008).

In the context of this study, *in situ* measurements using DGT and DET are even more important since sampling can take place directly within the sediments, under anoxic conditions without an increased chance of oxidation induced speciation changes (Bennett *et al.*, 2012). The results obtained from DGT and DET studies confirmed the above stated theory; the measured

arsenic (III) concentration was shown to increase with an increase in the concentration of iron (II) (Bennett et al., 2012).

### **2.5.3 Temporal trends**

Passive sampling can be used to assess temporal trends in the environment. A study conducted in India highlights the application of passive samplers in evaluating temporal and spatial trends (Pozo *et al.*, 2011). The study was focused on persistent organic pollutants (POPs). Due to the large increase in agricultural production, India has also seen a high increase in the use of pesticides. Measures have been made to try and limit the use and production of these pollutants. In order to assess the effectiveness of these control measure, proper monitoring has to take place. Passive samplers with polyurethane foam (PUF) discs were deployed on a quarterly basis in different areas, between 2006 and 2007 (Pozo *et al.*, 2011). From the results, the spatial trend of the POPs could be determined. The passive samplers were able to withstand the harsh storms that are occasionally experienced during the monsoon season. The temporal trends observed were however, not explicitly stated.

## CHAPTER THREE: RESEARCH METHODOLOGY

### 3.1 PART A: POLYMER INCLUSION BASED PASSIVE SAMPLER

#### 3.1.1 Chemicals and calibration standards

All chemicals used in this study were purchased as analytically pure reagents, and no further purification was done. Polyvinyl chloride (PVC), di-(2-ethylhexyl) phosphoric acid (D2EHPA), tetrahydrofuran (THF), nitric acid ( $\text{HNO}_3$ ), sulphuric acid ( $\text{H}_2\text{SO}_4$ ), hydrochloric acid (HCl), nickel(II) nitrate  $\text{Ni}(\text{NO}_3)_2$ , cobalt(II) nitrate hexahydrate ( $\text{Co}(\text{NO}_3)_2 \cdot 6\text{H}_2\text{O}$ ), Copper(II) nitrate,  $\text{Cu}(\text{NO}_3)_2$ , cadmium (II) nitrate ( $\text{Cd}(\text{NO}_3)_2 \cdot 4\text{H}_2\text{O}$ ) and iron (II) nitrate  $\text{Fe}(\text{NO}_3)_2$  were purchased from Sigma-aldrich (Johannesburg, South Africa). Metal stock solutions were conducted by dispersing a suitable amount of their metal salt in deionized water. The pH of the solutions was attuned by addition of 1M  $\text{HNO}_3$  and 1M NaOH solutions.

#### 3.1.2 Instrumentation

All metal ions measurements were performed on a Spectro Genesis inductively coupled plasma optical emission spectrometry (ICP-OES) (Spectro, Genesis, Germany). Conductivity and pH values were measured at several time intervals using a Hanna Combo pH/EC/TDS/C/PPM tester HI98129, Redox potential (ORP WP) both from Mettler Toledo (Johannesburg, South Africa). Deionized water was obtained from a Millipore water system (Massachusetts, USA), was used for the preparation of all solutions. All glassware was soaked for at least 24 h in 10%  $\text{HNO}_3$  and washed three times with deionized water prior to use. The morphology, structural configuration and roughness of the synthesized membrane were studied using an atomic force microscope, AFM Veeco Di3100 (Bruker, Boksburg, South Africa) and scanning electron microscope (SEM) with inverted light microscope (Nikon Eclipse Ma200). Small representative pieces of the membrane samples were coated with carbon and gold prior to analysis with the SEM microscope. Fourier transformed infrared spectrometry (FT-IR) (Tensor 27, Bruker, Germany) was used for the identification of functional groups present in the frequency range of  $4000\text{-}400\text{ cm}^{-1}$ . Thermal stability of each of the PIM sampler components was assessed by thermogravimetric analysis (TGA), using a TA Q600 SDT-Simultaneous Differential Scanning Calorimeter/thermogravimetric analyser. Phosphorus-31 NMR spectroscopy ( $^{31}\text{P}$  NMR) was used for determining the presence of D2EHPA in the membrane pores. ( $^{31}\text{P}$  NMR) is an analytical chemistry technique that uses nuclear magnetic resonance (NMR) to study chemical compounds that contain phosphorus. The ( $^{31}\text{P}$  NMR) spectra was analysed on a Bruker Avance III 500 MHz NMR Spectrometer. Water contact angle was measured using a Kruss Drop Shape Analyzer, DSA30 (KRUSS GmbH, Johannesburg). Film applicator was used for casting the membrane using Elcometer

4340 Motorised Film. The membrane thickness was further confirmed by electronic outside micrometre 0-25  $\mu\text{m}$ , 0.001  $\mu\text{m}$  shut geometrical metrology (Trossingen, Germany).

### 3.1.3 Experimental

#### 3.1.3.1 Preparation of membrane

Membranes were prepared by dissolving 400 mg of D2EHPA and 600 mg PVC in 10 mL of THF in a 100 mL glass beaker. The mixture was stirred for 3 h to form a homogeneous casting solution. The solution was casted using Elcometer 4340 Motorised Film Applicator which was kept on a levelled surface for uniform PIM formation. The homogenous membrane was casted on a glass Figure 8. Once the membrane was casted the glass was then covered to allow THF to evaporate over 24 h at room temperature. A transparent, flexible and mechanically strong membrane was formed. The membrane was then peeled from the glass plate, and the thickness was confirmed by using a micrometre. A round piece with diameter of 21.98 mm was cut out from its central section and used in the extraction experiments. The membrane was characterized for morphology and contact angle.



**Figure 8:** Casting membrane machine

#### 3.1.3.2 Passive sampler design

The passive sampler was designed from the PTFE rod shown in Figure 9. The designs were done by the Physics department at the University of the Witwatersrand using PVC tubular rods. All the design dimensions were provided by us. In this regard the designed passive sampler consists of a receiver solution chamber with a lumen as shown in Figure 10 a). The length of the receiver solution chamber was 24 mm and its lumen has the capacity to hold 5.5 mL of the receiver solution. The weight of the receiver solution chamber container is 41 g. The screw cap length was 21 mm. The enclosed screw cap Figure 10 b) has a window opening Figure 10 c) with a diameter of about 20 mm and tread depth of 1 mm which expose the

membrane to the source solution, and allow flow of the liquid from the source phase to contact the outer surface of the membrane. The screw cap has a weight of 31 g. The fully assembled passive sampler housing is shown in Figure 11. The length of the fully assembled passive sampler is 46 mm and weighs 72 g. With the aim of making the passive sampler lighter, easier to assemble and cheaper, we have designed it by using only PTFE material. Other studies have designed PMs using glass and the disadvantage with using glass is that it can easily cracked during deployment and Teflon tape was used to seal the glass threads to prevent leakage (Almeida et al., 2016).



**Figure 9:** Polytetrafluoroethylene rod

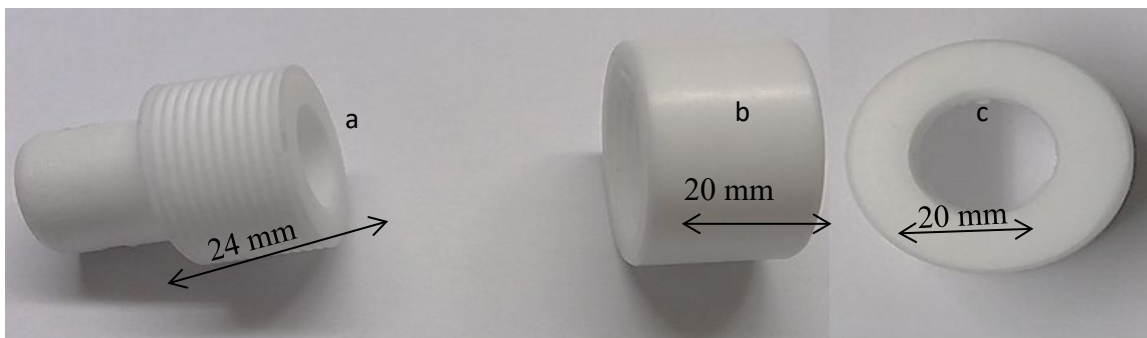


**Figure 10:** Components of the PIM a) receiver solution chamber, b) screw cap and (c) screw cap with a widow opening

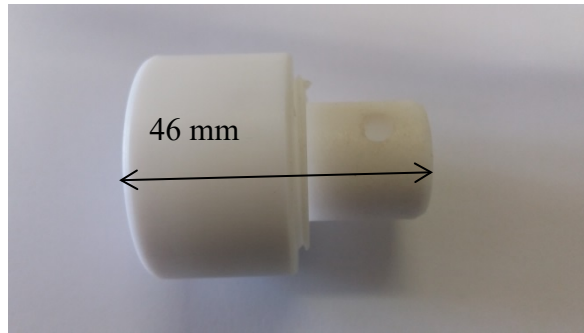


**Figure 11:** Fully assembled passive sampler housing

### 3.1.3.3 Assembling PIM components

The unassembled PIM with embedded membrane is shown in Figure 12. About 5.5 ml of the receiver solution was poured in the receiver solution chamber and the PIM membrane was used as a sealer to seal the receiver solution. The screw cap was then screwed down the receiver solution chamber using the threads, until the membrane was visible by the screw cap window and tightly bounded to the screw cap Figure 13.

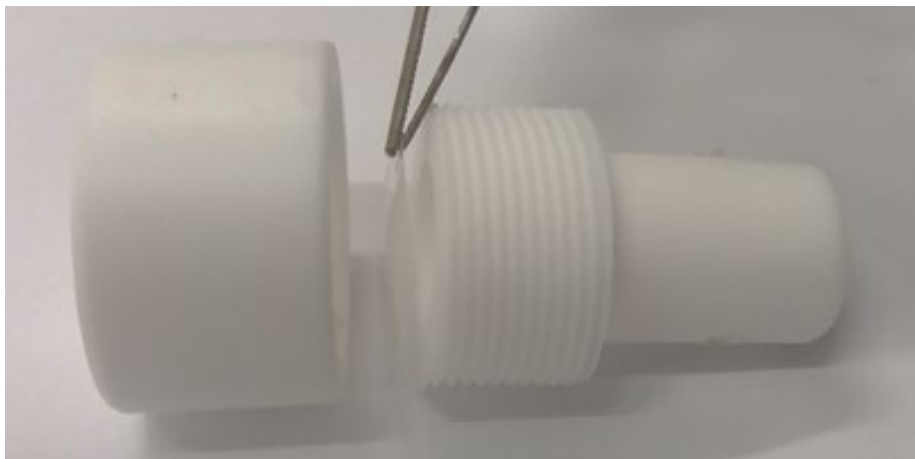


**Figure 12:** Unassembled PIM passive sampler

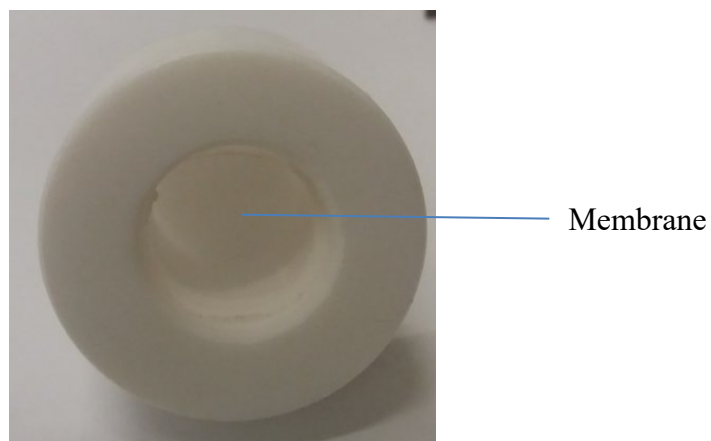


**Figure 13:** Assembled PIM passive sampler with exposure area

### 3.1.3.4 Passive sampler exposure area

The purpose of the study is to determine source solution metal ion concentration; hence it is required to calibrate the passive sampler in the laboratory before its application to the field. This involves an estimation of the impact of surrounding conditions on the performance of the sampler. In order to calibrate the passive sampler, it is necessary to construct an appropriate exposure area in the laboratory. Generally, samplers are exposed to continuous flow of analytes through the exposure area with a constant flow rate (Vrana et al., 2005). In order to have maximum sensitivity, a sampler design should have high (area and length) A/L ratio where A is the area and L is the length of the active device. Whatever design is employed, passive samplers mostly have a barrier between the sampled medium and the receiving phase. The barrier determines the rate at which analytes molecules are collected in the receiving phase. Some barriers have defined openings resulting into diffusion-based samplers. Others have the barrier in form of a non-porous membrane, referred to as permeation-based samplers (Vrana et al., 2005). Some factors that influence the uptake rate are sampler design, physio-chemical properties of the analytes and environmental variables (water turbulence, temperature and biofouling) (Nyoni et al., 2010). Hence for this study we first started by constructing two passive samplers with different window opening size for a non-porous membrane (Figure 14). The dimensions for the receiver solution chamber did not change; the only dimensions that changed were the screw cap exposure area. The dimensions for the larger exposure area were the same as those discussed earlier, which is 20 mm wide (Figure 14 b). The screw cap with the small exposure area was 10 mm (Figure 14 a). The optimisations of these windows opening are discussed in the results and discussion section.

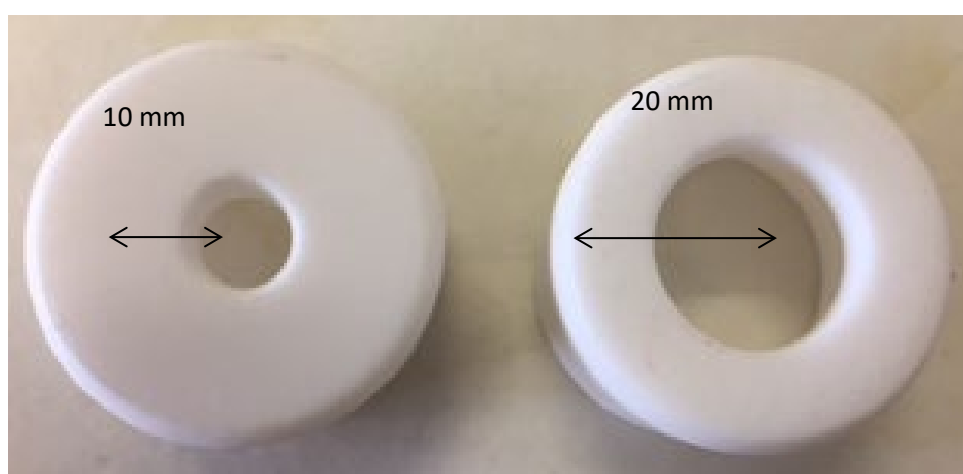


**Figure 14:** Dimensions of the a) small exposure area and b) large exposure area

### 3.1.3.5 Experimental set up of PIM pasive sampler

The passive sampler was set-up by incorporating a carrier with 10-40%w/w D2EHPA and a polymer 60-90%w/w PVC. PVC was chosen as the base polymer. The method was repeated by changing the composition of each component as shown in Table 1. The study of the PIMs always involves characterisation of the extraction of the target metal ion from a source into a membrane. This is frequently combined with simultaneous back extraction on the other side of the membrane into a receiver solution. Where extraction and back extraction occur simultaneously, the metal ion is transported across the membrane. These experiments were carried out in a system consisting of two compartment units a passive sampler and a glass beaker. A volume of 3.5 L of deionised water was spiked with 1 mg L<sup>-1</sup> of the metal ion concentration of Co, Cu, Ni and Cd. The PIM passive sampler device was immersed 5 cm in the sample solution in a vertical position under stirring conditions in a 5 L glass beaker container. In this study acidic receiving solutions were used. The PIM passive samplers were then placed in a passive sampler holder Figure 15 and then dipped in the source phase. The entire set up is shown in Figure 16. The solution in the source phase was continuously stirred at 200 rpm. The concentration of the target metal ion in the source phase and the receiver phase was monitored over time. The change in concentration in source phase and the receiver phase allows the determination of the rate of transport of the metal ion across the membrane (St John et al., 2012). During the PIM-transport experiments, the samples of the receiving phases were evaluated for metal ion concentration with ICP-OES. All the experiments were run at ambient temperature. Triplicate measurements were made and the standard deviations were used as error bars. The metal ion transport process is described by the first-order reaction as in Eqn below.

$$\ln (C_t/C_i) = -kt$$

Where  $C_t$  (mg L<sup>-1</sup>) is the concentration of the metal ion in the source solution at a given time,  $C_i$  (mg L<sup>-1</sup>) is the initial concentration of the metal ion in the source solution,  $k$  is the rate constant (h<sup>-1</sup>), and  $t$  is the transport time (h).

**Table 1:** PIM composition (total mass = 1 g)

Membrane	PVC (mg)	D2EHPA (mg)	Composition (%w/w)
1	900	100	90:10
2	800	200	80:20
3	700	300	70:30
4	600	400	60:40



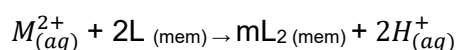
**Figure 15:** Passive sampler holder



**Figure 16:** Set up for polymer inclusion membrane passive sampler

### 3.1.4 Transport mechanism across the PIM

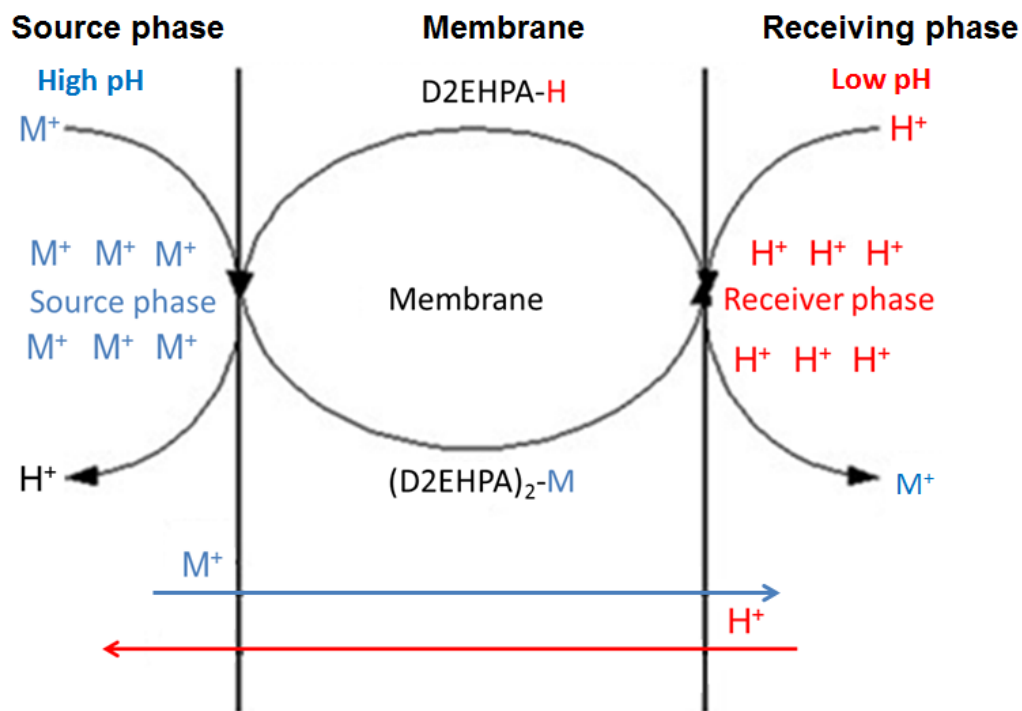
Transfer of analytes from the source phase to the receiver occurs through a carrier mediated mechanism. D2EHPA is used as the anionic carrier molecule that targets the cationic metal ions in solution in this study. Extraction and transport of a metal cation by an acidic carrier D2EHPA is directed by the exchange of the metal ion for protons of the carrier. D2EHPA replaces the carboxylic acids in metal extraction because of smaller extractant losses, higher metal loadings and faster equilibrium rates (Eljaddi et al., 2017). D2EHPA can also act as bidentate chelating agents. Therefore, counter-transport of protons is the driving force and is achieved by maintaining a suitable pH difference between the source and receiver solutions. In addition, careful pH control in the source solution can result in good selectivity as is the case in PIM passive samplers system using acidic reagents. When the extractant exhibits acidic properties, coupled counter transport takes place and the extraction reaction proceeds as in below.



Where  $M^{2+}$  is the target metal ion (Ni, Cu, Co and Cd), L is the dimer of the carrier D2EHPA in the PIM,  $mL_2$  represents the metal-D2EHPA complex.

PIM transport mechanism is studied in Figure 17. In the first step, the target solute after diffusing through the aqueous stagnant layer at the source solution/membrane interface reacts with the carrier at this interface to form a complex, which is then transported across this interface and replaced by another molecule of the carrier. In the second step, the complex diffuses across the membrane toward the receiving solution. The last step, at the membrane/receiver solution interface, the complex dissociates and the target solute is released into the receiving solution, which is essentially the reverse of the process occurring at the source solution/membrane interface. Thus, the source phase metal ion concentration is its total analytical concentration which is the sum of the concentrations of all chemical species containing this metal ion. Within the membrane phase, there is a concentration gradient of the target solute/carrier complex or ion-pair acting as a driving force for its transport across the membrane, despite the fact that the total analytical concentration of the target solute in the source solution can be substantially lower than in the receiving solution. In other words, uphill transport only takes place with respect to the total analytical concentration of the solute, while in the membrane phase it is actually downhill transport regarding the actual chemical species diffusing across the membrane. Many permanently charged compounds, especially metal ions can also be efficiently transported through PIM membranes by ionic carriers. In these cases, a gradient of counter ions from the receiving phase to the source phase provides the driving

force for the transport. Therefore, the metal carrier complex is transported through the membrane from the source to the receiver phase, and the counter ions are transported in the opposite direction (Zawierucha et al., 2016). The rate and selectivity of a PIM passive sampler separation is determined mainly by the membrane thickness, membrane, source and receiving composition.



**The transport mechanism depends on a high  $H^+$  ion concentration gradient between receiving phase and source phase**

**Figure 17:** Transport mechanism through PIM

### 3.1.5 Metal flux determination

Metal fluxes across the membrane are determined by monitoring their concentrations in the receiver and source phase. Flux ( $J$ ) is a measure for characterizing the performance of a PIM in an extraction experiment, where both sides of the membrane are exposed to the solution of the extracted species, (St John et al., 2012).

The value of the flux intake ( $J, mol m^{-2}s^{-1}$ ) at the PIM/solution interface was used to assess the extraction rate of the PIMs using the following Eqn below:

$$J = \left(\frac{V}{A}\right) \left(\frac{\Delta[M^{2+}]}{\Delta t}\right)$$

Where  $V$  is the feed solution volume,  $A$  is the membrane area exposed to feed solution,  $\Delta[M^{2+}]$  is the change in the metal ion concentration in receiver phase ( $mol\ m^{-3}$ ) at elapsed time (s).

### 3.1.6 Sampling rates determination

During initial deployment the accumulation rate is approximately linear, and during this period the mass of analyte in the receiving phase is dependent on the concentration to which the system has been exposed and the deployment time according to the relationship Eqn below

$$M_D = M_0 + C_W R_s t$$

where  $M_D$  is the mass (ng) of target analyte accumulated in the receiving phase over the deployment period,  $M_0$  the initial mass (ng) of the analyte in the receiving phase,  $C_W$  the TWA water concentration ( $ng\ L^{-1}$ ) over the deployment period, the effective sampling rate ( $R_s$ ) of the device ( $L\ day^{-1}$ ) and  $t$  is the deployment time (days) (Aguilar-Martínez et al., 2008). The sampling rate ( $R_s$ ) is equivalent the volume of water cleared per day by the device and is analyte specific. In the field, however,  $R_s$  is affected by variation in factors such as water temperature, turbulence, and biofouling of the diffusion membrane (Miege et al., 2015; Aguilar-Martínez et al., 2008).

### 3.1.7 Optimization of the PIM sampler

Fundamental parameters such as carrier concentration, pH of the aqueous phase, membrane thickness, receiver phase concentration, and effect of deployment time, effect of turbulence and membrane stability were monitored.

#### 3.1.7.1 Effect of carrier composition

The carrier concentration has a significant effect on the metal ion transport across the membrane. The effect of carrier concentration in the performance of PIMs was, investigated at 10, 20, 30, 40 and 50%w/w D2EHPA.

#### 3.1.7.2 Effect of source phase pH

The pH gradient between source and receiver phase generates the potential gradient across the membrane, which is the driving force for the permeation of metal complex towards the receiver phase. In order to assess the role of the source phase pH on the extraction of Co, Cu, Ni and Cd the pH of the source solution was investigated in this study.

#### 3.1.7.3 Effect of membrane thickness

The effect of the membrane thickness was studied with different thicknesses of 50 to 250  $\mu m$ . The thickness of a membrane was measured by the Elcometer film applicator, as the membrane was casted.

#### 3.1.7.4 Effect of receiver phase concentration

The concentration of the receiving solution plays an important role in the transport of metals across the membrane and the accumulation of metals in the receiving solution; it ultimately determines the accumulation capacity of the sampler. Hence, the effect of the concentration of HNO<sub>3</sub> in the receiving solution was studied in the range 0.25-1.5 mol L<sup>-1</sup>.

#### 3.1.7.5 Effect of stirring rate

Variation in stirring speed greatly affects the endurance, strength of the membrane and the transfer rate of metal ions from the source to the receiver solution. The effect of stirring rate was studied between 0 to 400 rpm.

#### 3.1.7.6 Membrane stability (recycle)

The PIM stability studies were carried out in this study. To study the stability of PIMs, three experiments were conducted under the same conditions without changing the membrane.

### **3.1.8 Application of PIM-based sampler**

#### 3.1.8.1 Sampling sites for PIM deployment

PIM passive samplers were deployed at two different sites affected by previous mining activities. Both sampling sites are found in Roodepoort, Johannesburg West. The first sampling site was near a mine tailing, with active AMD production. The second sampling site is Fleurhof dam Figure 18, the panoramic view shows that it is in close proximity to a mine tailing. Fleurhof Dam is situated on the Rand Leases (Vogelstruisfontein) G.M. Co Property; located on the farms Roodepoort 237 and Vogelstruisfontein 231.

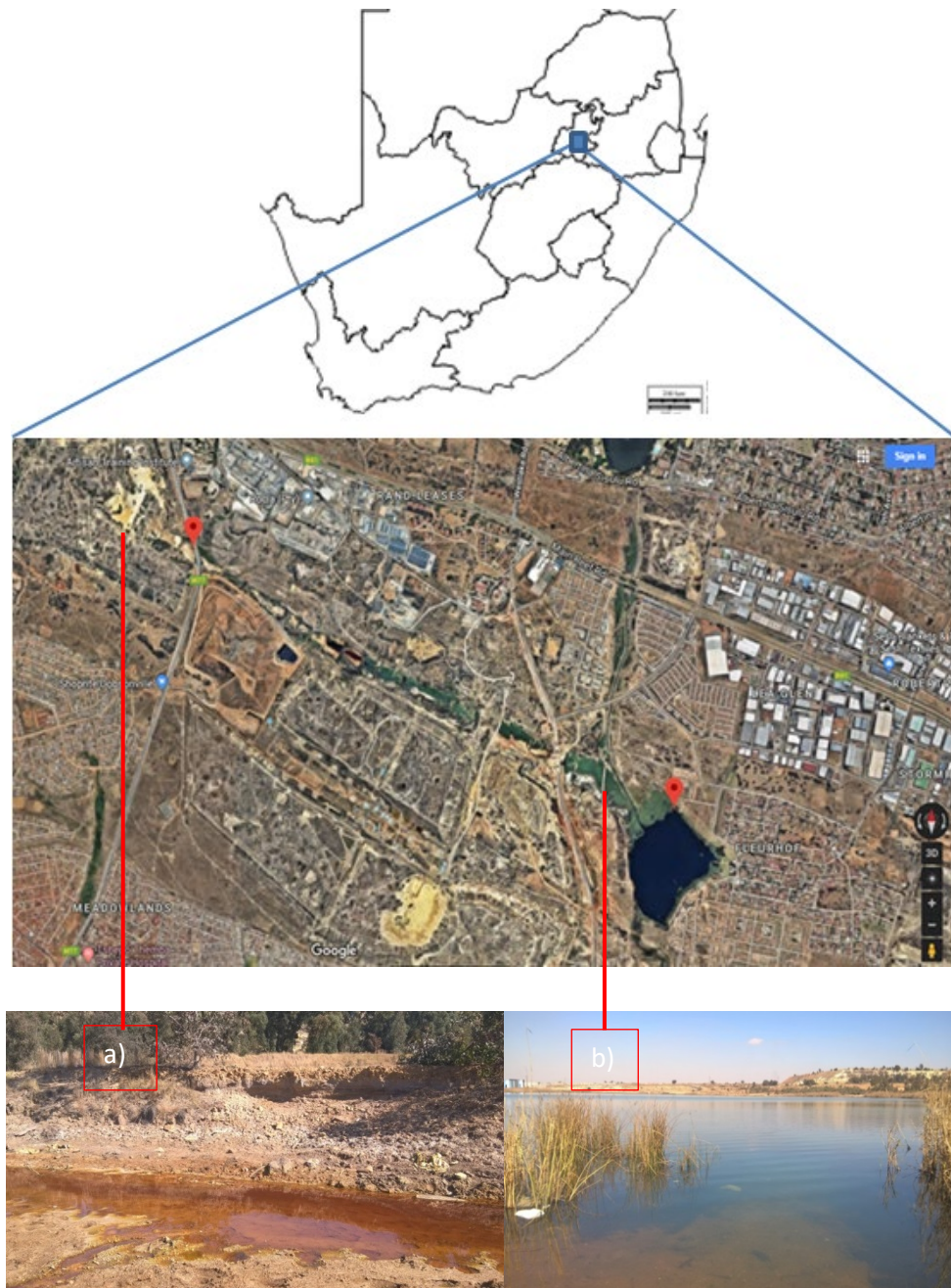


**Figure 18:** Sampling sites used for the deployment of PIM passive samplers, a) is the acid mine drainage impacted sampling site b) Fleurhof dam which is in close proximity to a mine tailing.

### 3.1.8.2 Construction of sampling cages

To protect the passive samplers at sampling sites, the first step was to design cages that could house the passive samplers during deployment. The passive sampling cages were designed such that they used cheap material that could protect the passive samplers during deployment in the field (Figure 19). The skeleton was made of threaded steel rods (Figure 19a) and a plastic mesh (Figure 19b) was wrapped around the steel rod structure in order to seal the cage

(Figure 19c) while allowing for water to flow through. The samplers were enclosed in stainless steel protective cages and taken to the field for deployment (Figure 19d). The number of samplers placed in each cage was three and the total number of cages was four.



**Figure 19**a) threaded steel rods and b) plastic mesh was wrapped around the steel rod structure in order to seal the Cages used for housing the passive samplers during field deployments, c) and d) deployment of the passive samplers, (e) picture of passive samplers submerged in the field.

### 3.1.8.3 Deployment of passive samplers in the dam and AMD

The cages were dipped approximately 2.5 cm below the water surface at random sites within the dam and AMD. Field parameters were recorded on the day of deployment and also on day 3, 5, 9 and 12 to check their variation during days of deployment of passive sampler. Grab samples were also collected on the same days and analysed for anions. It could be expected that anions might affect the transport of Cd, Co, Cu Ni and Fe due of competition with the carrier molecule.

### 3.1.9 Collection of passive samplers and analysis of metal ions

The passive samplers were then collected after day 12 and taken to the laboratory at the University of the Witwatersrand where they were carefully disassembled by unscrewing the top screw out of the PIM passive sampler housing. The membrane that sealed the receiver phase solution was removed from the receiver solution chamber. The receiver solution was

then poured inside the 15 ml plastic vial and immediately taken to ICP OES for quantitation of metal ions. No pre concentration steps were needed.

## **3.2 PART B: DIFFUSIVE GRADIENT IN THIN FILMS-BASED PASSIVE SAMPLER**

### **3.2.1 Materials**

PTFE rod for the manufacturing of passive samplers was purchased from Maizey plastics (Robertsham, Johannesburg). The polyethersulphone membrane was purchased from Merck. Polyethylenimine (PEI MW 25000), epichlorohydrin, 3-chloropropanesulfonyl chloride ( $C_3H_6Cl_2O_2S$ ), formaldehyde 38% ( $CH_2O$ ) were purchased from Sigma Aldrich and used without further purification. Sodium hydroxide, isopropanol, phosphoric acid, HCl, tetrahydrofuran were also used. Arsenate, selenite and mercury nitrate used to spike water were prepared from their nitrate salts:  $Na_3AsO_4$ ,  $Na_2SeO_3$  and  $Hg(NO_3)_2$ .

### **3.2.2 Instrumentation**

#### 3.2.2.1 Metal analysis

All elemental measurements were performed using Spectro Genesis inductively coupled plasma optical emission spectrometry (ICP-OES) (Kleve, Germany) and the Perkin Elmer inductively coupled plasma mass spectrometer (NexION 350D) (ICP-MS) (Massachusetts, United States).

#### 3.2.2.2 Fourier transform infrared (FT-IR) spectra analysis

The polymers were characterised using Fourier-transform infrared spectroscopy, Tensor 27 spectrophotometer (Bruker, Germany). The spectra was recorded between 4000 and 400  $cm^{-1}$ .

#### 3.2.2.3 Solid state NMR analysis

The solid state NMR spectra were obtained from Bruker Advance iii adapted with a 4 mm probe. The  $^{13}C$  CP-MAS, spinning at 500 Hz.

#### 3.2.2.4 CHNS analysis

CHNS analysis was performed on the polymers using Elementor vario EL cube. This technique was used to determine the percentage of carbon, hydrogen, nitrogen and sulphur.

### 3.2.2.5 Ion chromatography (IC)

A Metrohm 761 compact IC suppressor module, together with a Metrosep A Supp 5-150 column and guard column were used.

### 3.2.2.6 Field measurements

For field measurements, a portable Hanna combo meter that measures pH, conductivity, total dissolved solids (TDS), temperature.

## 3.2.3 Experimental procedure

### 3.2.3.1 Synthesis of polyethylenimine as a sorbent for DGT

#### **Cross-linked polyethylenimine (CPEI)**

CPEI was prepared as previously described by Saad et al. (2011), 10 g of polyethylenimine and 2 g of sodium hydroxide were dissolved in 25 mL ultra-pure Milli-Q water. The mixture was heated under reflux. Once the temperature had stabilised to 65°C, 1.2 mL of epichlorohydrin was added. A white rubbery solid was obtained within 10 minutes. The gel was then washed with water followed by isopropanol and left to dry overnight before use.

#### ***Sulphonated cross-linked polyethylenimine (SCPEI)***

CPEI was functionalised with sulphonyl groups in order to enhance selectivity of the polymer using a method adapted from Saad et al. (2013a) where 2.5 g of CPEI was dissolved in 65 mL of tetrahydrofuran. The mixture was heated under reflux until the temperature had stabilised to approximately 70°C, after which 2.4 mL of 3-chloropropanesulfonyl chloride (C<sub>3</sub>H<sub>6</sub>Cl<sub>2</sub>O<sub>2</sub>S) was added and the experiment was allowed to proceed overnight. An orange brown rubbery solid was obtained. It was washed with water several times to remove any unreacted product. The polymer was left to dry overnight.

#### ***Phosphonated cross-linked polyethylenimine (PCPEI)***

For the introduction of phosphate groups on the surface of CPEI, 2.5 g of CPEI was dissolved in 80 mL of 6 mol L<sup>-1</sup> HCl and 19.31 g of phosphoric acid using a method adapted from Saad et al. (2013b). This reaction mixture was heated under reflux to 90°C. Once the temperature had stabilised, 38 mL of formaldehyde was added drop-wise for one hour and the reaction was left to proceed overnight. The resulting dark brown solid was washed with water and left to dry overnight.

### 3.2.3.2 Batch studies

#### **SCPEI-PCPEI polymer mixture**

The efficiency of SCPEI-PCPEI-based DGT to accumulate arsenic and selenium would be determined by the ratio between the two polymers. The polymers were mixed in two different combinations: in the first 80% SCPEI to 20% PCPEI of the total mass was used. The second combination was 20% SCPEI to 80% PCPEI total mass. A solution containing  $1 \text{ mg L}^{-1}$  of arsenic and selenium was prepared and the pH was adjusted to 3 for one set and pH 7 for the other (pH 3 and pH 7 were selected because they represent AMD and natural water, respectively). Afterwards, 20 mL of either solution was poured into a 25 mL sample vial. 0.3 g of each resin combination was added to the sample vials. For each resin combination the samples were prepared in triplicate. The samples were left on a shaker for 1.5 hrs after which they were filtered. The remaining polymers were desorbed using 5 M nitric acid as suggested by Saad et al. (2013a; 2013b). Both the filtrate and the desorbed polymers were analysed using ICP-OES.

#### **Elution efficiency of different solvents**

Obtaining quality information from DGT depends on the proper elution of analytes accumulated within the resin layer. The elution factor as previously shown in equation (2.5) and (2.6) is required for the determination of TWA concentrations (Zhang and Davison, 1995). Saad et al. (2011) had prescribed 5 M nitric acid as the best elution solvent. Efforts were made to find a solvent that would be as effective but at a much lower concentration. Resin gels discs (resin that was embedded in agarose and cut into discs after the polymerisation of agarose) were prepared and each disc was deployed in 20 mL of ultra-pure Milli-Q water containing  $1 \text{ mg L}^{-1}$  of arsenic, and selenium. After 12 hours the resin gels were removed and rinsed with ultra-pure Milli-Q water and placed into different sample vials containing 20 mL of either  $1 \text{ mol L}^{-1}$  nitric, sulphuric, hydrochloric or phosphoric acid as well as sodium hydroxide and thiourea (dissolved in  $1 \text{ mol L}^{-1}$  hydrochloric acid). The resin gels were removed after 12 hours, the remaining solutions were filtered and analysed using ICP-OES.

### 3.2.4 The elution factor calculations

The elution factor ( $f_e$ ) was calculated using equation below:

$$f_e = \frac{M_e}{M_i - M_f}$$

Where  $M_e$  is mass eluted,  $M_i$  and  $M_f$  are the initial mass and mass remaining in solution, respectively (Davison, 2016).

### 3.2.5 Construction of passive sampler

#### 3.2.5.1 Construction of sample holders

DGT sample holder units used in this study were manufactured from a 30 cm diameter polytetrafluoroethylene (PTFE) rod (Figure 20). The dimensions used in the construction of the units were based on those prescribed for commercial DGT; both the piston and cap were 2.5 cm in diameter, in addition, the cap had a 2.0 cm exposure window (Warnken et al., 2005). Further modifications were made on the design of the DGT cap to allow for multiple uses unlike commercial DGT caps which are disposable.



**Figure 20:** PTFE rod used in the construction of DGT sample holder units

#### 3.2.5.2 Preparation of resin embedded in agarose

In commercial DGT, the receiving layer is made up of the Chelex® resin incorporated in an agarose-derivative gel designed by Lancaster University (Zhang and Davison, 1995a). Consequently, 0.5 g of SCPEI-PCPEI mixture was evenly spread out in a Perspex container. Warm agarose was poured on the polymer mixture, ensuring that the polymer was completely covered. This was left to polymerise at room temperature. It was also important to ensure that polymerisation took place on an even surface. The side containing the gravity-deposited polymer faced upwards on the DGT. A PES membrane was placed on top of the resin gel

layer and sealed with a DGT cap. These DGT devices were deployed in a solution containing  $1 \text{ mg L}^{-1}$  of arsenic and selenium. The passive samplers were deployed for 15 days with samplers removed every 3 days.

### 3.2.5.3 Preparation of diffusive gel layer

An agarose-based diffusive gel was made from 1.5% (w/v) of agarose. The required amount of agarose was weighed into a 250 mL Erlenmeyer flask and dissolved with Milli-Q water and sealed with a 50 mL Erlenmeyer flask. The agarose was placed in a conventional microwave oven and allowed to dissolve. Once dissolved, the hot mixture was poured into a Perspex mould with 0.08 cm plastic spacers. The Perspex mould was sealed with a lid to ensure an even surface. The agarose was allowed to polymerise after which the agarose was cut up into 2.5 cm discs using a 2.5 cm custom-made disc cutter. Gel thickness was measured using a digital calliper. The thickness of the agarose diffusive gel normally ranged between 0.068 cm and 0.08 cm.

### 3.2.6 Experimental set up of DGT-based sampler

The new SCPEI-PCPEI DGT passive sampler was assembled by placing 0.8 g of SCPEI-PCPEI resin directly on the DGT Teflon piston followed by a diffusive gel and PES membrane, respectively. During assembly, each layer was moistened with Milli-Q water to ensure that the resin and agarose diffusive gel do not dry up. To complete the assembly, the DGT cap was placed on top, ensuring that the passive sampler was completely sealed. These steps are summarised in Figure 21.

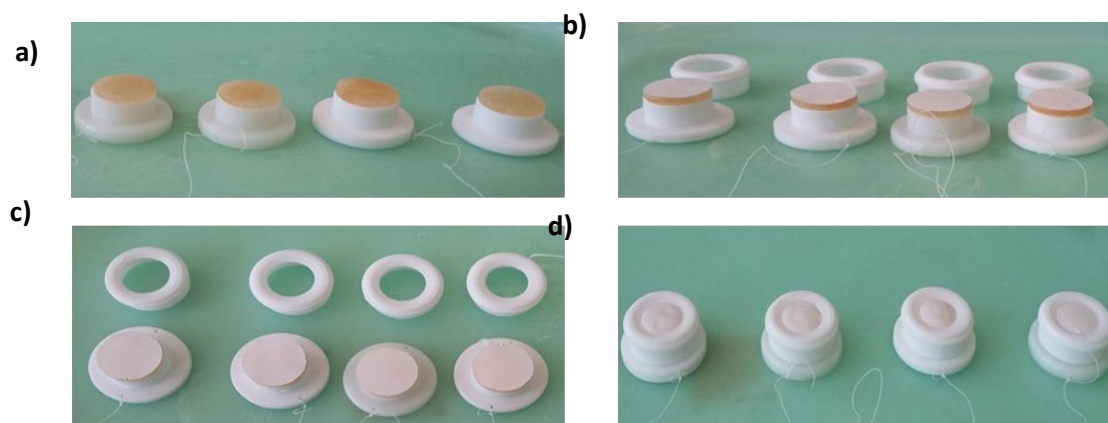


**Figure 21:** DGT was assembled by a) placing SCPEI-PCPEI resin mixture directly on the DGT piston b) this was followed by the agarose diffusive gel disc and c) PES membrane d) the samplers are sealed with a DGT cap.

SCPEI-PCPEI DGT passive samplers were deployed in 6 L Borosilicate glass containers filled with 5 L solutions spiked with a known concentration of arsenic and selenium. Depending on

the required conditions, the containers were placed on magnetic stirrers (stirred at 60 rpm) and deployed for a prescribed number of days. This experimental set-up is depicted in Figure 22.



**Figure 22:** Laboratory-based deployment of passive samplers in Spiked Milli-Q water.

### 3.2.7 Optimisation of DGT-based passive sampler

#### 3.2.7.1 Performance of SCPEI-based DGT

In passive sampling, the resin plays a crucial role in retaining the analytes of interest. Due to the ubiquity of sulphur and its strong association with multiple elements SCPEI was the initial polymer of choice. In preliminary studies, a simple experiment was set up by weighing 0.4 g of SCPEI and placing it on the DGT piston, a PES membrane was placed directly on top of the SCPEI. These contents were sealed with a DGT cap, 2 other DGT devices were prepared following the procedure stated above. These were deployed in a solution spiked with arsenic, selenium and mercury with a final concentration of ( $1 \text{ mg L}^{-1}$ ) and deployed for 12 days. A DGT sampling device was removed after 6, 9 and 12 days.

#### 3.2.7.2 Performance of SCPEI-PCPEI-based DGT embedded in agarose

Agarose vs no agarose

#### 3.2.7.3 The effect of resin mass on uptake of metals

The unique nature of this resin mixture and its ability to swell upon contact with water warranted further investigation on how it would best serve as a resin. A decision was made

not to embed the resin mixture in agarose but to instead use it as it is in DGT. An arbitrary mass of 0.4 g was selected since this was the minimum amount that could provide complete coverage of the DGT piston base. Furthermore, 0.8 g was the maximum amount that would still allow the structural integrity of DGT to be maintained. The resin layer was therefore prepared by weighing either 0.4 g or 0.8 g of the polymer mixture and placing it directly onto the DGT Teflon piston. This layer was smoothed out as much as possible before placing a PES membrane and sealing with a DGT cap.

#### 3.2.7.4 Role of the diffusive gel layer in SCPEI-PCPEI-based DGT

To test the requirement of a diffusive gel, DGT passive samplers were assembled in 2 different ways: The first layout involved placing a PES membrane on top of 0.4 g SCPEI-PCPEI resin mixture and sealing with a DGT cap. In the second, an agarose diffusive gel was placed between the resin mixture and a PES membrane everything was sealed with the DGT cap. The Diffusive gel was 0.07 cm. The passive samplers were deployed in Milli-Q water spiked with arsenic and selenium ( $1 \text{ mg L}^{-1}$ ). The passive samplers were deployed for 6 days, and removed after day 1; day 3 and day 6.

#### 3.2.7.5 The effect of diffusive gel thickness

#### 3.2.7.6 The effect of turbulence on DGT uptake

An experiment similar to the one described in section 4.4.5 was set up. The final concentration was  $1 \text{ mg L}^{-1}$  under stagnant conditions. The experiment was also allowed to proceed for a total of 12 days, with samplers removed every 3 days.

#### 3.2.7.7 The effect of sample concentration on DGT uptake

The DGT passive samplers were deployed in solutions at pH 3 containing a final concentration of  $0.25 \text{ mg L}^{-1}$ ,  $0.5 \text{ mg L}^{-1}$  and  $1 \text{ mg L}^{-1}$  for both arsenic and selenium. pH 3 was used because it was found to be optimal. These experiments were allowed to continue for 12 days, and samples were removed every 3 days.

#### 3.2.7.8 The effect of sample pH on DGT uptake

The pH plays an important role in the speciation of both arsenic and selenium. It was important to ensure that this newly developed DGT passive sampler could work under different pH conditions and to evaluate whether any significant effects on transport of target analytes occurred as a consequence of pH changes. Passive samplers were assembled and deployed in  $1 \text{ mg L}^{-1}$  arsenic and selenium water solutions, the pH was set to 3, 5 or 8. The samplers

were deployed for 15 days. This experiment provided both accumulation of mass over time as well as the effects of pH over time. The pH was checked every few days to ensure that no significant changes had occurred.

### **3.2.8 Calculation of the diffusion coefficient and DBL**

#### **3.2.8.1 The diffusion coefficient**

SCPEI-PCPEI DGT passive samplers were deployed in Milli-Q water spiked with arsenic and selenium ( $1 \text{ mg L}^{-1}$ ). The total deployment time was 16 hours, 3 DGT devices were removed after 4, 6, 8, 10, 14 and 16 hours. The resin was removed from the samplers, desorbed, filtered and the filtrate analysed using ICP-OES.

#### **3.2.8.2 The diffusive boundary layer (DBL)**

The thickness of the DBL ( $\delta$ ) was determined by deploying SCPEI-PCPEI DGT devices with varying diffusive gel thickness (0.06, 0.08, 0.1 and 0.12 cm) in spiked Milli-Q water for 3 days, after which they were removed and analysed.

### **3.2.9 Determination of the blank and method detection limit (MDL)**

DGT blank concentrations were obtained by preparing DGT devices comprising of the 0.014 cm thick PES filter membrane, 0.07 cm thick diffusive gel and resin. The devices were deployed in Milli-Q water for 24 hours; the resin was retrieved and desorbed with  $1 \text{ mol L}^{-1}$  of sulphuric acid for 12 hours, after which it was filtered and the filtrate analysed using ICP-OES. The method detection limit was calculated as three times the standard deviation of the blank.

### **3.2.10 Field application of optimised SCPEI-PCPEI-based DGT**

#### **3.2.10.1 Construction of sampling cages and deployment**

The passive sampling cages were designed such that they use affordable material that could be easily accessed and replaced in the same way as PIM-based sampler. These cages served the purpose of protecting the passive samplers during deployment in the field. The skeleton was made of threaded steel rods; a plastic mesh was wrapped around the steel rod structure in order to seal the cage while allowing the free flow of water (Figure 23).



**Figure 23:** a) and b) Cages used for housing the passive samplers during field deployments, c) passive samplers attached to the sampling cage d) picture of passive samplers submerged in the field.

DGT passive samplers were deployed at two different sites affected by previous mining activities as described already (Figure 24). Both sampling sites are found in Roodepoort, west of Johannesburg, with mine tailings in clear view. The first sampling site was near a mine tailing (GPS coordinates: 26°11'07.8"S 27°52'51.2"E) with active AMD production. The second sampling site was Fleurhof dam (GPS coordinates: 26°11'53.4"S 27°54'33.5"E). Physiochemical properties of the sampled water such as temperature, pH, redox potential and conductivity were obtained on site and in the lab. From each sampling site, 25 L of water was collected; however no preservative measures were taken as this would alter the pH prior to deployment of the DGT passive samplers.



**Figure 24:** a) Google Earth map of the area where water samples and DGT passive samplers were deployed. Site A is the site with active AMD seepage and site B is Fleurhof dam, which is in close proximity to mine tailings and active AMD b) and c) are the areas where AMD water was collected, which correspond to site A. d) Fleurhof dam which corresponds with site B on the map.

### 3.2.10.2 Application in Fleurhof dam water

SCPEI-PCPEI-based DGT units were assembled as described in the experimental a day prior to the sampling expedition. The DGT devices were deployed in Fleurhof dam for a total of 15 days. Three DGT sampling devices were removed after 3, 6, 9 and 15 days. The physiochemical properties of the water were measured on site.

For the laboratory-based experiments, 30 L of Fleurhof dam water was collected and used immediately. Two laboratory-based experiments were set up. In the first, two 6 L containers with 5 L of the Fleurhof dam water spiked with arsenic, selenium and mercury to a final concentration of  $0.5 \text{ mg L}^{-1}$ . Six DGT devices were placed in each container and they were deployed for a total of 9 days, with DGT devices removed after 3, 6 and 9 days.

In the second experiment, 6 L Borosilicate containers were filled with 5 L of Fleurhof dam water. Six DGT devices were deployed for a total of 9 days with samplers removed after 3, 6 and 9 days.

Prior to analysis, the resins were removed and placed in sample vials containing 20 mL of  $1 \text{ mol L}^{-1}$  of sulphuric acid. These vials were left at room temperature over-night, filtered and analysed using IC-MS. ICP-OES was used to analyse to measure the metals that were simultaneously accumulated in DGT.

### 3.2.10.3 Application in efflorescent crusts from AMD impacted sampling site

Efflorescent crusts were used to mimic AMD in order to assess matrix effects and measurement of bioavailable fractions of arsenic, selenium and mercury. The ratio used was 1 g of crust dissolved in 100 mL of Milli-Q water. Prior to analysis using ICP-OES, solutions were filtered several times using  $0.45 \mu\text{m}$  syringe filter. A 5 L solution of the dissolved crust was prepared for the deployment of DGT passive samplers. This solution was spiked with arsenic, selenium and mercury ( $1 \text{ mg L}^{-1}$ ). DGT devices were deployed for 19 days and three devices were removed every three days. The pH, redox potential, conductivity, anion concentration and background metals were analysed. The dry and ground efflorescent crust along with the experimental set up along shown in Figure 25.

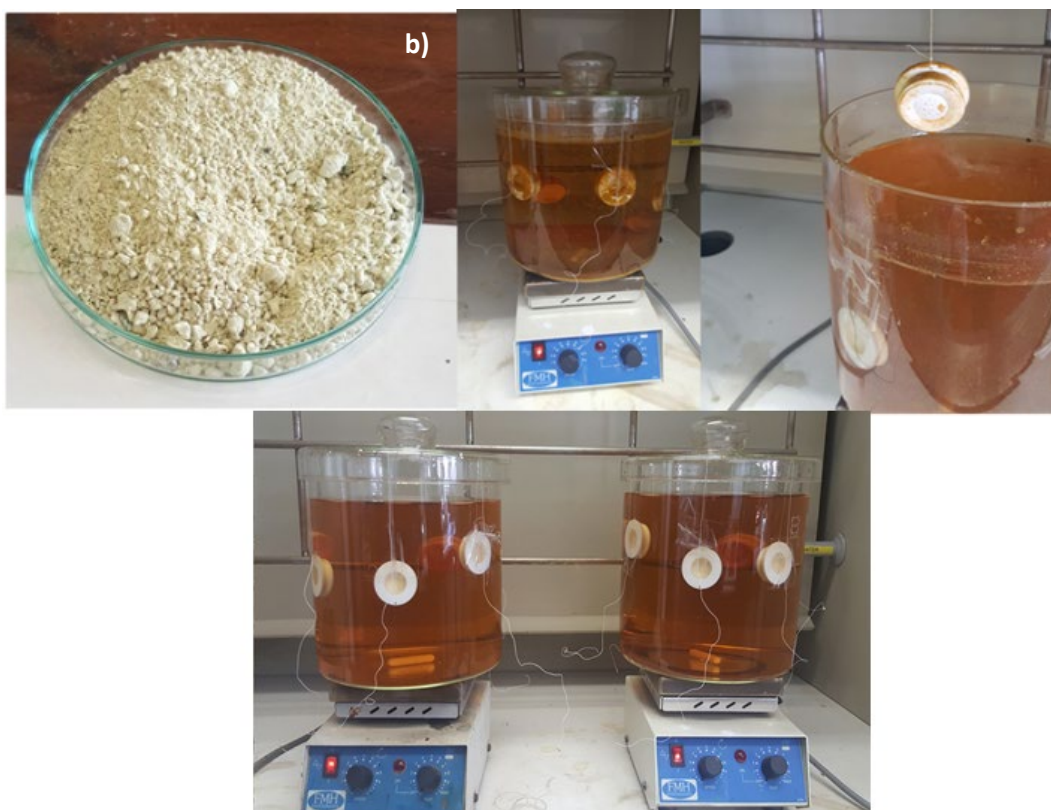


**Figure 25:** a) The efflorescent crust used in this study. b) The experimental set up of DGT in the dissolved efflorescent crust. DGT deployed in AMD water.

#### 3.2.10.4 Application in AMD water

AMD water was collected from site A shown in the map above. The water was spiked with  $0.5 \text{ mg L}^{-1}$  of arsenic, selenium and mercury. DGT devices were deployed for 5 days to avoid significant precipitation of the drainage water. DGT sampling devices were also deployed in the field for 5 days. The laboratory-based experimental set up is shown in Figure 26. Prior to analysis, the resins were removed and placed in sample vials containing  $20 \text{ mL}$  of  $1 \text{ mol L}^{-1}$  of sulphuric acid. These vials were left at room temperature over-night, filtered and analysed using IC-MS.



**Figure 26:** Experimental set up of SCPEI-PCPEI-based DGT sampling devices in AMD water.

### 3.2.11 PHREEQC modelling software

PHREEQC modelling software was used to gain better understanding of the species distribution in the environmental samples of selenium, arsenic and mercury.

## CHAPTER FOUR: RESULTS AND DISCUSSION

### 4.1 PART A: POLYMER INCLUSION MEMBRANE-BASED SAMPLER

#### 4.1.1 Polymer inclusion membrane optimisation

The components of a PIM (base polymer, PVC and carrier D2EHPA) which determine its extraction and transport performance were tested in this chapter.

##### 4.1.1.1 Effect of D2EHPA composition

The effect of D2EHPA carrier concentration composition in the membrane pores was investigated at 10, 20, 30, and 40 and 50%w/w D2EHPA for the transfer extraction of Co, Ni, Cu, Cd and Fe ions Figure 27.

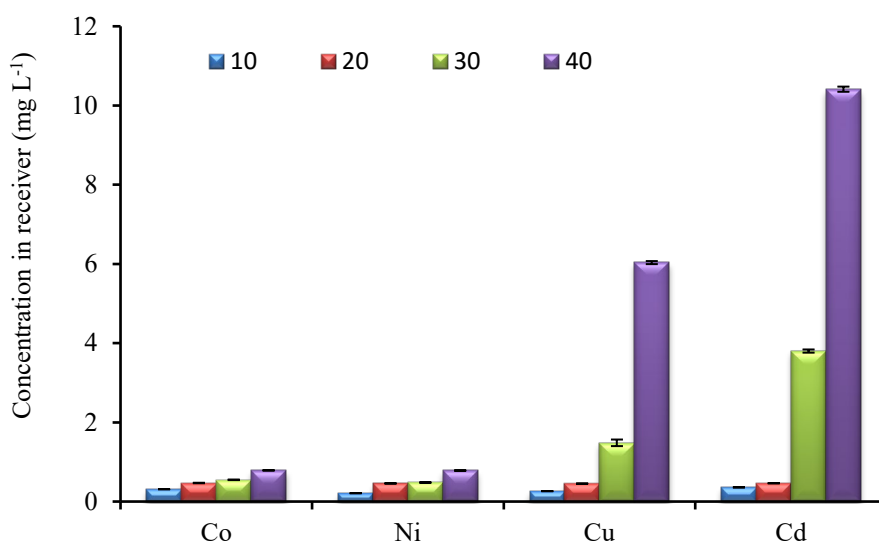


**Figure 27:** Effect of extractant (D2EHPA) concentration in the membrane (n = 3, SD)

The prepared membranes in PIM set were all homogeneous and transparent with an oil free surface and met the requirements of a stable PIM. The concentration of metals extracted was determined in the receiver solution. The amount of metal extracted increased with increasing the D2EHPA content in the membrane composition. Of the five compositions tested, only the 40%w/w D2EHPA membrane transported appreciable amounts of metals over the 5 days sampling period. Results for the transport of metals across PIMs containing lower concentrations of D2EHPA indicated that either metals diffusion coefficients were too low to ensure appreciable trans-membrane transport during the sampling period. As shown in previous work by Zhu et al., (2012), the transport rate may be increased by adding a plasticizer to the membrane composition. Membrane containing 50%w/w D2EHPA had limited

mechanical stability as reported by Kolev et al. (2009). The 40%w/w D2EHPA composition was therefore selected for further experiments. This optimum D2EHPA composition has been reported by other research Almeida et al. (2014) also and found to be around 40%w/w.

#### 4.1.1.2 Effect of receiver solution

Effective stripping of the metals from the membrane is necessary for the system to be used in practical situations. Three different receiver solutions containing 1M H<sub>2</sub>SO<sub>4</sub>, 1M HCl and 1M HNO<sub>3</sub> were used to evaluate the stripping of Co, Ni, Cu and Cd from PVC/D2EHPA PIM. The experiment was run for 2 days at pH 3 (Figure 28) and pH 6 (Figure 29). High metal ions concentrations were observed at pH 3 as compared to pH 6. However, it is notable that the stripping concentration of HNO<sub>3</sub> was the highest followed by HCl and H<sub>2</sub>SO<sub>4</sub>. It appears that facilitative transport of Co, Ni, Cu, and Cd through PVC/D2EHPA PIMs can be achieved with hydrogen ion concentration gradient across the membrane faster from nitric acid. Nitric acid has been reported in literature as a good metal ion stripping solution (Kim et al., 2001). Further experiments were thus conducted using 1M HNO<sub>3</sub>.

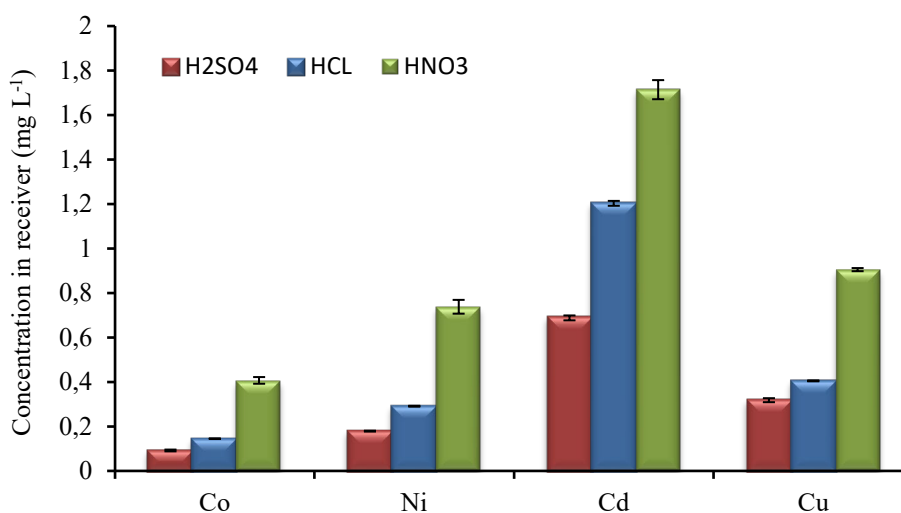


**Figure 28:** Effect of various acids as receiver solution at sample of pH 3 (n = 3, SD)

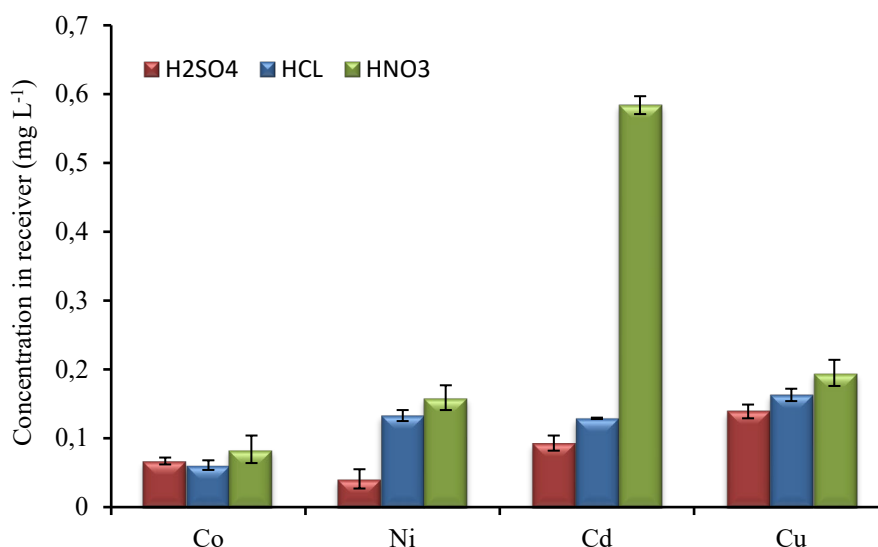


**Figure 29:** Effect of various acids as receiver solution at sample of pH 6 (n = 3, SD)

#### 4.1.1.3 Effect of pH in the source solution

The pH of the source solution plays an important role in the complex formation by acidic extractant. The influence of pH is related to the form of metal ions in solution, as well as the functional group of the extractant. Since D2EHPA is an acidic extraction reagent it is expected that the extraction concentration can be enhanced by increasing the pH of the metal ions solution. In this study the effect of pH on the extraction of the membrane containing 40%w/w D2EHPA and 60%w/w PVC was investigated at pH range of (3-7). Results are shown in Figure 30. The experiment was run for 1 day.

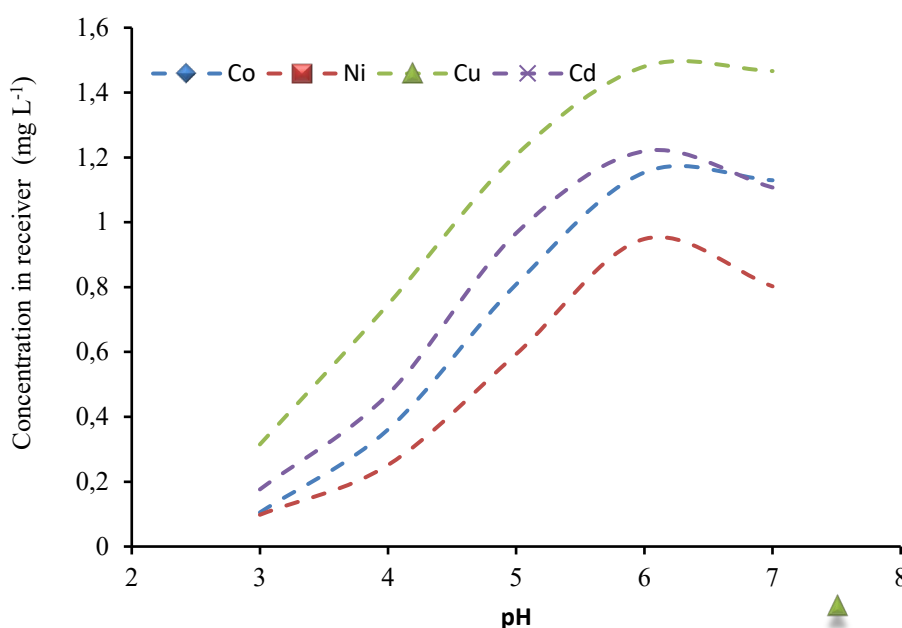
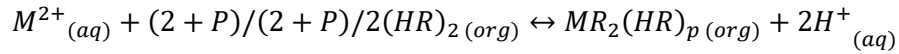


**Figure 30:** The effect of pH on the membrane extraction capacity (n = 3, SD)

The extraction could be interpreted from the general extraction Eqn below between divalent metal ions and D2EHPA molecules.



Where  $(HR)_2$  is a dimeric form of D2EHPA and P is the number of molecules of D2EHPA engaged in the reactions. In these cases, P has a value of 2 for Cd, Cu, Ni and Co when DE2HPA is used. According to Eqn above, as the pH increases there are is a decrease of  $H^+$ . It was observed that the amount of metal ion extracted decreased beyond pH 6, due to the fact that an increase of pH higher than 6 leads to the precipitation of the trace metal ions. This is due to the excess availability of phosphoric acid in D2EHPA and decreasing of the pH solution with the liberation of  $H^+$  ions. Further experiments were conducted at the optimum pH of 6. Results in Figure 30 seem to contradict those in figures 29 and 30 where sample pH of three was found optimum. This contradictions could be due to large time lag in this PIM-based sampler as observed later.

#### 4.1.1.4 Effect of membrane thickness

The diffusion of the complex formed by metal ion with D2EHPA across the membrane is a critical process of the PIM transport. Membrane thickness is one parameter that influences the transport rate of the formed metal ion-D2EHPA complex. The influence of membrane thickness was investigated at four different thicknesses (50, 100, 150 and 200  $\mu\text{m}$ ). It was observed in Figure 31 that the metal ion transport rate decreased as the thickness increased after the experiment was run for 1 day, which indicated that the mechanism of transport was in line with Fick's first law of diffusion in Eqn 13 (Kaya et al., 2013; Zaheri et al., 2017).

$$J = D \frac{C_{f,0}}{d}$$

Where d is the membrane thickness and D is the apparent diffusion coefficient of metal ion studied through the membrane and  $C_{f,0}$  are the initial and final concentration (Zaheri et al., 2017). In this study, it was observed that increasing membrane thickness from 50 to 100  $\mu\text{m}$  did not affect much the transport. At 200  $\mu\text{m}$  thickness, the metal ion transfer decrease. The 100  $\mu\text{m}$  membrane thickness was therefore accepted as optimum and used in further studies.

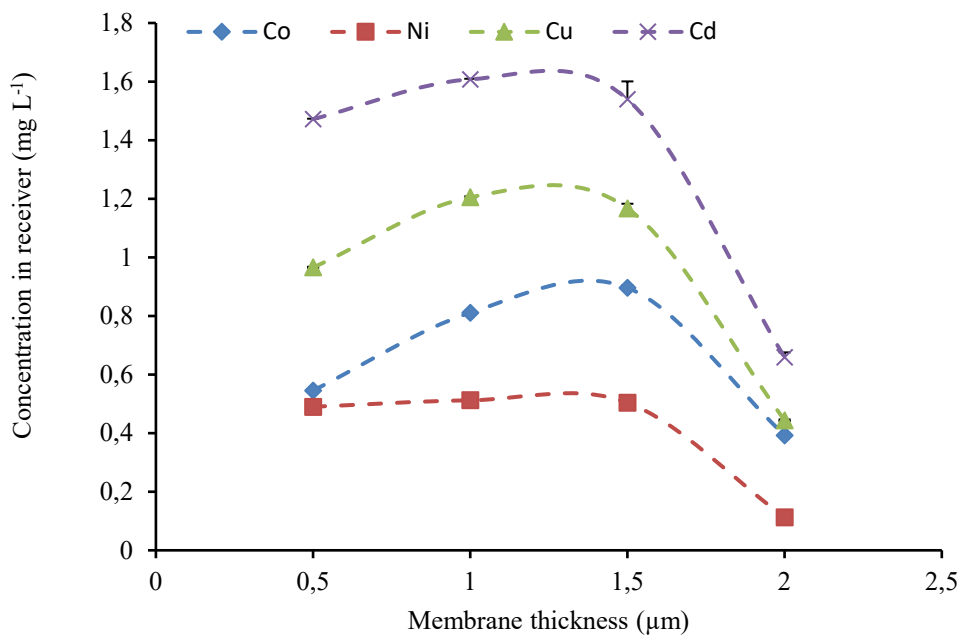


**Figure 31:** Effect of the thickness of PIM on the transport (n = 3, SD)

#### 4.1.1.5 Effect of receiver phase concentration

For a membrane composition of 40% w/w D2EHPA/ 60%w/w PVC, the effect of the nitric acid concentration in the stripping phase on the of metal ion concentration was studied from 0.25-1.5 mol L<sup>-1</sup> after 5 days of deployment. As shown in Figure 32 the metal ion flux through the PIM increases with increasing HNO<sub>3</sub> concentration up to 1 mol L<sup>-1</sup>, this could be attributed due to high concentration of protons in the receiver phase which leads to an increase in the driving force, which accelerates the separation of the metal ion-D2EHPA complex at the membrane-receiver interface. However, the optimum concentration was 1 M, from 1.5M HNO<sub>3</sub> the metal ion flux reduces. This might be related to degradation of the membrane by the acid or poor ionisation of the acid at high concentration

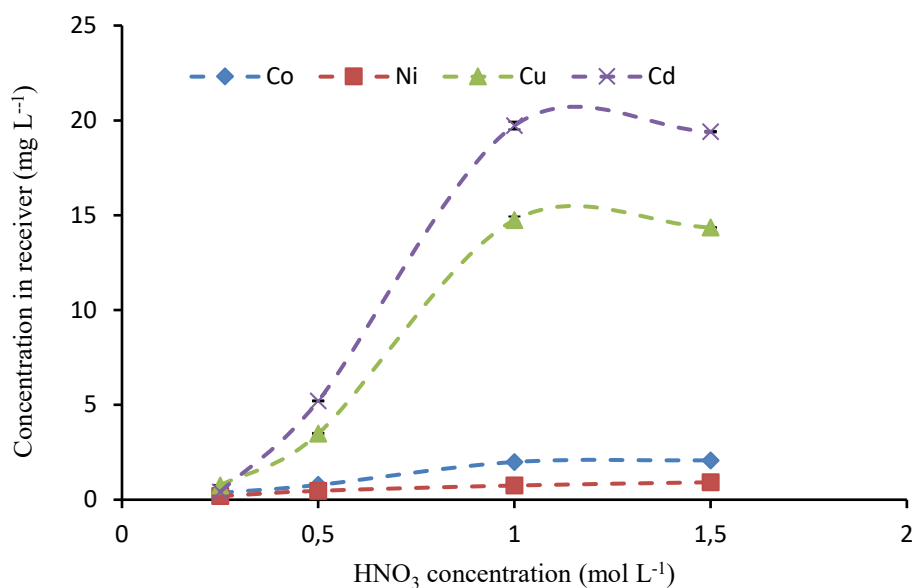


**Figure 32:** Effect of stripping phase concentration on the extraction of metal ions (n = 3, SD)

#### 4.1.1.6 Effect of stirring rate

The passive sampler with a different stirring rate speed liquid barrier between the source solution and the membrane was studied with the aim of investigating any stirring effects on the rate of accumulation of metal ion in the receiving solution. The effect of stirring rate of the source phase in case of metal ions concentration in the receiver solution using PIM was determined by varying the stirring speed from 0-400 rpm as in **Figure 33**.

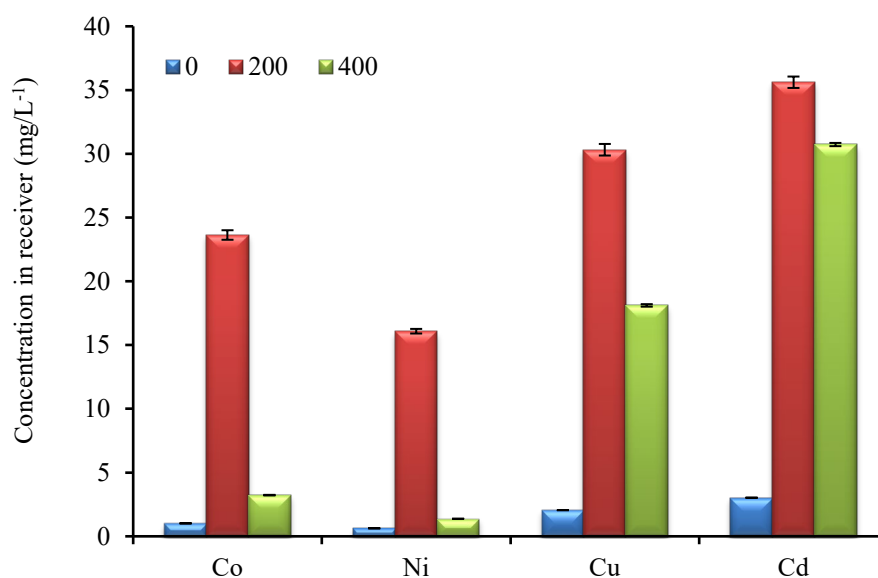


**Figure 33:** The effect of different stirring speed on concentration in the receiver solution of the passive sampler was investigated at 0, 200 and 400 rpm (n = 3, SD)

At 0 rpm the concentrations were very low and a significant increase was noticed once the stirring rate was increased to 200 rpm. Thereafter a decrease at 400 rpm was observed which is due to the aqueous boundary layer thickness decreasing continuously with increasing stirring speed up to 400 rpm. The increase of stirring speed beyond 200 rpm leads to stirring rate which then causes the release of the DE2HPA out from membranes pores (Benosmane et al., 2015). It was observed that the concentration of Co, Ni, Cd and Cu reached its optimum at 200 rpm after 10 days. Hence, the stirring speed of 200 rpm was selected for further experiments

#### 4.1.1.7 Effect of passive sampler exposure area

PIM passive sampler exposure area was tested. The study was performed using the optimum conditions which are 40%w/w D2EHPA, 1M HNO<sub>3</sub>, 100 μm, pH6 and 200 rpm stirring rate. The experiment was conducted for two days. The result Figure 34 shows that the larger exposure area of passive sampler was more effective and its extraction was higher than that of the small exposure area of the passive sampler. Cd was extracted more in the larger contact area with a concentration of 3.5 mg L<sup>-1</sup>, whereas the small contact area had the highest extraction of Cu with a concentration of 0.5 mg L<sup>-1</sup>. These results are evidence that the larger contact areas of the PIM passive sampler improve the rate of transport metal ion concentration uptake.

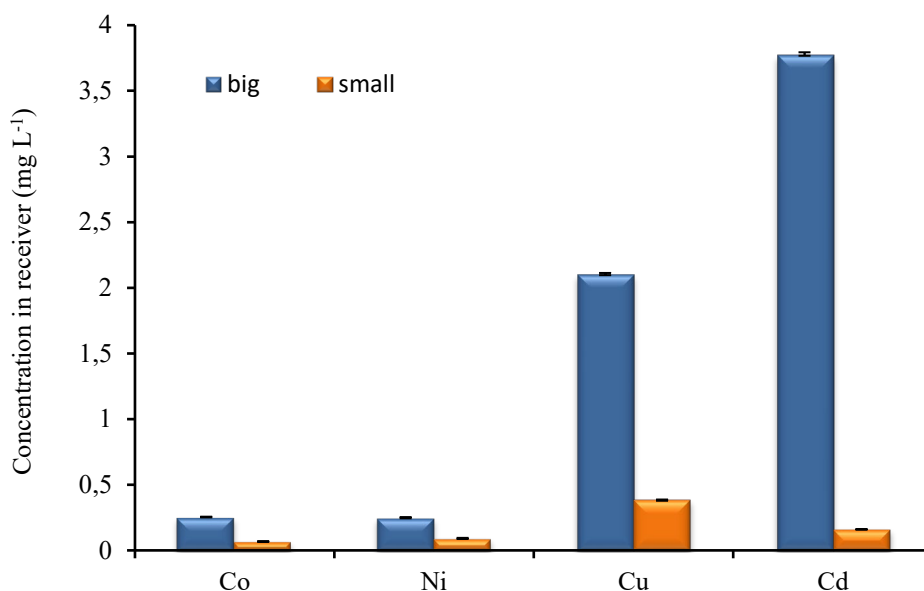


**Figure 34:** pH 6 PIM passive sampler window opening results after day 2 (n = 3, SD)

#### 4.1.1.8 Deployment time

The influence of sampling time on metal ions accumulation in the receiver phase was investigated over 13 days using the optimum results of the PIM passive as discussed above. The dependence of metal ion accumulation on the transport is shown in Figure 35.

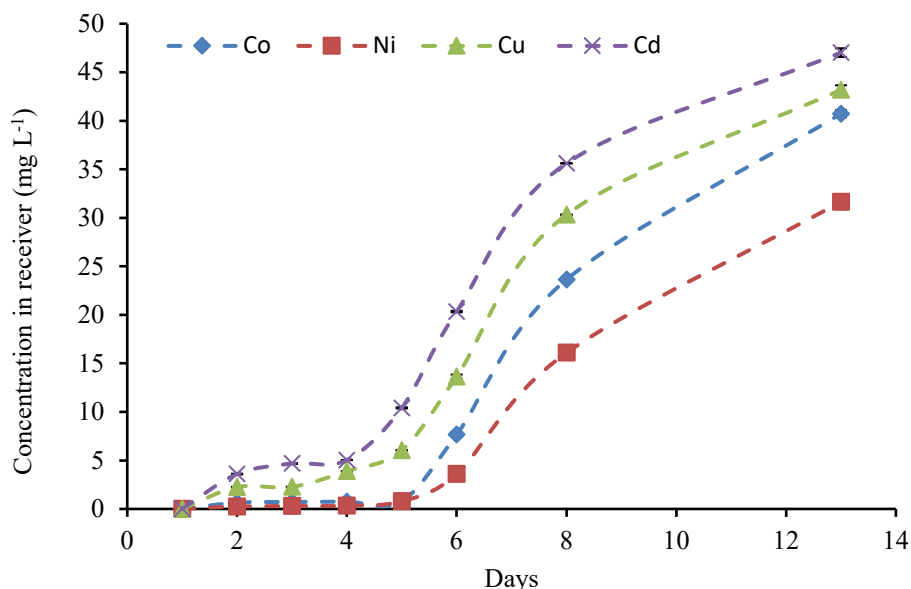


**Figure 35:** Transport of metal ion across PIM (n = 3, SD)

Lower transport kinetics was observed up to day 5. The concentration increased after day 6 and an uptake was observed up to day 13 which showed that PIM containing D2EHPA as carrier and PVC as polymer can facilitate the transport of Co, Ni, Cu and Cd. An uptake of metal ion was only obtained between day 6 and day 13. The change in concentration of metal ions in the receiver phase after a 13-day deployment time and other optimized parameters was used to calculate the flux of metal ions across the membrane using Eqn 11. The results showed that Co ions had the highest flux of  $685.17 \times 10^8 \text{ mol m}^{-2} \text{ s}^{-1}$ , followed by Cu with  $674.98 \times 10^8 \text{ mol m}^{-2} \text{ s}^{-1}$ , Ni with  $532.41 \times 10^8 \text{ mol m}^{-2} \text{ s}^{-1}$  and finally Cd with  $416.78 \times 10^8 \text{ mol m}^{-2} \text{ s}^{-1}$ .

#### 4.1.1.9 PIM stability and re-use

To study the stability of PIMs, three experiments were conducted under the same conditions without changing the membrane. The source and receiving phases were renewed for each experiment while the used PIM was first soaked in water set at pH 3 for 5 mins and allowed to dry at ambient temperature before reuse. The results in Figure 36 indicate that the metal ion concentration was higher in the first cycle.

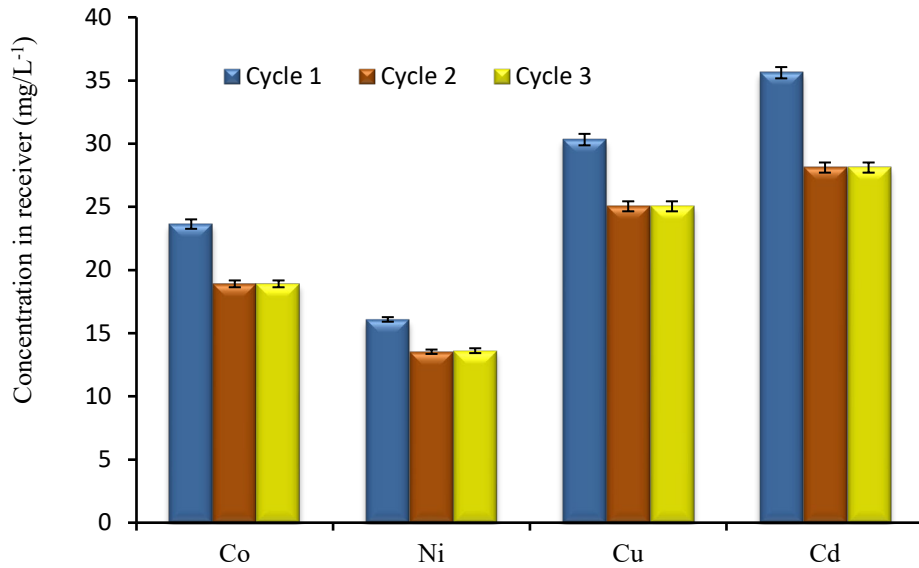


**Figure 36:** Stability of PIM for three consecutive experiment (n = 3, SD)

After that, the transport efficiency decreases, which may be caused by the leaching of the extractant to the source solutions, the difference in percentage between first cycle and second cycle for Co, Ni, Cu and Cd is 20%, 15%, 17% and 21% respectively. After the decrease between the first and the second cycle, the membrane was stable and there was no change between the second and third cycle. The mass of membrane weighted after transport was less than the one weight before transport. The percentage mass loss of the PIM from first cycle to second cycle was 5.1%. The visual observation of the membrane colour before transport is homogeneous, clear and colourless Figure 37 a), after transport the membrane colour changes to white and the membrane pores are visible Figure 37b).

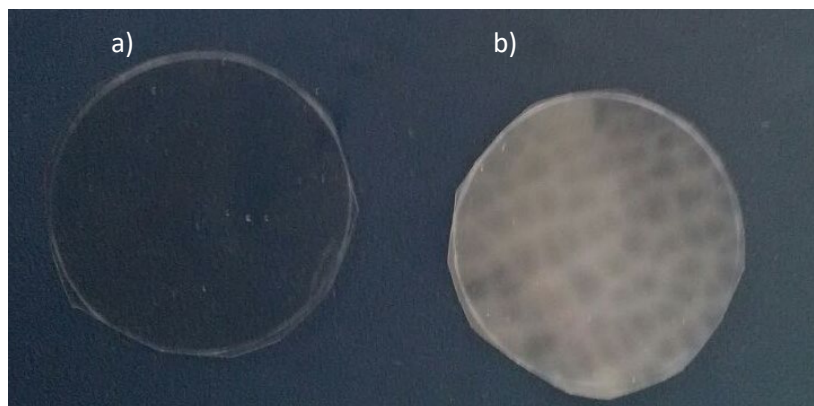


**Figure 37:** Membrane before a) and after b) extraction.

#### 4.1.2 Characterisation of stability

Membrane microstructure is one of major aspects affecting the separation of metal ions. PIM have a specific structure, depending on the particular type polymer film. In the case of PIMs, which are prepared by pouring out a polymer solution containing a carrier, the resulting membrane may have a different structure, depending on the type and concentration of the reactants. Scanning electron microscopy (SEM) provides information on how the carrier is distributed within the base polymer. By means of these techniques the actual picture of membrane morphology can be obtained. The stability of the PIM was further tested using thermogravimetric analysis (TGA) and nuclear magnetic resonance ( $^{31}\text{P}$  NMR). Contact angle measurements were studied.

##### 4.1.2.1 Scanning electron microscopy (SEM)

The SEM images of the PIM before application in Figure 38a) show a membrane surface with homogenous pores filled with liquid micro-domains containing the extracting agent. This observation supports the idea of coalescence of the aqueous carrier molecules to create liquid pathways that relay the analytes across the membrane (Gherasim et al., 2011). After extraction the membrane surface seems to collapse into irregular wells Figure 38b). The liquid domains at the pore openings have also been lost exposing the pores. The absence of liquid carrier domains at the pore openings might be an indication that the carrier liquid now exists inside the pores only. This might be responsible for the reduction in metal ion transfer across the membrane. When the PIM is reused for the third time, the transfer is not affected because the liquid membrane now exist inside the pores and there is minimal loss.

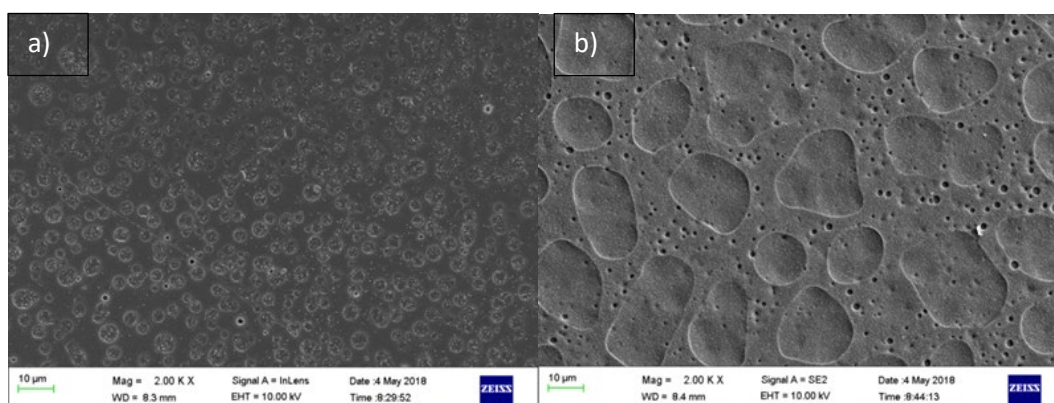


**Figure 38:** SEM image surface of the a) before extraction and b) after extraction of PIM.

##### 4.1.2.2 Thermogravimetric analysis (TGA)

TGA analysis was done to determine the stability of PVC and the PIM (PVC impregnated with D2EHPA) before and after extraction as a function of temperature. The results are presented

in Figure 39. The thermogram curve shows that the thermal degradation of PVC and PIM before extraction have common degradation temperatures at 260 and 400°C due to loss of the original weight followed by the decomposition of the polymer chain. This result was consistent with the thermogram of PVC and D2EHPA in a study by Ling et al., 2017. The thermogram for the PIM shows degradation of D2EHPA at about 300°C. The PIM before extraction shows a total D2EHPA loss of 35% while after extraction the percentage loss due degradation of D2EHPA was about 15%. These D2EHPA composition results coincide with the SEM images and repeatability results.

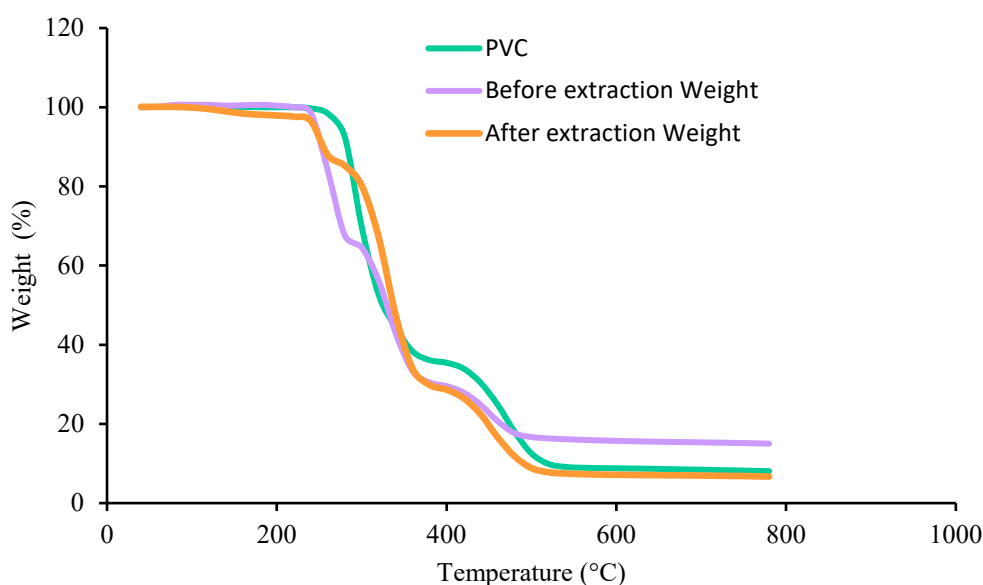


**Figure 39:** Thermogram a) PVC, b) before, and c) after extraction of PIM

#### 4.1.2.3 Nuclear magnetic resonance ( $^{31}\text{P}$ NMR)

The presence of D2EHPA in the pores of the PIM was confirmed using  $^{31}\text{P}$  NMR. The  $^{31}\text{P}$  NMR spectrum for PVC, DE2HPA and the PIM before and after extraction are shown in Figure 40. The PVC spectrum as expected did not show any phosphorus peak. The D2EHPA had a sharp peak, which was a clear indication of the presence of phosphorus atoms in its structure. The phosphorus peak was visible in the spectrum for PIM both before and after extraction. However, a chemical shift of 1.6 ppm for the phosphorus peak for D2EHPA in the PIM was observed. This might be due to the effect of THF that was used to dissolve the D2EHPA and the PVC. The peak also appears in the PIM spectrum after extraction an indication that the extraction process did not remove D2EHPA from the membrane pores. The PIM can therefore be reused for more experiments. However, the intensity of the peak decreased and broadens as compared to that of the PIM before extraction. This might be due to the fact that a small amount of D2EHPA might be lost during extraction, something that was confirmed by the TGA thermograms, SEM images and reusability results.

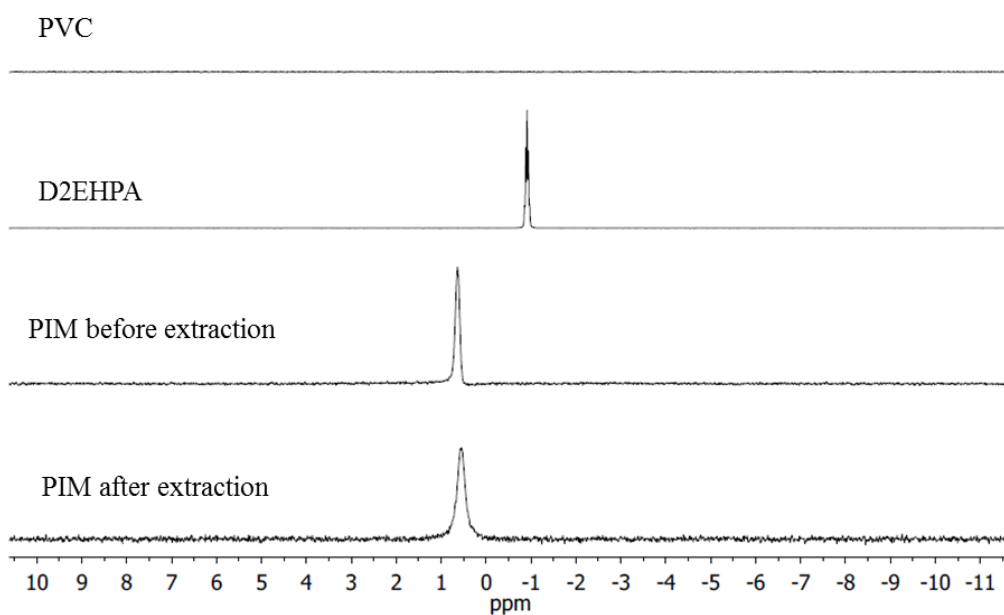


**Figure 40:**  $^{31}\text{P}$  NMR spectrum of PIM Composition

#### 4.1.2.4 Contact angle

The contact angle is a measure of the ability of a liquid to spread on a surface. The method is used to measure the angle between the outline tangent of a drop deposited on a solid and the surface of this solid. The contact angle measurements give the following information: The affinity of a liquid to a solid surface: if water is used to measure the contact angle one can deduce the hydrophobic (great angle,  $>90^\circ$ ) or hydrophilic (small angle,  $< 90^\circ$ ) character of the surface. In this study, contact angle measurements were taken at room temperature for PIM containing 40%w/w D2EHPA of carrier. The angle was found to be  $78.80 \pm 2.58^\circ\text{C}$ . When a solid surface is hydrophilic, the contact angle will be lower than  $90^\circ$ . This phenomenon can be the result of changes in surface morphology and the hydrophilic quality of carrier in the membrane.

### 4.1.3 Optimisation field water samples of dam water and AMD

#### 4.1.3.1 Effect of stirring rate in laboratory-based experiments

The effect of stirring rate in which dam water was used as the source phase was also investigated from 0 to 300 rpm as was the case with spiked deionized water. The results are shown in Figure 41. The dam water was spiked with  $1 \text{ mgL}^{-1}$  of Cd, Co, Cu, Ni and Fe. It was observed that just like in spiked deionized water, the optimum stirring rate was also 200 rpm. This was an indication that stirring rate was not affected by presence of potential matrices.

However, application in real samples with varying turbulence still requires considerations of the stirring rate. In our case, the PIM passive sampler was deployed where turbulence was very minimal due to the nature of the site with lots of reeds.

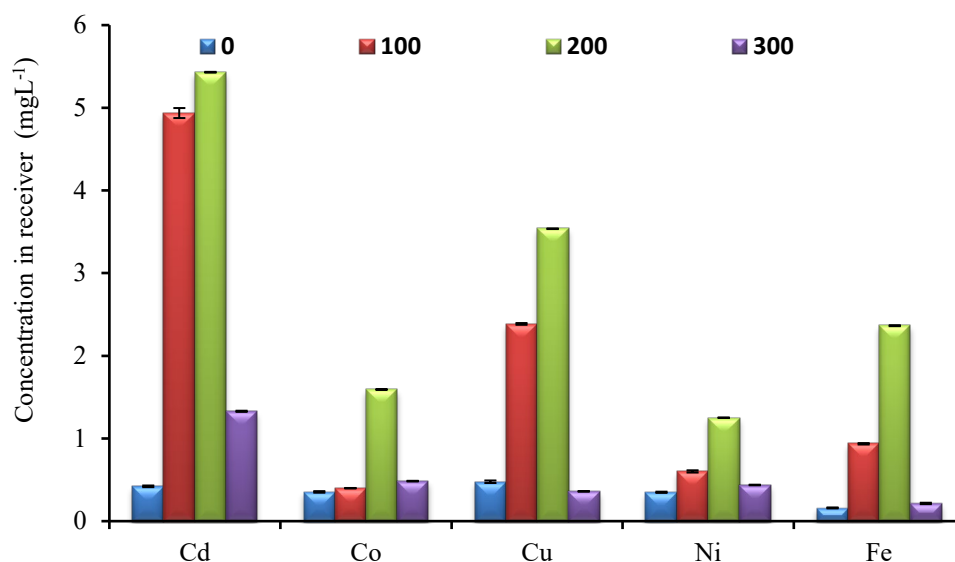


**Figure 41:** Effect of stirring rate using Fleurhof dam water spiked with 1 mgL<sup>-1</sup> of each metal ion (n = 3, SD)

For AMD, the results are shown in **Figure 42**. The stirring rate was only investigated at 0 to 100 rpm, due to Fe (II) precipitation. The hydrodynamic condition also had an effect on the concentration of Cd, Co, Cu, Ni and Fe transport. This effect was more observed in the AMD that had started to precipitate. Metal ions were made to be more bioavailable due to low pH as Fe precipitated. Increase in turbulence still could not result into more increased uptake. This suggests that precipitation reactions had reached near completion and stirring did not reverse process.

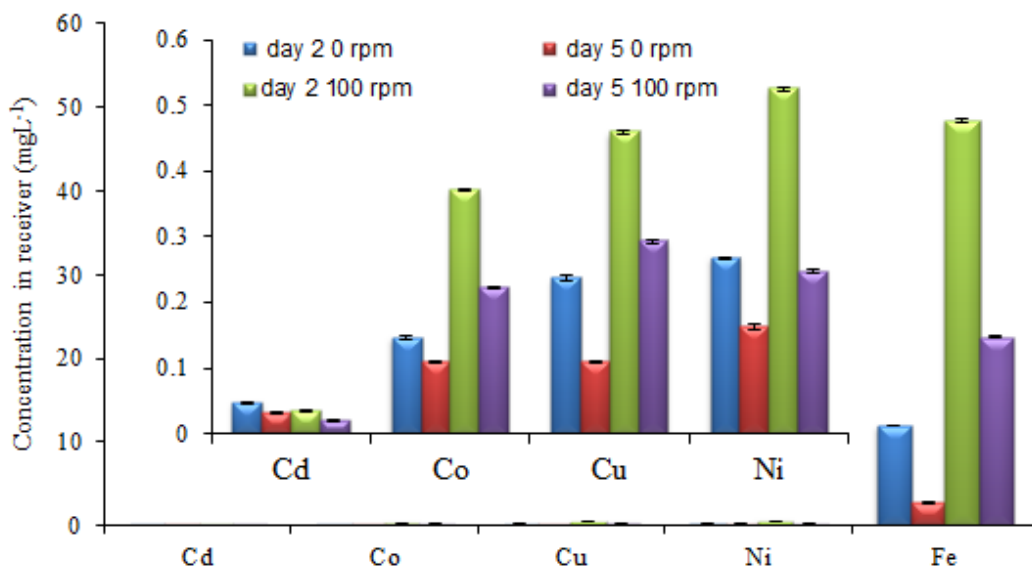


**Figure 42:** Effect of stirring rate on uptake of PIM passive sampler in AMD in the laboratory (n = 3, SD)

#### 4.1.3.2 Effect of contact time in laboratory-based experiments

The passive sampler was deployed in water samples obtained from Fleurhof dam and spiked with  $1 \text{ mg L}^{-1}$  metal ions as shown in Figure 43. A linear kinetic uptake of metal ion concentration was observed up to day 12. The linearity of the uptake was noted in the laboratory-based spiked water samples. This could be attributed to increased bioavailable fraction. The measured pH of the dam water was 6 which coincided with the optimum source phase pH for efficient metal ion flux across the membrane. The metal ion concentration in the spiked source phase was corrected for concentrations already existing in the dam water. The flux values dropped significantly by a factor of between 4 and 9 lower than the values obtained for spiked deionized water. In environmental samples, metal ions exist as complexes with organic acids. Even though some researchers have observed that the formation of the D2EHPA-metal ion complexes is fast Li et al., 2017 and Meng et al., 2017, the impact of the metal-humic acid complexes on the D2EHPA/D2EHPA-metal complex equilibrium cannot be ignored.

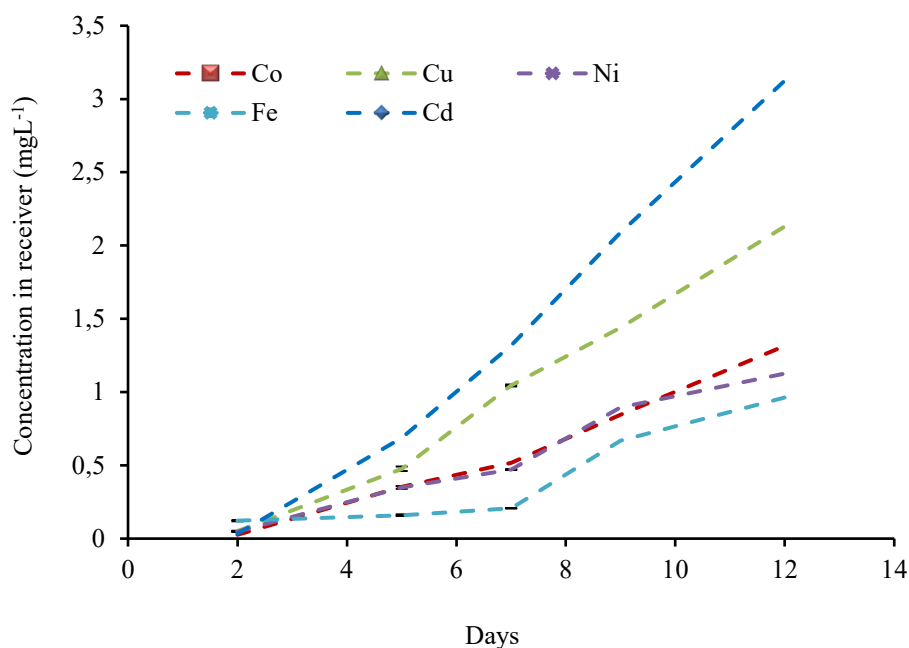


**Figure 43:** Uptake of metal ion in the laboratory using Fleurhof dam spiked with 1 mgL<sup>-1</sup> metal ion (n = 3, SD)

Observing this difference, the deployment time was investigated again this time using the dam water un-spiked (Figure 44 a&b). Results show Cu was far much more up taken than other metals followed by Fe, Co, Ni and Cd. A linear up take was observed between days 2 up to day 9 for Cu. Fe increased from day 2 up to day 5 and then it reached equilibrium up to day 12. It was observed that the flux values maximised at day 12. The calculated flux values were  $1.73 \times 10^8 \text{ mol m}^{-2} \text{ s}^{-1}$  for Co,  $38.74 \times 10^8 \text{ mol m}^{-2} \text{ s}^{-1}$  for Cu,  $1.65 \times 10^8 \text{ mol m}^{-2} \text{ s}^{-1}$  for Ni  $0.67 \times 10^8 \text{ mol m}^{-2} \text{ s}^{-1}$  for Cd and  $11.29 \times 10^8 \text{ mol m}^{-2} \text{ s}^{-1}$  for Fe. These observations are an indication that optimization of the passive sampler should be done using environmental water as compared to deionized water. Day 12 was therefore adopted as the optimum number of days for deploying the passive samplers in the field.

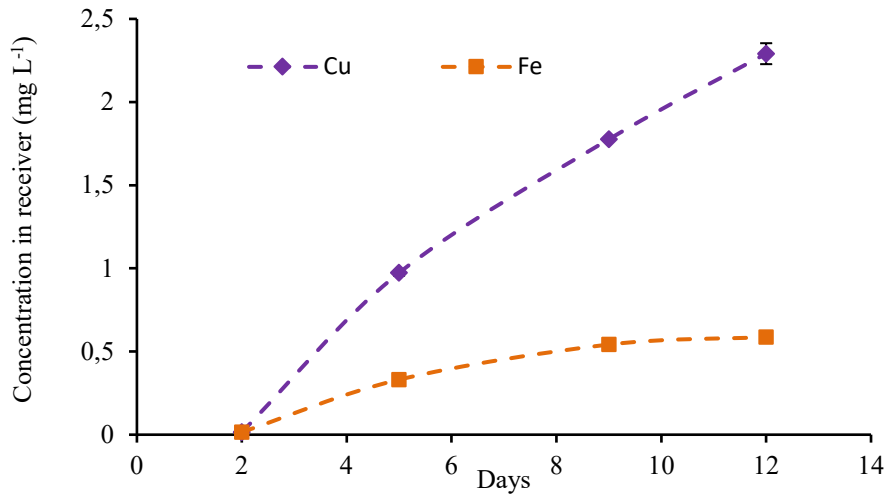


**Figure 44a:** Uptake of Cu and Fe in in the laboratory using dam unspiked (n = 3, SD)

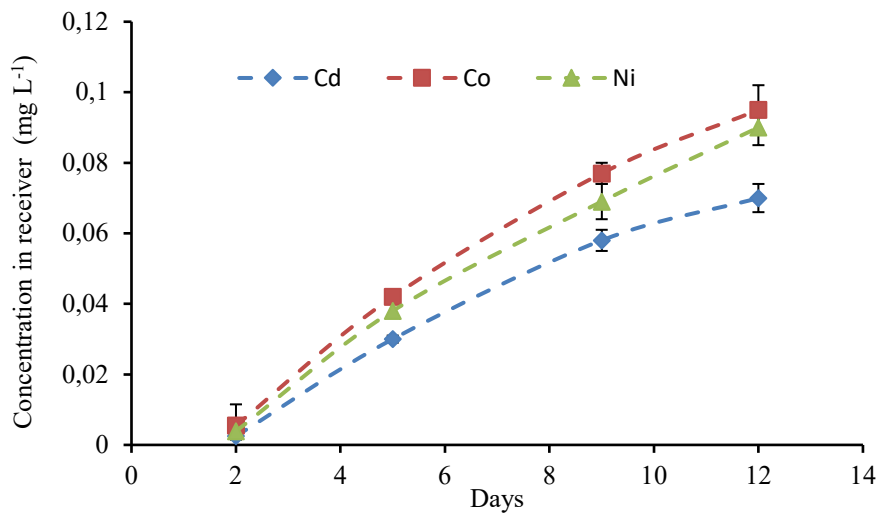


**Figure 44b:** Uptake of Co, Ni and Cd in in the laboratory using Fleurhof dam unspiked (n = 3, SD)

Figure 45 shows AMD laboratory results. The result shows a drastic decrease of metal ions concentration after 5 days of deployment. The decrease in the total metal ion concentration after day 5 is attributed to precipitation reactions. AMD water samples are susceptible to precipitation when kept stagnant due to changes in the water chemistry. The concentration of Fe decreased from 48 mg L<sup>-1</sup> to 22 mg L<sup>-1</sup>. A lot of solid precipitate was observed settling at the bottom after 5 days and the colour changed from a brown colour to an orange colour Figure 46. For this reason, the experiment was only carried out for 5 days instead of 12 days. These results were also confirmed by the decrease of metal ions concentration of AMD water

that was standing in the laboratory at room temperature for a period of 5 days as shown in Table 2. This means precipitation reactions reduced the bioavailability of the metals. The decrease was much more observed with Fe which means Fe is a major driver of the precipitation reaction. Cd and Co seem least affected but could be co-precipitated with Fe. The precipitation of Fe (II) to Fe (III) could be due to lack of oxygen, as samples are being stored in the laboratory. Thus passive sampler optimisation in AMD can best be done in the field. In the laboratory, it can be used to study the metal bioavailability after system is perturbed.

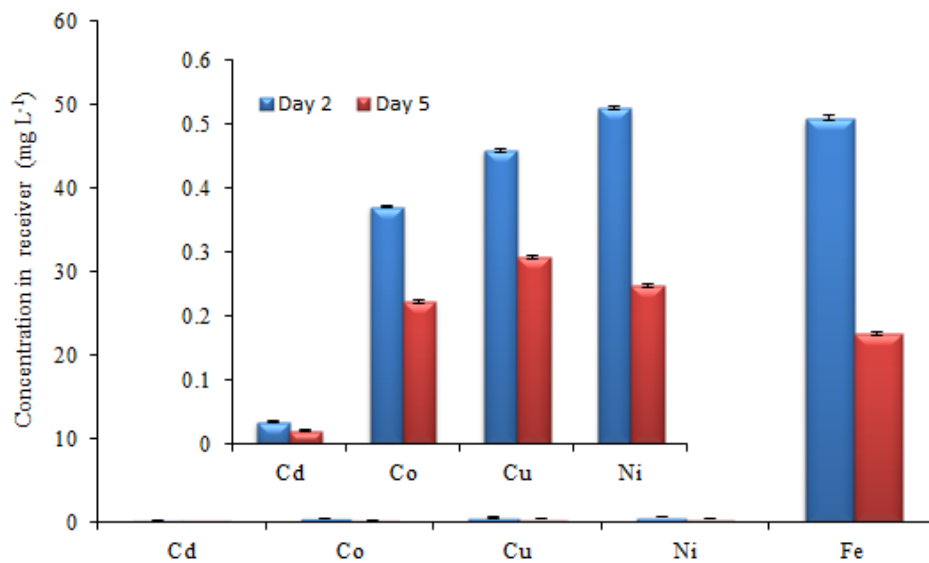


**Figure 45:** Metal ion deployed in AMD water in the laboratory (n = 3, SD)



**Figure 46:** Fe precipitation after day 5 in the laboratory set up (n = 3, SD)

**Table 2:** Metal ion concentration in the AMD sampled in one batch but analysed different days and kept at room temperature.

Metal (mg L <sup>-1</sup> )	Cd	Co	Cu	Ni	Fe
AMD immediately after sampling	0.53	19.06	14.48	28.70	1142.5
					0
AMD analysed after 5 days	0.16	10.23	9.73	23.62	817.79

#### 4.1.3.3 Receiver solution parameters

The relationship between the redox potential (Eh) and pH of the receiver solution, and its influence on the redox equilibrium was investigated because redox reactions are often sensitive to pH. The measured Eh and pH of the receiver solution over the 12-day deployment time are given in Figure 47 a&b. It was observed that as the Eh decreases with the increasing number of days while pH increased. This was in agreement with the PIM transport mechanism as discussed above.

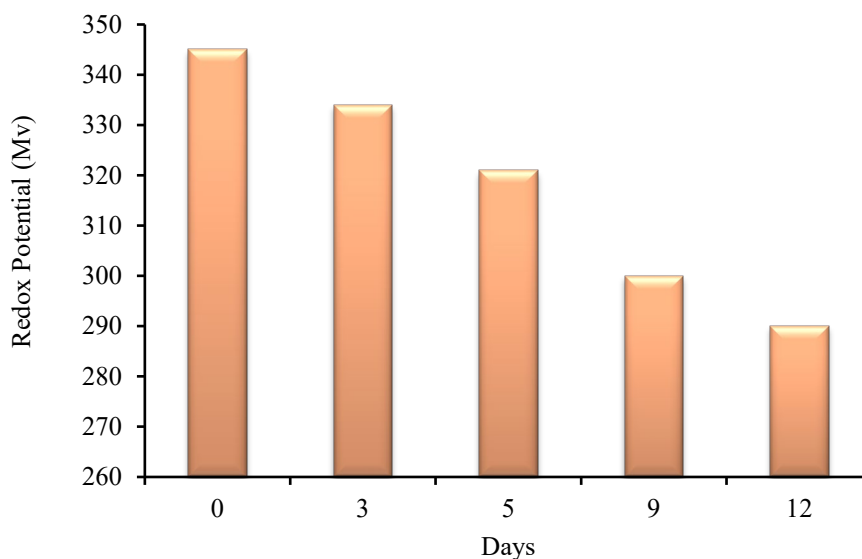


**Figure 47a:** Receiver solution Eh results

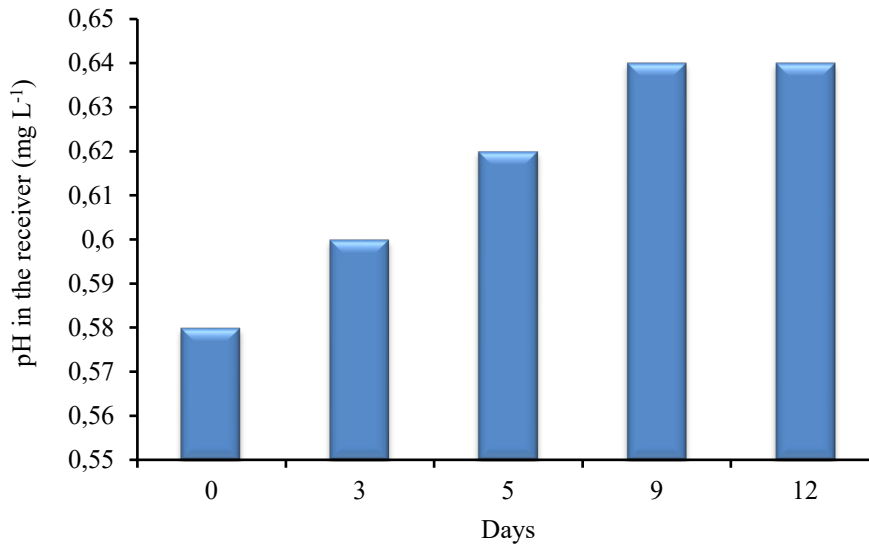


**Figure 47b:** Receiver solution pH results

When the dam water was spiked with the metal ions at  $1 \text{ mg L}^{-1}$ , the increase in pH of the receiver phase is more pronounced as shown in Figure 48. For example, the pH of the receiver phase for the spiked sample at day 12 was 0.84 compared to 0.64 in the unspiked setup. At higher metal ion concentration in the source phase, there are more metal ions that are transferred to the receiver phase, In turn, more  $\text{H}^+$  ions are transferred in the counter direction resulting in an increase in the pH of the receiver phase.

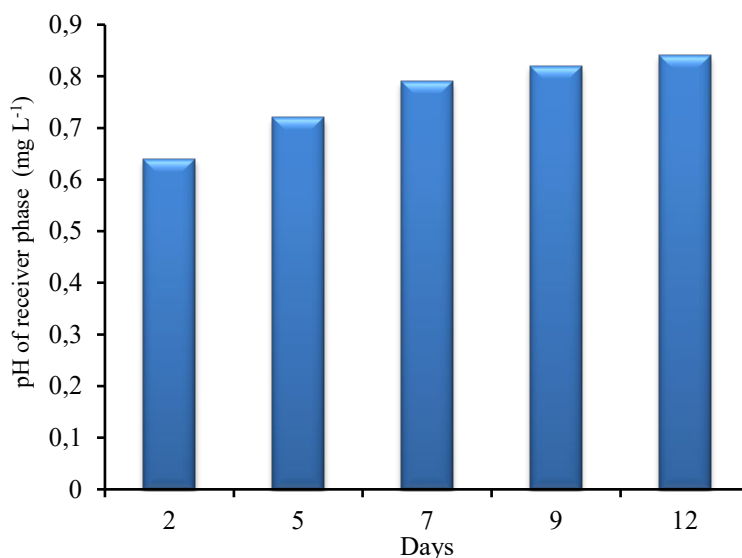


**Figure 48:** pH of the receiver solution in PIM sampler deployed for different days in the laboratory using Fleurhof dam (n = 3, SD)

The pH of the acceptor solution was also investigated at AMD. Results in Figure 49 shows the same trend that was observed in the study where passive sampler was deployed in the Fleurhof dam. the pH in the receiver solution increased as the number of days increased. The pH of the receiver phase for the AMD samples at day 12 was 0.95 compared to 0.64 in the un-spiked and 0.84 spiked setup. This might be due to low pH in the AMD and this accelerates the H<sup>+</sup> ions transfer resulting in an increase in the pH of the receiver phase.

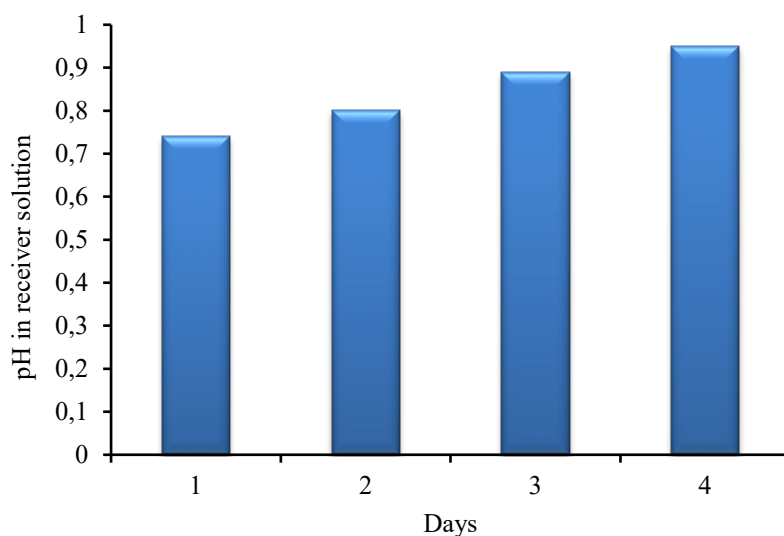


**Figure 49:** pH of the receiver solution in PIM sampler deployed at different days at AMD (n = 3, SD)

#### 4.1.4 Application in dam water

##### 4.1.4.1 Field parameters

Various field parameters recorded at the passive sampling site are summarised in Table 3. Parameters that changed drastically in the water during exposure controlled the changes in water chemistry during exposure in the laboratory. These parameters are pH, redox potential and nitrate. All these parameters increased with time during exposure and thus their behaviour is inter-related. As the pH decrease, redox potential increase and thus increased come of nitrate ions. Thus it can be concluded that oxygen and nitrogen was involved in the redox increase and the water chemistry. Other parameters remained relatively constant. Changes in physical-chemical parameter also illustrate the changes of optimizing passive samplers under laboratory conditions. At lower pH the metal bioavailable is expected as metal ions became more water soluble. However in this case seems not the case as conducting did not

increase drastically. This means that metal bioavailability was not very much affected during exposure time in the laboratory

**Table 3:** The source solution parameters and anions

Parameters	Day 0	Day 3	Day 5	Day 9	Day 12
pH	6.37	5.66	4.95	3.90	2.42
Conductivity (Ms)	0.36	0.39	0.40	0.44	0.99
Total-dissolves solid (ppt)	0.16	0.19	0.22	0.30	0.48
Redox-potential (Mv)	317	325	335	353	385
$F^-$ (mg L <sup>-1</sup> )	0.11	0.090	0.089	0.090	0.082
$Cl^-$ (mg L <sup>-1</sup> )	19.68	20.43	21.27	20.16	20.49
$Br^-$ (mg L <sup>-1</sup> )	0.053	0.059	0.073	0.067	0.060
$SO_4^{2-}$ (mg L <sup>-1</sup> )	138.48	139.81	147.79	141.68	143.51
$NO_3^-$ (mg L <sup>-1</sup> )	6.92	21.35	27.39	21.01	79.92

#### 4.1.4.2 Total metal ion concentrations in Fleurhof Dam

Table 4 summarises the maximum permissible water concentrations of our study elements according to WHO, EU and DWARF guidelines. The concentrations found at Fleurhof dam are also given in Table 4. Metal ions concentrations were 6x (Ni – WHO and EU standards), 2x (Ni – DWARF standards), 1.4x (Cu), 3x (Fe – EU standards only) and 23x (Cd – DWARF and EU), 38x (Cd – DWARF and EU) higher than the recommended regulation guidelines standards. Co is not listed in the WHO, EU and SA guidelines. The reason why metal ions concentrations were above the regulations guidelines range was because metal ions from AMD tailing dumps moves into the dam since it is close proximity to a mine tailing.

**Table 4** Maximum permissible water concentrations of metal ions and the concentrations found in dam water.

Metals ions	WHO (mg L <sup>-1</sup> )	European Union (mg L <sup>-1</sup> )	DWARF (mg L <sup>-1</sup> )	Fleurhof Dam (mg L <sup>-1</sup> )
Ni	0.02	0.02	0.07	0.114
Cu	2.0	2.0	2.0	2.989
Fe	-	0.2	-	0.616
Cd	0.003	0.005	0.005	0.115
Co	-	-	-	0.077

Adapted for Water Quality for Ecosystem and Human Health, 2006 (prepared and published by the United Nations Environment Programme. Water Programme for South African water affairs. Blank cells indicate that no, citable information was available.

The field metal ion uptake results are shown in Figure 50a&b. Results show Cu was far much more up taken than other metals followed by Fe, Cd, Ni and Co respectively. The same trend was observed with lab deployment. A linear up take between day 2 up to day 9 for Cu. Thereafter equilibrium was reached from day 9 up to day 12. Cu has the highest metal ion concentration in the dam and its uptake is expected to be the high since its concentration was highest in the dam. These results correlates with those reported by Singh et al., 2002, where Cu was extracted quantitatively in the pH range 6.0 to 8.0 with using D2EHPA as a carrier. Fe (II) increased from day 2 up to day 5 and then it reached equilibrium up to day 12. The concentration selectivity orders of the metal ions transport through PIM from the aqueous source phase (dam) into the receiving aqueous phase using D2EHPA was Cu > Fe > Cd > Ni > Co.

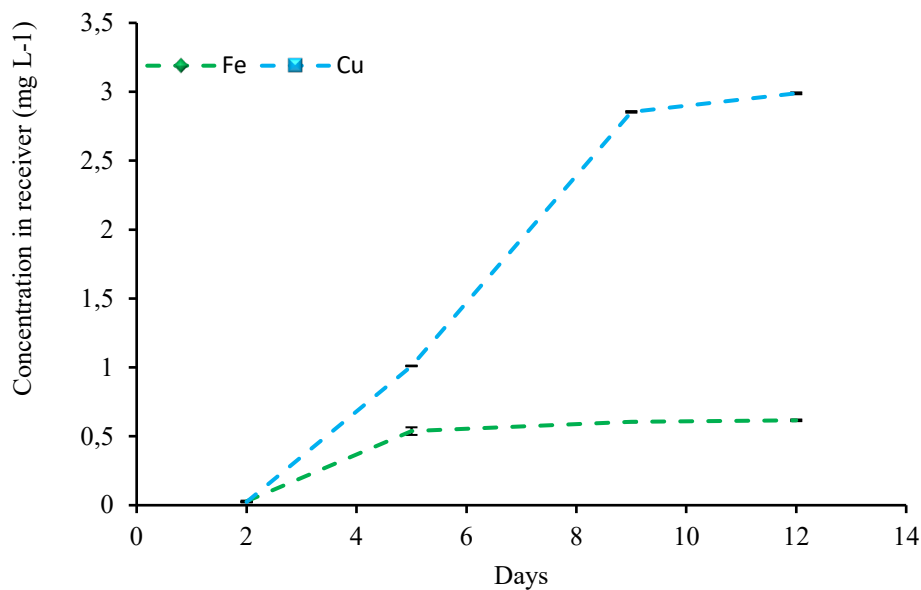


**Figure 50a:** Uptake of Cu and Fe in PIM sampler deployed at Fleurhof dam (n = 3, SD)

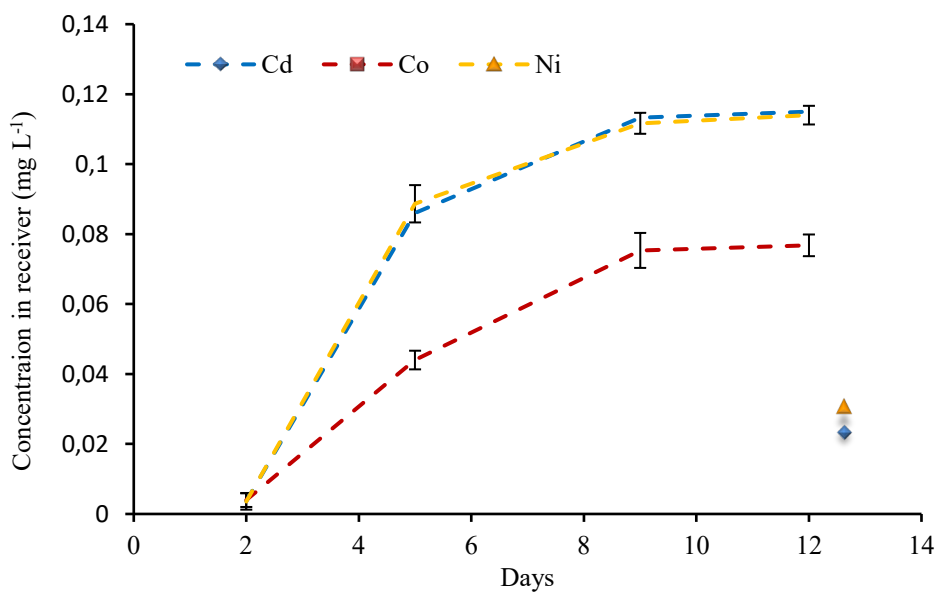


**Figure 50b:** Uptake of Cd, Co, Ni and Fe in PIM sampler deployed at Fleurhof dam (n = 3, SD)

#### 4.1.4.3 pH changes in the acceptor phase of the PIM passive sampler deployed at Fleurhof Dam for different days

The pH of the acceptor solution was measured for the acceptor solution before and after deployment for each period. The results are shown in Figure 51. pH of the acceptor solution increased with deployment time and remained steady after 9 days of passive sampler deployment. The increase in pH is expected since the transport mechanism involves transporting  $H^+$  to the source phase while transporting metal ions to the receiving phase. The  $H^+$  in the receiving phase are therefore the driving process for the transport. Due to the

continuous slow transport of the acid in the receiving solution across the membrane to the sample solution, it is expected that the pH at the interface between sample solution and membrane to be substantially lower than the bulk pH value of 6.25 of dam water. This acidic interfacial pH can be expected to enhance the PIM selectivity for Cd, Co, Cu, Ni and Fe over other metal ions and inhibit its fouling.

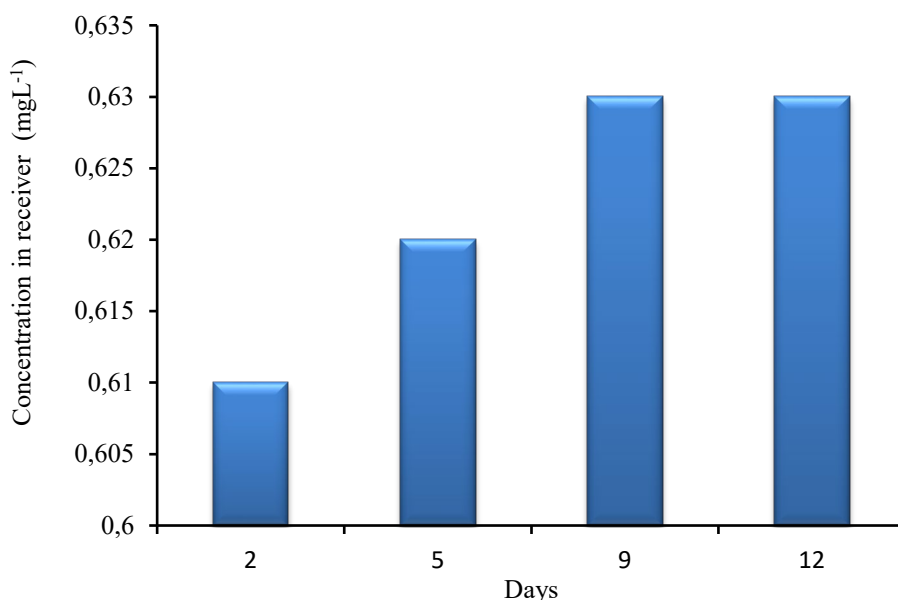


**Figure 51:** Comparison of the receiver solution pH in PIM sampler deployed at different days at Fleurhof dam (n = 3, SD)

#### 4.1.4.4 State of the deployed passive sampler at Fleurhof dam

Pictures of PIM passive sampler cage on deployment day and on collection day (day 12) at Fleurhof dam are shown in Figure 52 a & b. The cages still looked clean with very little fouling of the membrane after day 12. The PIM after 12 days was still transparent with no sign of precipitation or fouling on the membrane surface (Figure 53). FTIR was used to confirm that the functional groups observed before application of the membrane were still present after 12 days of deployment. This is discussed in detail later.

It was noted that in day 12, the wetland reeds that form part of the dam had been burned but the deployed passive sampler was not affected. This was a reflection of the challenges associated with passive sampler deployments in the field. In addition, the cages can be stolen by thieves for selling to metal scrap yards.

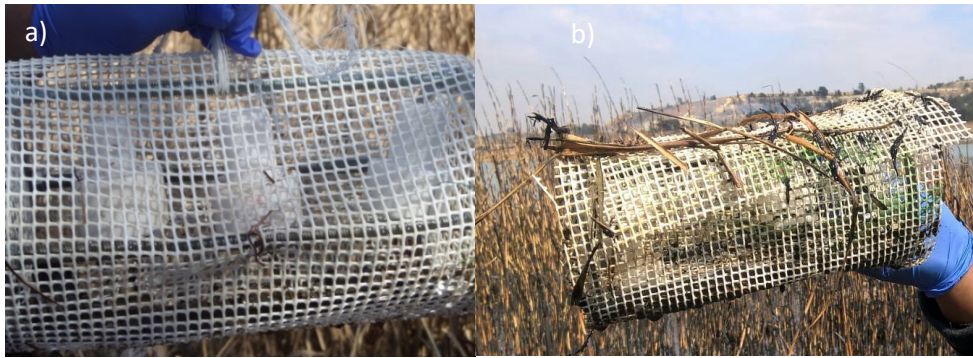


**Figure 52:** Picture of PIM-based passive sampler cages a) on day of deployment and b) day 12 at Fleurhof Dam

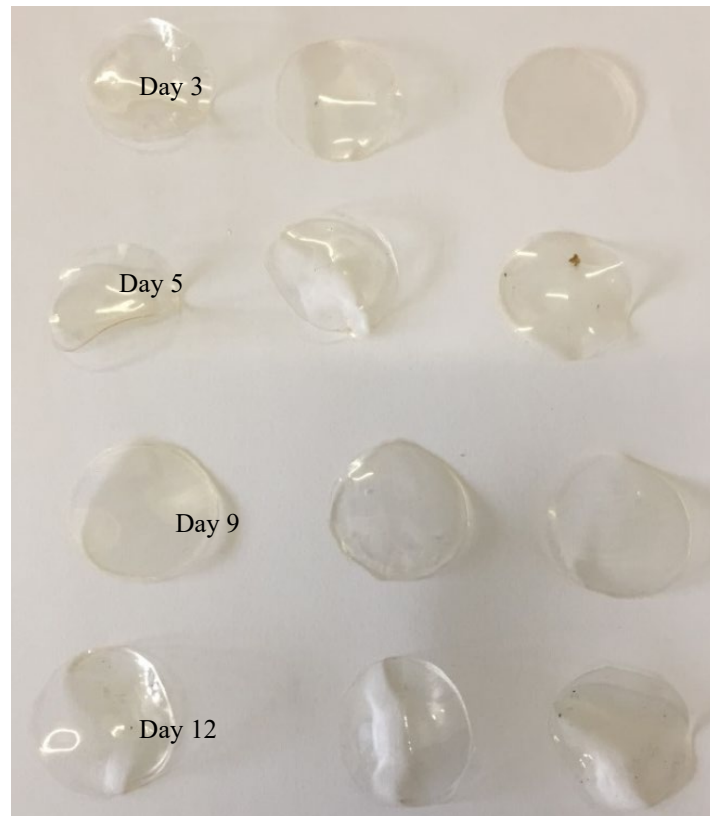


**Figure 53:** Picture of PIM deployed different days at Fleurhof Dam.

#### 4.1.4.5 Comparison of the bioavailable fraction of the metals in PIM sampler deployed in the field and in laboratory from Fleurhof dam water

Passive samplers are often optimised in the laboratory under similar environmental condition so that they can be applied to estimate the bioavailable fraction in the field. Results of the comparison of the PIM passive sampler deployed in the field and in the same dam water in the laboratory are shown in Figure 54. For most metals, the concentrations obtained in the

PIM passive sampler while in the field and that in the laboratory are comparable. This shows the PIM passive sampler calibration in the laboratory was successful and can be used to estimate the bioavailable fraction in the field. However, for Fe and Cu, the concentrations obtained in the field were much higher than in the laboratory. This means that taking the water samples from the field and leaving it standing in the laboratory perturbs the water system. This probably makes Cu and Fe less bioavailable. This is why passive samplers are very good at studying the bioavailable fraction after a system has been perturbed. This also suggests that some physical-chemical parameters of the water in the lab changed, and that copper was involved in driving these changes too.

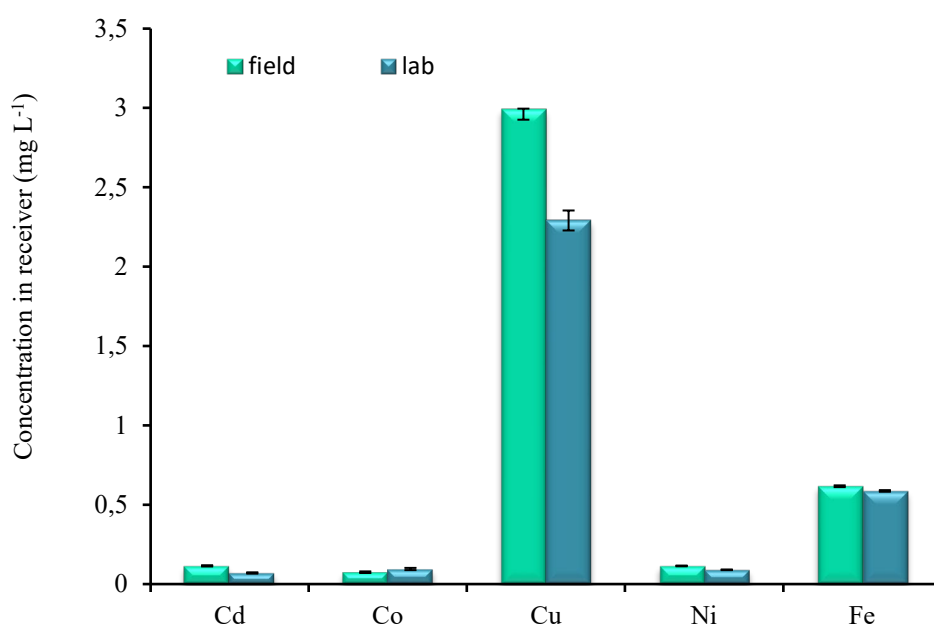


**Figure 54:** Comparison of the metal ion bioavailable fraction in PIM sampler deployed over 5 days in laboratory and field (n = 3, SD)

#### 4.1.4.6 Uptake of other metals in uptake by PIM sampler

In the field the source medium will almost certainly contain other cations which may potentially be transported together with Cd, Co, Cu, Ni, and Fe, across the PIM. Metal ion selectivity order in which the D2EHPA carrier extracted other metal ions were Zn > Mn > Mg > Na > K > Cu > Al > Cr > Ca > Fe > Ni > Cd and Co respectively. The metal ions of interest in this study followed the selectivity order Cu > Fe > Ni > Co and Cd as shown in Figure 55. The concentration of Zn was the highest with 1200 mg L<sup>-1</sup>, while Cu was the highest metal ion extracted from the metals interest in this study with a concentration of 2.989 mg L<sup>-1</sup>. This preference towards Zn has also been observed by (Almeida et al., 2014) in natural waters at pH above 6. This acidic interfacial pH can be expected to enhance the PIM selectivity for Zn

over other metal ions. The dam water experiments provided good evidence that the PIM-based sampler could be employed successfully in the passive sampling of other metals in natural waters.

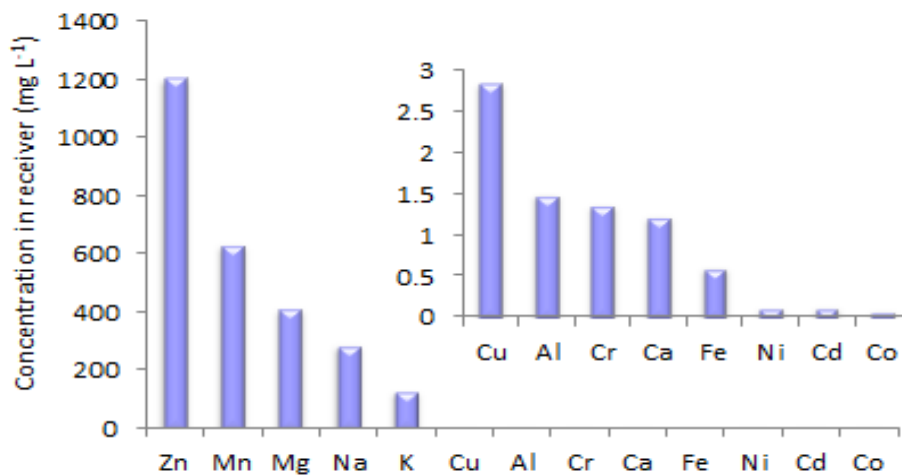


**Figure 55:** Other metal ion up take by PIM passive sampler after day 9 at Fleurhof Dam (n = 3, SD)

#### 4.1.4.7 Sampling rates determination in PIM passive sampler

**Figure 56** shows the obtained sampling rates in PIM passive sampler from various samples. To determine the TWA concentration of Cd, Co, Ni, Cu and Fe in dam water it is necessary to know the metal ion specific sampling rate (Rs expressed as L day<sup>-1</sup>) for the prevailing environmental conditions. The sampling rates shows that for most metals the laboratory experiments had the highest sampling rates. As expected changes in the water matrix had an important effect on the sampling rate for all metal ions and was most marked for Cu where sampling rates were more pronounced in the field.

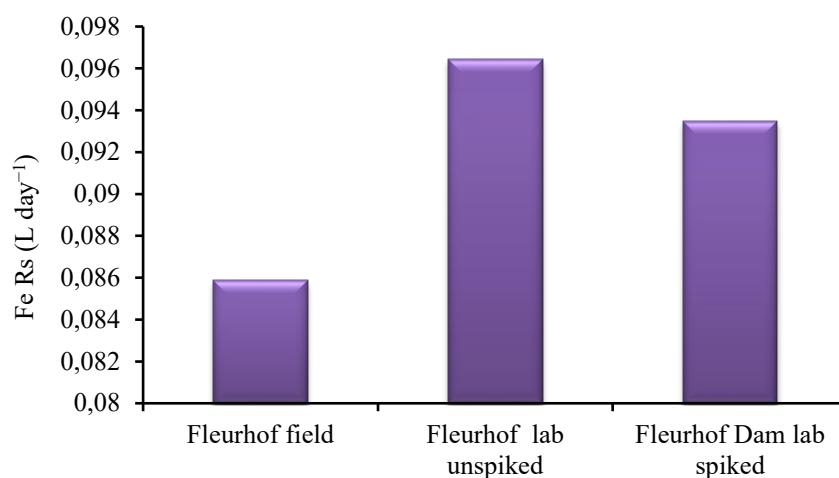


**Figure 56a:** Sampling rates in PIM passive sampler for iron (n = 3, SD)

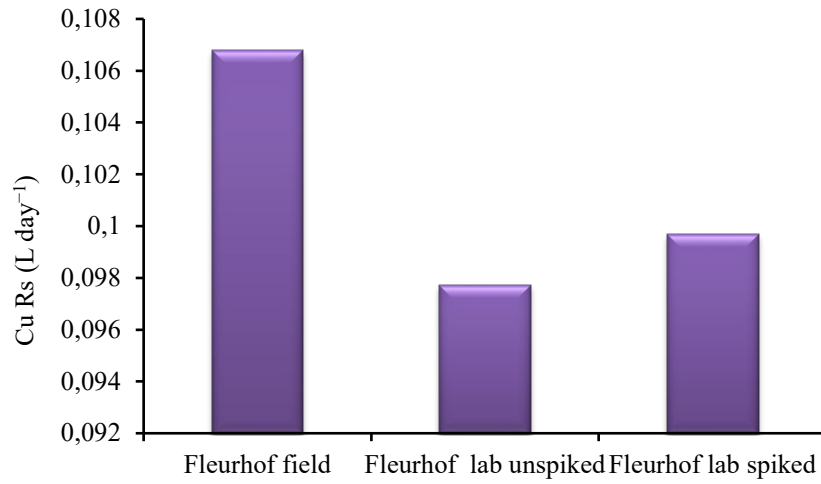


**Figure 56b:** Sampling rates in PIM passive sampler for copper (n = 3, SD)

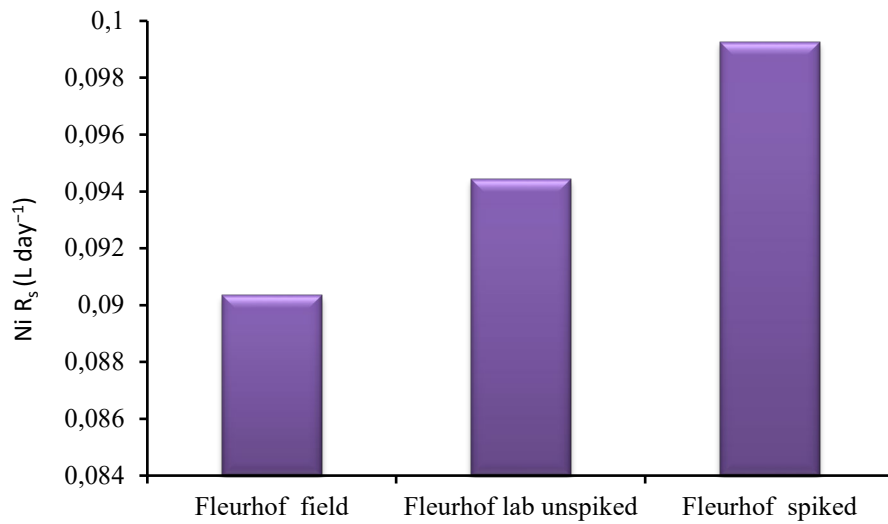


**Figure 56c:** Sampling rates in PIM passive sampler for nickel (n = 3, SD)

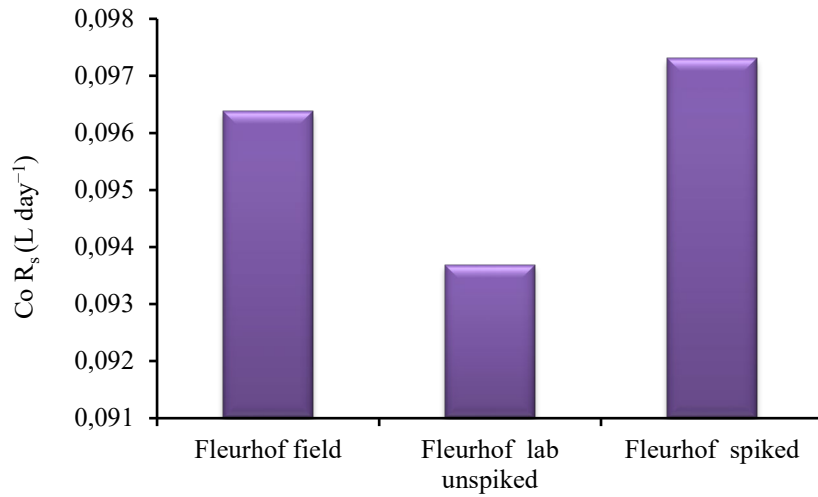


**Figure 56d:** Sampling rates in PIM passive sampler for cobalt (n = 3, SD)

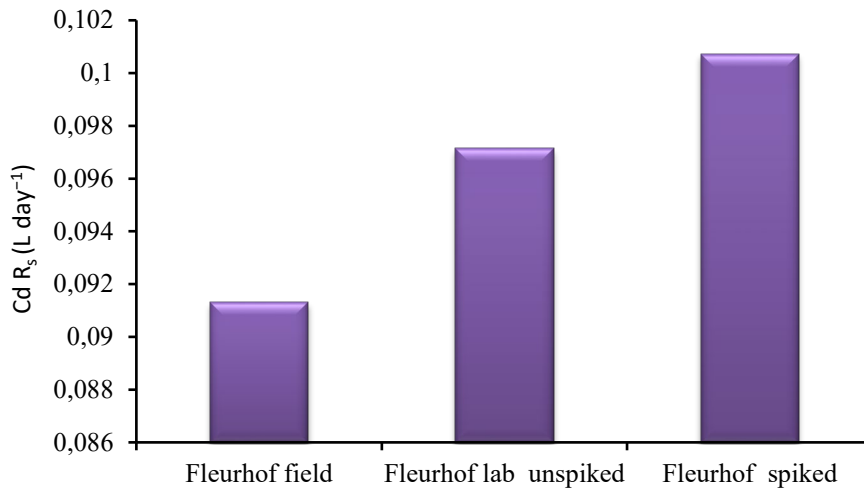


**Figure 56e:** Sampling rates in PIM passive sampler for cadmium (n = 3, SD)

#### 4.1.5 Application in acid mine drainage

##### 4.1.5.1 Field parameters

The total metal ion concentration are summarised in Table 2 and anion concentrations were measured in the AMD water. The concentrations of anions were 18728.76 mg L<sup>-1</sup> for  $SO_4^{2-}$ , 2030.79 mg L<sup>-1</sup> for  $PO_4^{2-}$ , 38.94 mg L<sup>-1</sup> for  $Cl^-$ . The parameters for AMD water were pH 2.83, conductivity and 10.76 mS and redox potential 346 mV. The result shows the pH of the AMD was very acidic compared to dam samples. The conductivity of the AMD was also about 30 times that of the dam water.

#### 4.1.5.2 Total metal ion concentrations in AMD

Maximum permissible water concentrations of metal ions found in AMD are discussed in Table 5. The result shows that at AMD site, all the metal ion concentrations were found to be above the recommended regulation guidelines. The concentrations were 2733x (Ni – WHO, EU standards), 780x (Ni – DWARF standards only), 57x (Cu), 3265x (Fe) and 433x (Cd – EU and DWARF), 722x (Cd – WHO only) higher than the recommended guidelines standards. Co is not listed in the WHO, EU and SA guidelines. This is an indication that the AMD is highly polluted with metal ions. This was expected since AMD water has low pH which dissolves the metal ions.

**Table 5:** Maximum permissible water concentrations of metal ions and the concentrations found in AMD.

Metals ions	WHO (mg L <sup>-1</sup> )	European Union (mg L <sup>-1</sup> )	DWARF (mg L <sup>-1</sup> )	AMD (mg L <sup>-1</sup> )
Ni	0.02	0.02	0.07	54.65
Cu	2.0	2.0	2.0	114.6
Fe	-	0.2	-	6529
Cd	0.003	0.005	0.005	2.167
Co	-	-	-	38.26

Adapted for Water Quality for Ecosystem and Human Health, 2006 (prepared and published by the United Nations Environment Programme. Water Programme for South African water affairs. Blank cells indicate that no, citable information was available.

The passive samplers deployment results in AMD are shown in Figure 57. The complexation rate at source phase/PIM interface increases and on the other site of the membrane the decomplexation rate also increases at the PIM/ receiving phase interface. Hence the result shows an increase in the metal ion uptake deployed in AMD. A linear up take was observed between 5 to 12 days. This can be explained by the fact that in acidic solutions the PIM is able to uptake metal ions. The accumulation of metal ions follows a linear regression. This suggests that PIM passive sampler is operating within the kinetic region from day 5 to day 12. Between day 2 and 5 a time lag was observed. The time-lag could be attributed to either the delay caused by the slow diffusion of the analyte across the rate limiting barriers, or the time taken to saturate binding sites in the diffusion limiting membrane before breakthrough is achieved. This time-lag depends on experimental conditions (Aguilar-Martínez et al., 2008). The

selectivity order for metal ions concentration in AMD is as follows: Fe > Ni > Cu > Co > Cd. Fe was expected to have high selectivity order since AMD has a lot of Fe.

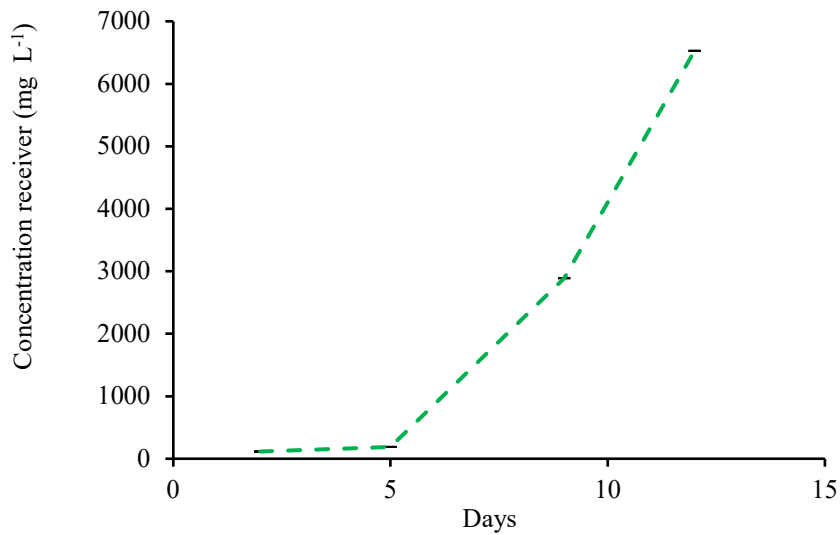


**Figure 57a:** Uptake of iron at AMD site (n = 3, SD)

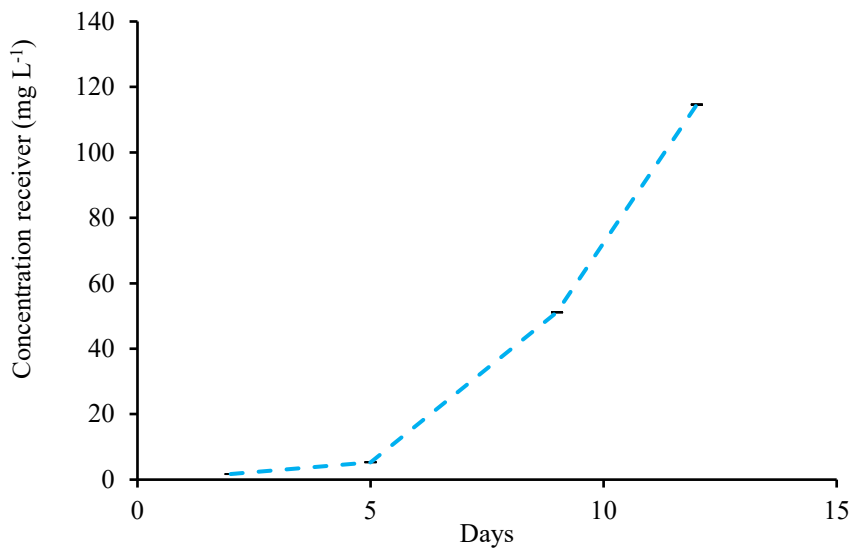


**Figure 57b:** Uptake of copper at AMD site days (n = 3, SD)

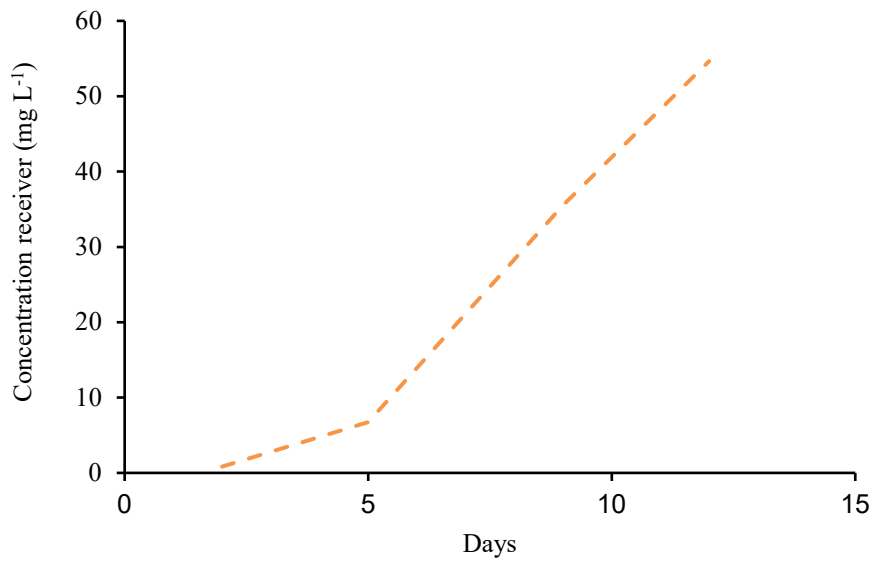


**Figure 57c:** Uptake of nickel at AMD site (n = 3, SD)

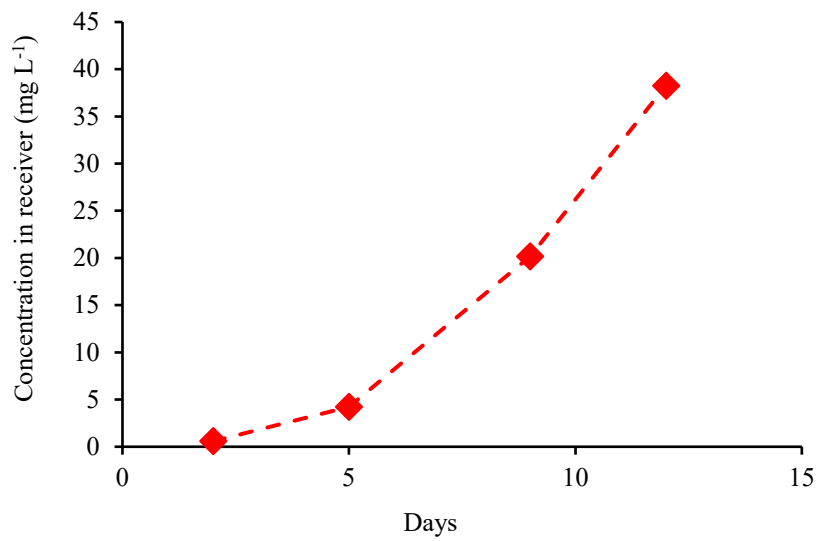


**Figure 57d:** Uptake of cobalt at AMD site (n = 3, SD)

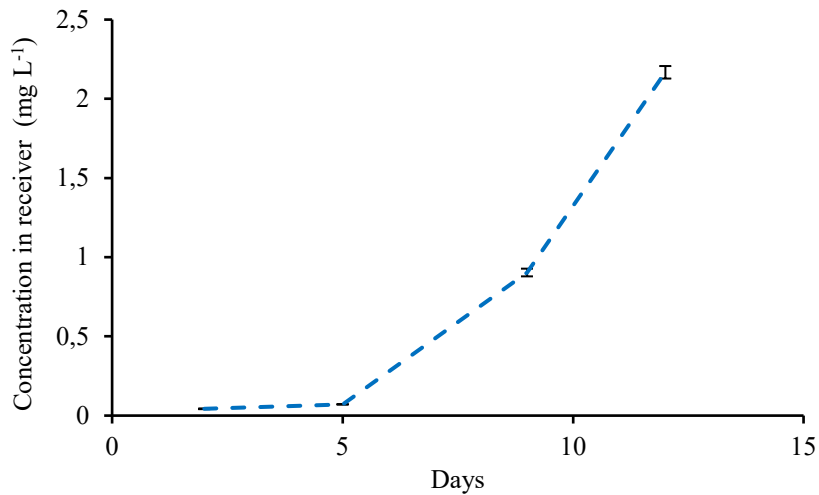


**Figure 57e:** Uptake of cadmium at AMD site (n = 3, SD)

#### 4.1.5 .3 pH changes in the acceptor phase at AMD site

The pH of the acceptor solution was compared before and after passive sampler deployment as in Fleurhof dam. Results in Figure 58 shows the same trend that was observed in the study where passive sampler was deployed in the Fleurhof dam. The pH of the acceptor solution increased from day 2 up to day 12. The increase in pH again can be attributed to the transport of protons across the acceptor to the source solution.

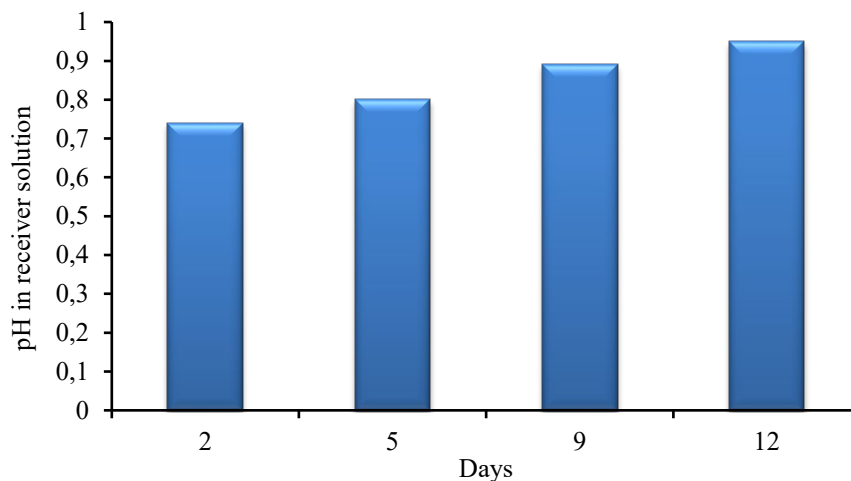


**Figure 58:** pH of the receiver solution in PIM sampler deployed at different days at AMD (n = 3, SD)

#### 4.1.5.4 State of the deployed passive sampler at AMD

Deposition of Fe precipitate was observed in the PIM passive sampler cage (**Figure 59a**) and on top of a membrane surface after day 12 as shown in **Figure 59b**. A deposition on the membrane surface is normally a sign of fouling. The fouling is caused by the undesirable

accumulation of solutes inside the membrane or on the membrane surface which can be attributed to the high hydrophobicity of the polymer. Which then result in a decline in the life span of the membrane, (Khalid et al., 2017). From theory, the PIM passive sampler is expected to transport the metal ions across the membrane to receiver phase until the protons in the receiver phase are nearly depleted or pH of the receiver phase is near that of the source phase. It also shows the versatility of PIM-based passive sampler.



**Figure 59a:** Picture of PIM-based passive sampler cages after deployment of a) day 2 and b) day 12 at AMD

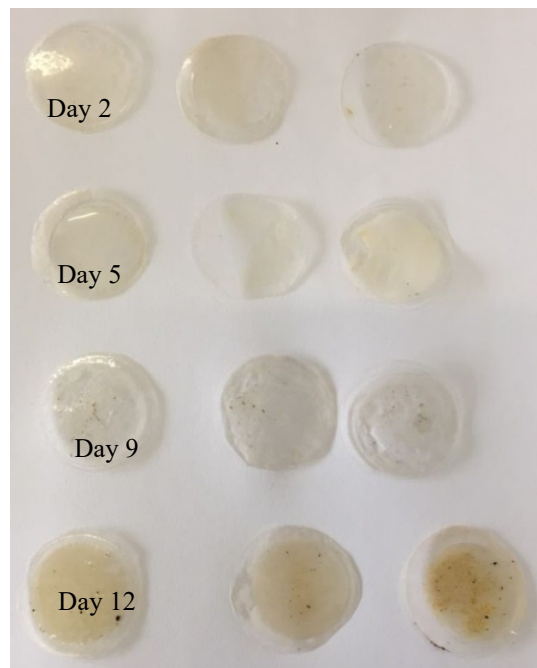


**Figure 59b:** Picture of polymer inclusion membrane after deployment at AMD site

#### 4.1.5.5 Comparison of the bioavailable fraction of the metals in PIM sampler deployed in the field and in laboratory from AMD water

**Figure 60** shows a comparison of the bioavailable fraction of the metals in the laboratory and in the field with similar exposure for AMD. Results support the thinking that less amount of metal ions are bioavailable in the laboratory due to changes in water chemistry. This result also proves that the PIM-based passive sampler is more effective with field samples when they are deployed in the field rather than in the laboratory.

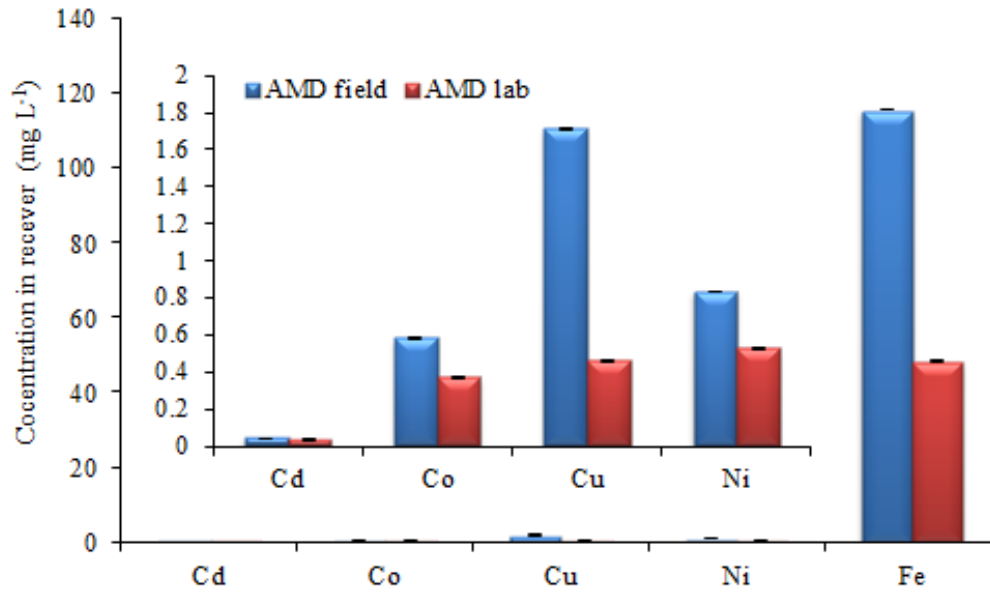


**Figure 60:** Comparison of uptake of metals in PIM passive sampler deployed in AMD water in the laboratory and in the field (n = 3, SD)

#### 4.1.5.6 Other metal ion uptake by PIM passive sampler after day 9 at AMD site

There are a number of inorganic and organic ligands that may complex the metal ions and thus affect their transport across the membrane in low pH medium water. Figure 61 shows other metal ions that have been up taken by PIM passive sampler after day 12 of deployment. As expected in AMD water Fe was extracted more, the concentration was 2800 mg L<sup>-1</sup>. This can be explained by the fact that in acidic solutions the PIM is selective for Fe in the presence of other metal ions, followed by Al, K, Mg, Na, Zn, Cu, Ni, Mn, Co, Ca, Cr and Cd.

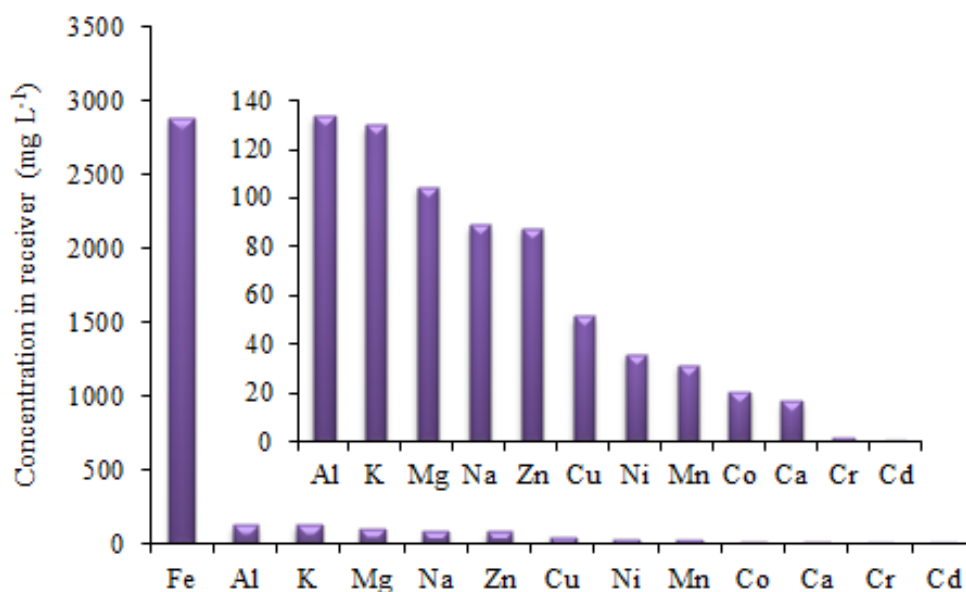


**Figure 61:** Other metal ions up take by PIM passive sampler after day 9 at AMD (n = 3, SD)

#### 4.1.5.7 Characterisation of PIM before and after field deployment

##### FTIR

The PIM membrane consisting of 60%w/w PVC and with 40%w/w D2EHPA was taken for FTIR analysis before (Figure 62a) and after field exposure at Fleurhof dam Figure (63b) and AMD site (Figure 62c) over 12 days. FTIR spectral characterization was used to determine functional groups present in each samples and to check for fouling. The functional groups of the polymer PVC and the carrier D2EHPA are present and this was confirmed by a band at 2959  $\text{cm}^{-1}$ , indicating the C-H stretching of the aliphatic C-H group assigned to PVC, while the C-H band also exhibited from 2959 to 2861  $\text{cm}^{-1}$  (Salima et al., 2012; Zioui et al., 2017). The peak at 1228  $\text{cm}^{-1}$  and 1018  $\text{cm}^{-1}$  correspond to P=O and P-O stretching were due to D2EHPA. The overlapping of some characteristic bands of PVC/D2EHPA was observed at 2959, 1228 and 1018  $\text{cm}^{-1}$ . The PIM before extraction and after extraction at Fleurhof dam had the same intensities and wavelength shifts. This proves that there was no fouling of the membrane at Fleurhof dam after day 12.

After 12 days of metal ions extraction at AMD site, the intensities of the characteristic peaks decrease, illustrating that the P=OOH group of D2EHPA is involved in the extraction reaction with metal ions. The peak of 3239  $\text{cm}^{-1}$  corresponding to the O-H stretching vibration could be caused by the depletion of the O-H groups of the D2EHPA molecules (Ling et al., 2017). These results demonstrate that the metal ions-D2EHPA complexes gradually infiltrate the membrane phase from the source solution/interface of the membrane to the interface of membrane/meta-ion crystal trough. The change in shift peaks intensity and shift in wavelength

could be attributed to fouling. This may be responsible for the reduction in transport studies for AMD described earlier and may be due to solubility or degradation of the extractant because of the chemical conditions established by the source phase

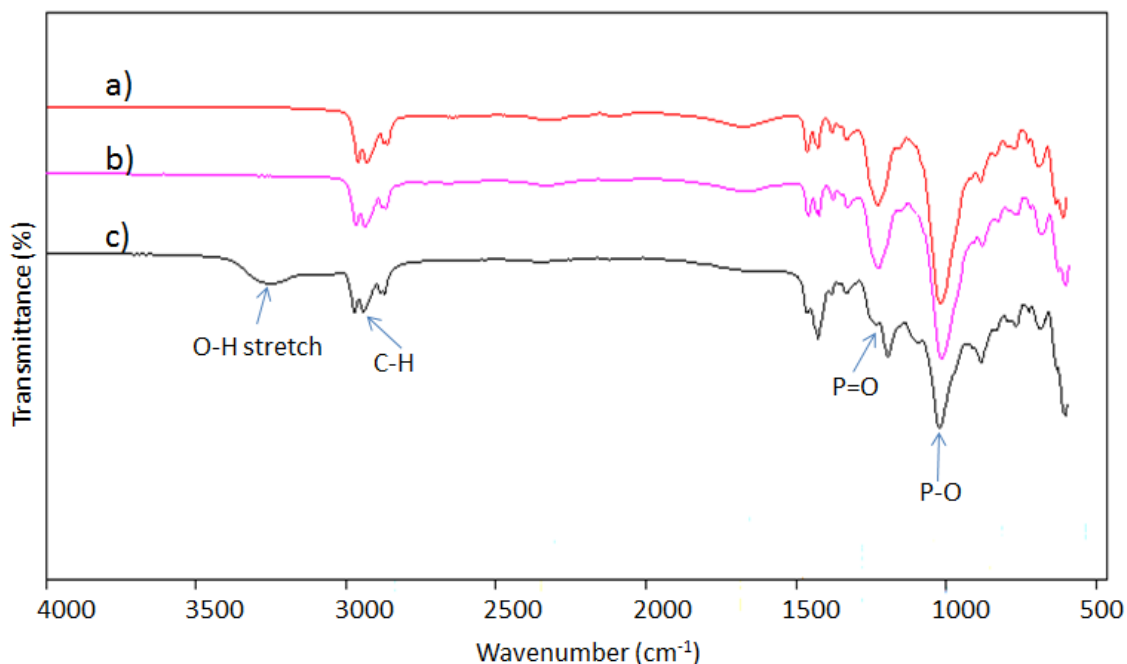


**Figure 62:** FTIR spectrum of PIM a) before extraction, b) after extraction at Fleurhof dam and c) AMD

The 2D and 3D AFM images are shown in Figure 63 which indicates the carrier distribution in the investigated membranes, after the evaporation of THF, the membrane is homogeneous throughout the entire surface. AFM has proved to be a useful tool in detecting the leakage of D2EHPA and the extracted complex from the surface of a PVC-based membrane. The performance of AFM analysis enables quantitative determination of membranes mean roughness ( $R_a$ ) and membrane mean square roughness ( $R_q$ ) (Ghazanfari et al., 2017). The membrane  $R_a$  value difference after extraction at Fleurhof dam was 1x while the ( $R_a$ ) value at AMD was 9x respectively. The lower  $R_a$  values for membrane after extraction at Fleurhof dam (Figure 63a) indicate that the uniform parts of the membranes have well-defined pores. A significant difference was noticeable with the AMD where high  $R_a$  values showed that the membrane structure pores have been deformed (Figure 63b). The porosity and roughness of the membranes is determined by the kind and concentration of the ion carrier (Radzaminska-lencik et al., 2015).

Mean square roughness ( $R_q$ ) values for membranes before and after extraction at Fleurhof dam and AMD site were calculated in Table 6. There was a noticeable increase of mean square roughness after membrane extraction at AMD site; this confirms that there was membrane fouling with AMD samples (Figure 63c). The metal ions transport happening within the membrane penetrates its irregular surface and caused its roughness. Membranes with rough surface are prone to fouling. Surface roughness is considered as the most important factor to improve antifouling ability of the membranes.

**Table 6:** Mean square roughness values after 12 days of sampling at Fleurhof dam and AMD

	Before extraction	After extraction	Difference
Dam $R_q$ , nm	12.42	13.42	1.00
AMD $R_q$ , nm	12.42	114.70	102.28

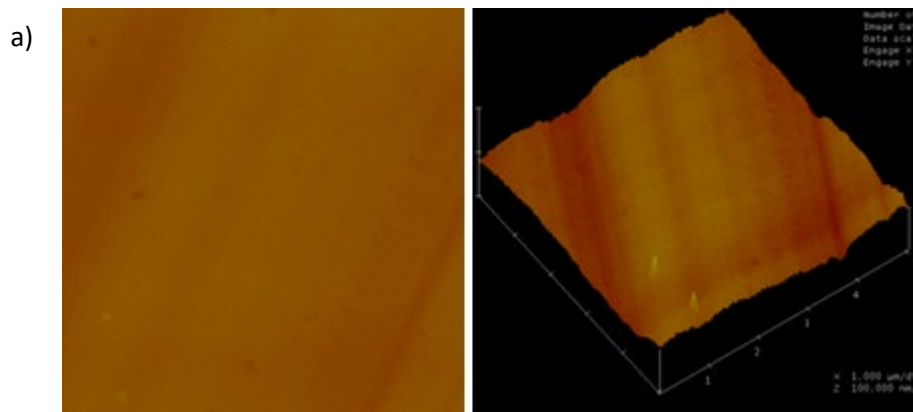


**Figure 63a:** 2D and 3D-AFM images of PIM before extraction

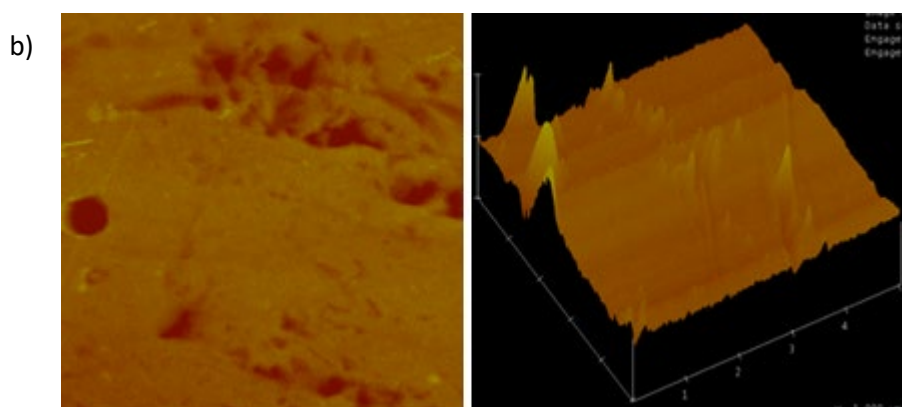


**Figure 63b:** 2D and 3D-AFM images of PIM after 12 days extraction at Fleurhof dam

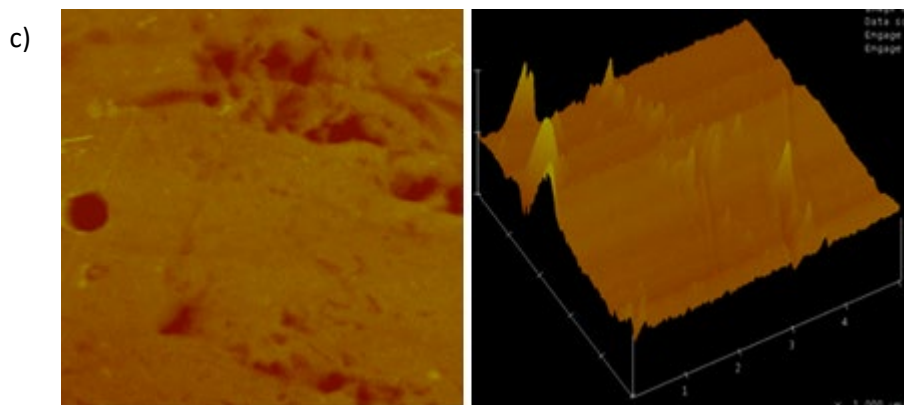


**Figure 63c:** 2D and 3D-AFM images of PIM after 12 days extraction at AMD site

## 4.2 Part B: Diffusive gradient in thin films-based passive sampler

### 4.2.1 Characterisation of functionalised CPEI using FTIR, solid state NMR and CHNS

CPEI is a transparent amorphous solid that turns white over time, SCPEI and PCPEI are characteristically orange and dark brown in colour, respectively (Figure 64). All three polymers are rubbery and extremely sticky in nature. Upon contact with water they swell up, implying that they are also hygroscopic.

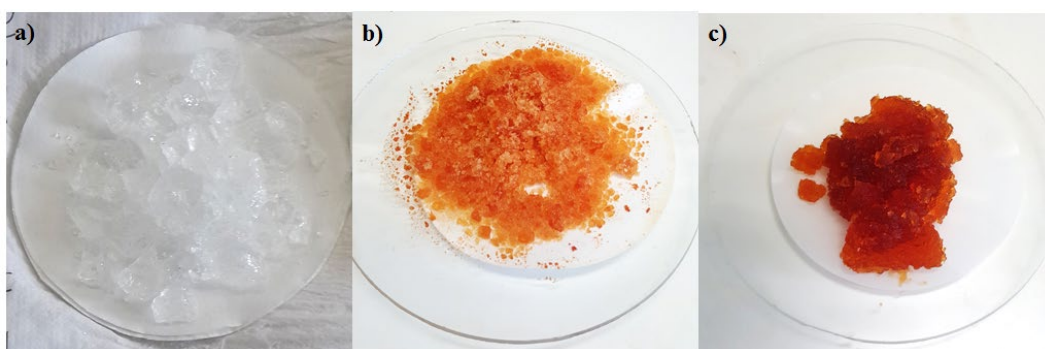


**Figure 64:** a) cross linked-polyethylenimine b) sulphonated and b) phosphonated polymers shortly after synthesis.

#### 4.2.1.1 FTIR analysis

Figure 65 shows the spectral differences between un-functionalised CPEI, SCPEI and PCPEI. The absorption bands of the relevant functional groups are summarised in Table 7. The FTIR spectrum of CPEI is indicative of a structure with large number of amine groups as shown by the absorption bands at 3317, 1633 and 1031  $\text{cm}^{-1}$ . In addition, there is an alcohol group represented by an absorption band at 1315  $\text{cm}^{-1}$ . These main features are in accordance to

the structure of CPEI (Saad et al., 2011). These bands were further compared to those usually obtained for PEI, the building block of CPEI. PEI has a characteristic N-H band between 1559 and 1592  $\text{cm}^{-1}$  (Amit et al., 2017; Ma et al., 2011; Wang et al., 2015) and another N-H band usually observed between 3100 and 3700 (Wang et al., 2015). These are in agreement with bands obtained for CPEI. In addition, Pang et al. (2011a) also quotes a characteristic C-N band at 1267  $\text{cm}^{-1}$  which appeared at 1031  $\text{cm}^{-1}$  in CPEI.

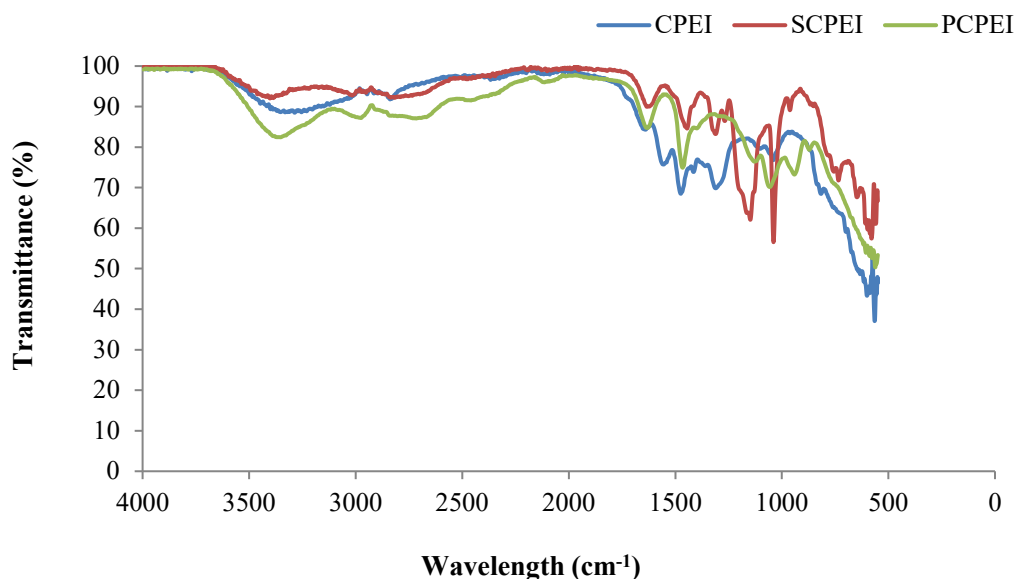


**Figure 65:** FTIR spectra of CPEI, sulfonated CPEI, phosphonated CPEI.

**Table 7:** Description of the absorption bands observed in figure 65

Wavenumber ( $\text{cm}^{-1}$ )			Bond and functional group
CPEI	SCPEI	PCPEI	
3317	3408	3371	N-H stretch; 1°, 2° amines and amides
1633	1670	1627	N-H bend, 1° amine
1550	-	-	N-O asymmetric stretch, nitro compound
1473	1423	1465	N-O asymmetric stretch
1315	1315	-	C-O stretch alcohols
-	1147	-	$\text{CH}_2\text{X}$ where $\text{X} = (\text{SO}_3)$
1031	1039	1066	C-N aliphatic amine
-	-	947	P-OH
565	613	555	

Upon functionalisation the absorptions bands for the primary, secondary and tertiary amine groups, as well as the N-O asymmetric stretch bond and the C-N bond were retained. There was however, loss of the N-O asymmetric stretch bond in both SCPEI and PCPEI, suggesting that this bond could have a role in functionalisation. Additionally, the C-O stretch bond at

1315  $\text{cm}^{-1}$  observed in both CPEI and SCPEI spectra is not found in the PCPEI spectrum, which implies a different mode of functionalisation in PCPEI. Changes in absorption bands of PEI as a result of functionalisation have been documented in previous studies: Ma et al. (2014) showed that modification of PEI with biochar resulted in a shift of the N-H stretch band from 1559 to 3398  $\text{cm}^{-1}$ . Pang et al. (2011) further suggested that after adsorption of target analytes the peak at 3419  $\text{cm}^{-1}$  would continue to shift depending on analyte adsorbed

Furthermore, SCPEI has an absorption band at 1147  $\text{cm}^{-1}$  ( $\text{CH}_2\text{X}$ ) which is not present in either CPEI or PCPEI. This band most likely represents the sulphonyl group. Similarly, PCPEI has a band at 947  $\text{cm}^{-1}$  which could be due to the phosphate group.

Mady et al. (2011) studied the interaction between DNA and PEI, a phosphate absorption band was observed at 1236  $\text{cm}^{-1}$ . Conversely, in Table 5.1, the absorption band related to the phosphate group is observed at a lower frequency. This could be attributed to the fact that the phosphate groups are in different environments; in the study by Mady et al. (2011) the phosphate could belong to either PEI or DNA whereas in this study they are attached to a PEI backbone. The characteristic phosphate absorption band observed at 947  $\text{cm}^{-1}$  corresponds to the one obtained by Saad et al. (2013b). It can therefore be assumed that functionalisation of CPEI was successful as depicted by the distinct features in the three spectra.

#### 4.2.1.2 Solid state NMR

$^{13}\text{C}$  solid state NMR was used instead of solution NMR for structural analysis because the CPEI functionalised derivatives are insoluble in most solvents. The  $^{13}\text{C}$  NMR spectrum of SCPEI and PCPEI are shown in Figure 66a. The spectrum for SCPEI appears broad and unresolved suggesting a more amorphous structure whereas the sharper lines observed in the PCPEI spectrum suggests a less amorphous, slightly crystalline structure. In addition, there is a strong correlation between the predicted chemical shifts (Figure 66b) and actual measurements: SCPEI shows a unique peak near 30 ppm (peak 2), according to the prediction software this peak belongs to  $^{18}\text{C}$  and  $^{21}\text{C}$ , which are in close proximity to the sulphonyl groups. Shielding by the sulphonyl groups causes the peak to appear at a lower chemical shift. The obvious differences between the two spectra suggest two different functional groups; ( $-\text{SO}_3\text{H}$ ) and ( $-\text{PO}_4^{2-}$ ). To further validate this notion it would have been ideal to assess PCPEI using  $^{31}\text{P}$  solid state NMR.

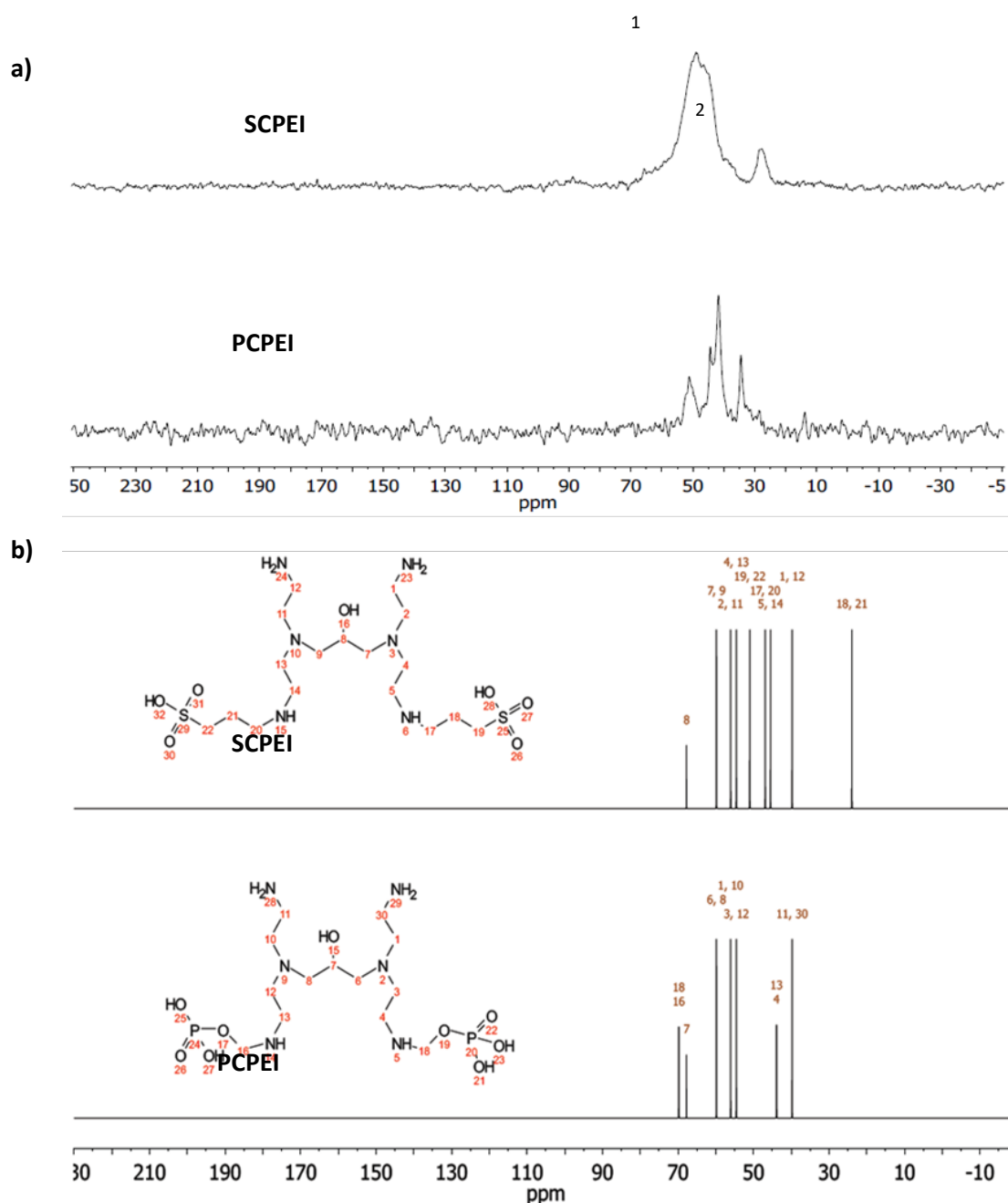


**Figure 66:** a)  $^{13}\text{C}$  solid state NMR spectra for SCPEI and PCPEI b) the predicted chemical structures and spectra of SCPEI and PCPEI.

#### 4.2.1.3 CHNS analysis

Elemental analysis of the CPEI and the functionalised derivatives shows that CPEI has the highest percentage of carbon (32.8%), hydrogen (8.16%) and nitrogen (14.0%) compared to SCPEI and PCPEI (Table 8). The polymeric structure of CPEI comprises of a carbon-nitrogen backbone (Figure 66) which explains the composition trend and the least sulphur content (0.034%). Alternatively, SCPEI had the highest sulphur content due to the incorporation of the sulphonyl functional group. SCPEI had a slightly higher percentage of carbon compared to

PCPEI, the values of hydrogen and nitrogen were similar. The polymer mixture contained an average of the components found in SCPEI and PCPEI.

**Table 8: Elemental analysis of the polymers**

Sample	C (%)	H (%)	N (%)	S (%)
CPEI	32.8	8.16	14.6	0.034
SCPEI	29.5	7.38	11.2	6.47
PCPEI	26.3	7.81	9.87	0.042
SCPEI-PCPEI mixture*	28.2	7.53	10.9	4.66

*C = carbon, H = hydrogen, N = nitrogen, S = sulphur*

*\* Mixture is a combination of SCPEI and PCPEI in an 80% to 20% ratio*

## 4.2.2 Batch studies

### 4.2.2.1 SCPEI-PCPEI resin mixture

According to Figure 67, pH has no significant impact on the uptake abilities of either (80% S: 20% P) or (20% S: 80% P). However, when (80% S: 20% P) was used, the mass of mercury was higher at pH 3 compared to pH 7. The resin mixture with the higher portion of the sulphonated resin (80% S: 20% P) accumulated higher amounts of selenium and mercury. On the other hand having a higher ratio of PCPEI to SCPEI (20% S: 80% P) did not improve the uptake of arsenic, instead the mass of selenium and mercury remained high. Relative to the results obtained from the (80% S:20% P) resin combination there was a slight reduction in the mass of selenium and mercury because of the reduced sulphur content.

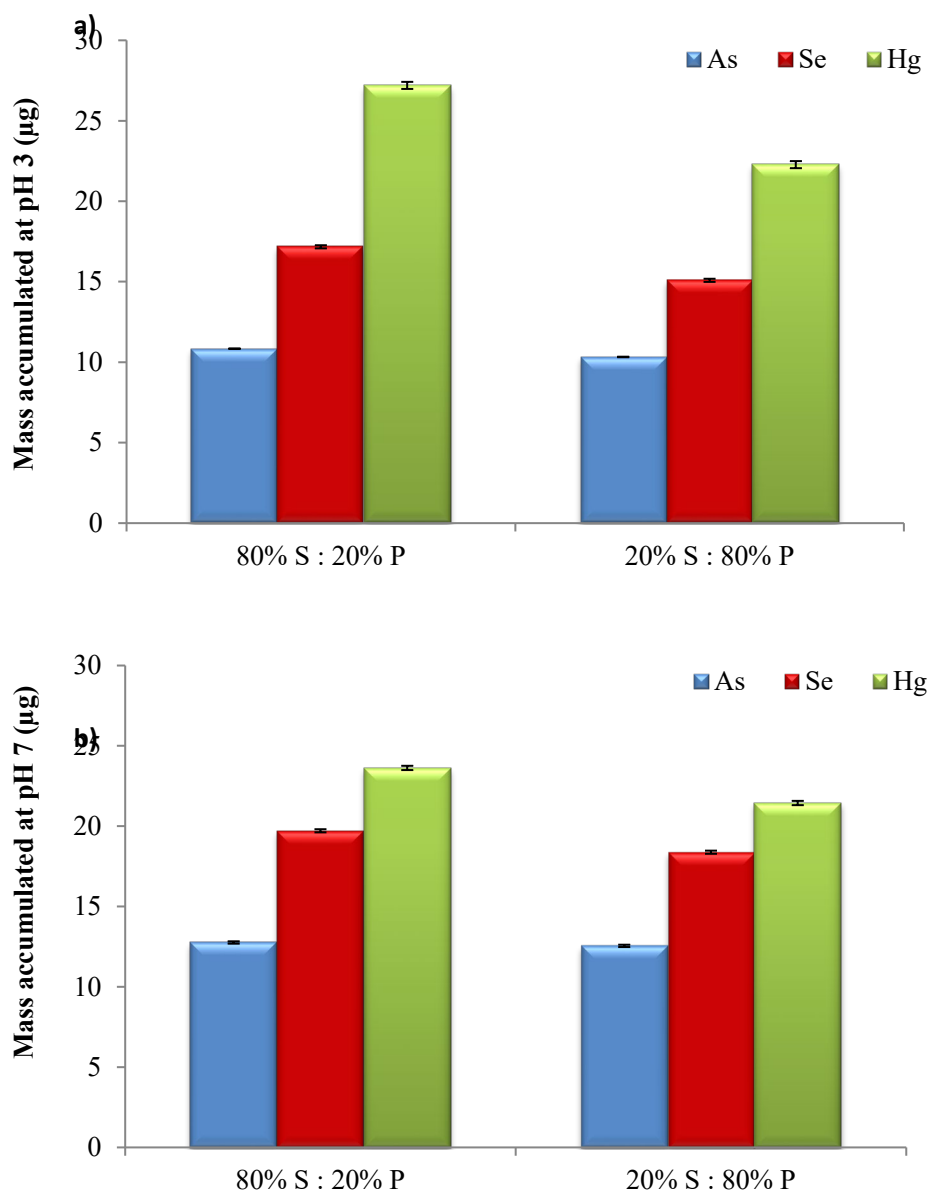


**Figure 67:** The influence of mixing the sulphonated (S) and phosphonated (P) polymers in different ratios at a) pH 3 and b) pH 7.

Selenium and mercury are able to adsorb onto the SCPEI-PCPEI resin irrespective of the total percentage of SCPEI. This has two implications; firstly, selenium and mercury could be the first to bind onto the resin, with much ease, occupying majority of the sites, sterically hindering arsenic from binding. Selenium and mercury bind onto SCPEI using two different modes: selenium binds via an anion exchange with the sulphonyl group whereas mercury forms a strong complex with the sulphonyl group. Additionally, it can be assumed that

The Second and reason could be the proportion of sulphonyl groups per CPEI polymer is higher in SCPEI compared to the proportion of phosphate groups per CPEI of the same quantity. Indeed, Mason et al. (2005) suggest that mixed binding layers may experience uneven distribution which could result in some analytes having to travel further to reach their binding sites, than they would in a single resin binding layer. This leads to underestimation of the diffusion layer thickness. Therefore, the distribution of sulphonyl groups in SCPEI-PCPEI are better compared to phosphate groups which is why the mass of selenium was always be higher than arsenic.

Unfortunately due to the nature of the polymers no technique could be used to quantify the ratio of sulphonyl and phosphate groups in in SCPEI and PCPEI, respectively. 80% S : 20% P was selected as the best combination. The lack of obvious differences between the two polymer combinations did not warrant further investigation into different ratio combinations. Despite these challenges combination of the two resins enhanced the selectivity towards arsenic and selenium. Also, the addition of PCPEI did not significantly compromise the capacity of SCPEI for selenium.

#### 4.2.2.2 Elution factor ( $f_e$ ) and elution efficiency

Saad et al. (2011) recommended 5 mol L<sup>-1</sup> of nitric acid as the best extraction solvent for CPEI and the functionalised derivatives. This recommendation was based on the individual resins and not their combination. The extraction of arsenic, selenium and mercury from SCPEI-PCPEI using 7 mol L<sup>-1</sup> resulted in the lowest value of  $f_e$  relative to the values obtained for arsenic and mercury (Figure 68). It is also apparent that 5 mol L<sup>-1</sup> produced better results compared to 7 mol L<sup>-1</sup>. This is in agreement with Saad et al. (2011). Despite giving better results, 5 mol L<sup>-1</sup> cannot be considered suitable since it did not effectively remove all 3 elements from the resin mixture.

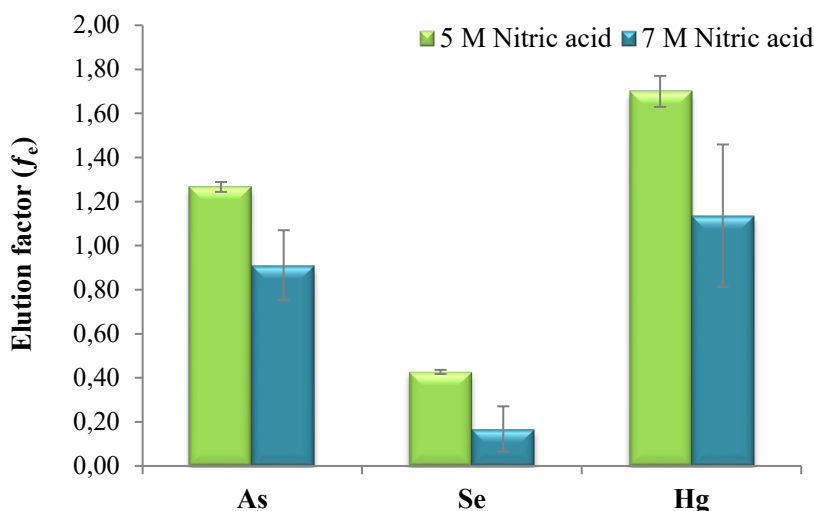


**Figure 68:** The elution factors of arsenic, selenium and mercury with 5 and 7 mol L<sup>-1</sup> of nitric acid (n = 3).

When other extraction solvents were used at lower concentrations the general trend was similar to the one obtained using 5 and 7 mol L<sup>-1</sup> of nitric acid: mercury shows the highest elution factor for all solvents and concentrations followed by arsenic, then selenium (Figure 69). Both 0.5 and 0.25 mol L<sup>-1</sup> of thiourea were ineffective at extracting selenium.

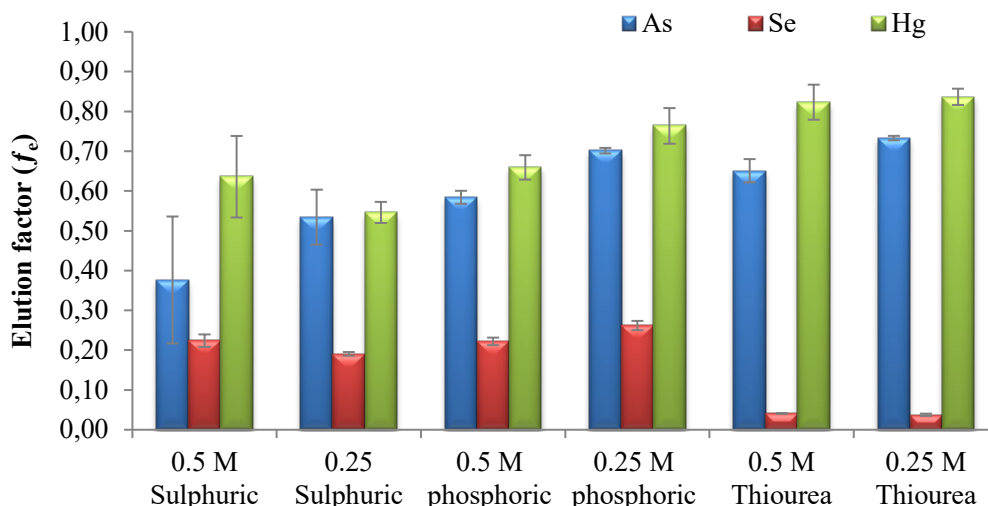


**Figure 69:** Extraction of arsenic and selenium using different solutions (n = 3)

Figure 70 shows the elution factors obtained for arsenic and selenium. 1 mol L<sup>-1</sup> nitric acid is still a good extraction solvent considering the low disparity between arsenic and selenium  $f_e$

values compared to those obtained for hydrochloric acid, thiourea and sodium hydroxide. Sulphuric and phosphoric acid were deemed the best extraction solvents because  $f_e$  values higher than 0.80 were obtained for both arsenic and selenium compared to the other solvents. Selection of sulphuric acid as the optimum solvent was due to the slightly higher elution factor together with high reproducibility. Elution factors for mercury were not determined, however, based on the previously observed trends it can be assumed that the  $f_e$  value for mercury was higher than 0.80. What was most surprising was that at

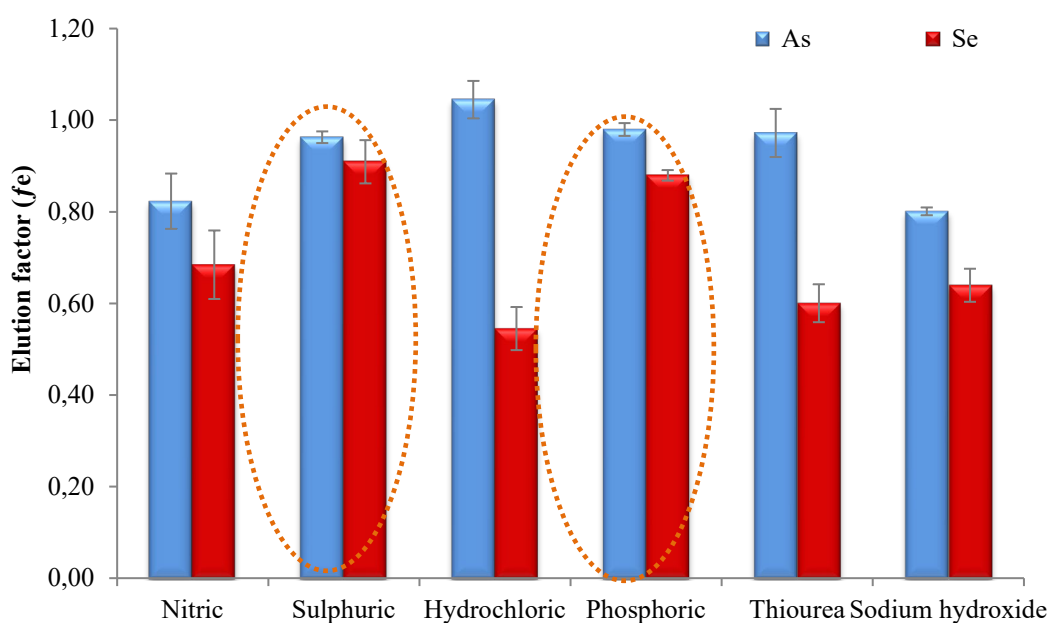


**Figure 70:** The elution factors obtained after using 1 mol L<sup>-1</sup> of different solutions (n = 3)

In this study the elution volume was 20 mL instead of 1 mL that is commonly used during the extraction of the resin layer (Zhang and Davison, 1995; Devillers et al., 2017). Devillers et al. (2017) showed that higher  $f_e$  values were obtained when higher elution volumes were used. This is because higher elution volumes eliminate errors usually associated with smaller elution volumes. This is especially true if the concentration of the extraction solvent is low. Furthermore, to obtain 100% recovery, Zhang and Davison (1995) suggested that for resins that are not incorporated in a gel it is best to use column elution instead of batch elution.

#### 4.2.3 Design and construction of DGT sample holder units

DGT sample holders were manufactured to eliminate the costs associated with the use of commercial units that have disposable caps. Sample holders were designed and manufactured from PTFE rods according to the dimensions specified for commercial DGT. Additionally, to the original design of the DGT cap, grooves were added to allow removal and replacement of the cap without damage or leakage. Figure 71 compares the structural designs of the constructed DGT sample holder with commercial DGT holder. The design and dimensions of the piston base and the diameter of the sampling window were kept the same.

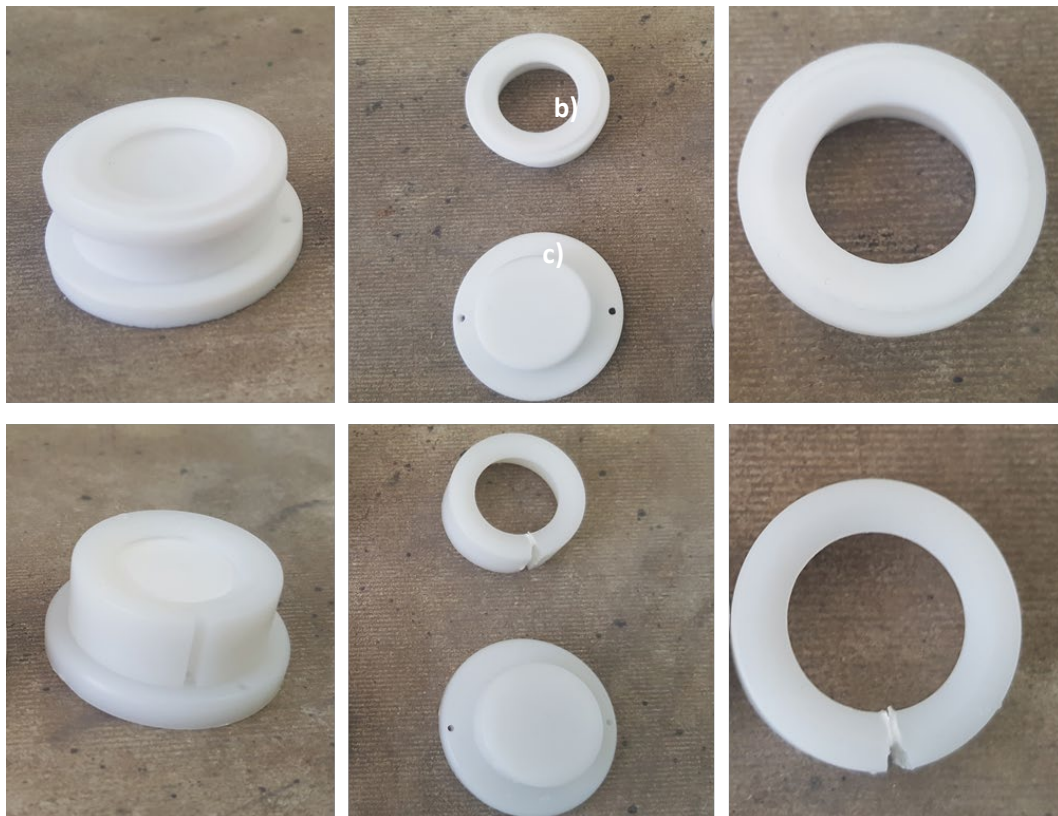


**Figure 71:** a) Fully assembled unit of the new DGT sample holder, b) the modified DGT cap and the piston base c) close-up of the modified DGT cap with grooves. d) Fully assembled commercial DGT sample holder unit, e) the commercial DGT and piston base, f) close up of commercial DGT cap.

With regards to the physical structure of the DGT sample holders, it was imperative to have a proper seal at all times so that the resin and diffusive gel layers inside the sample holder are protected from the external environment. This would ensure that entry into the passive sampler is exclusively via diffusion through the diffusive gel layers. Secondly, although the DGT cap was altered externally, the geometry of the sampling window remained the same because

equations used in DGT are described in terms of  $3.14 \text{ cm}^2$ , which is the geometric area of the sampling window (Zhang and Davison, 1995).

Ding et al. (2016) also designed new DGT sample holders. For sample holders that had a similar configuration to commercial DGT, they did not carry out any performance test because they assumed that the behaviour would be the same. Similarly, for this study, the addition of grooves on the cap was not expected to have any major implications on DGT uptake trends.

#### **4.2.4 Optimisation**

##### 4.2.4.1 Performance of SCPEI-based DGT

SCPEI-based DGT was able to accumulate selenium during the 12 day deployment period (Figure 72). It was however, unsuccessful at accumulating arsenic and mercury: their masses were negligible relative to selenium. Despite the low mass, arsenic did display a linear uptake trend. Conversely, mercury did not display any mass increase with deployment time. Despite better retention by SCPEI-based DGT, the accumulation of selenium was non-linear. From these results, it was concluded that SCPEI was not ideal for arsenic and mercury. The results pertaining to mercury were unexpected considering the strong complexation with the sulphonyl group. It is possible that during longer deployments, as more sulphonyl groups are replaced by the selenite anion, the complexation of  $\text{Hg}^{2+}$  is no longer favoured. On the other hand the Saad et al. (2013) recommends PCPEI as the best option for arsenic; in their study it was able to effectively remove 88% of arsenic from mine waste water. Subsequent experiments involved a combination of SCPEI and PCPEI.

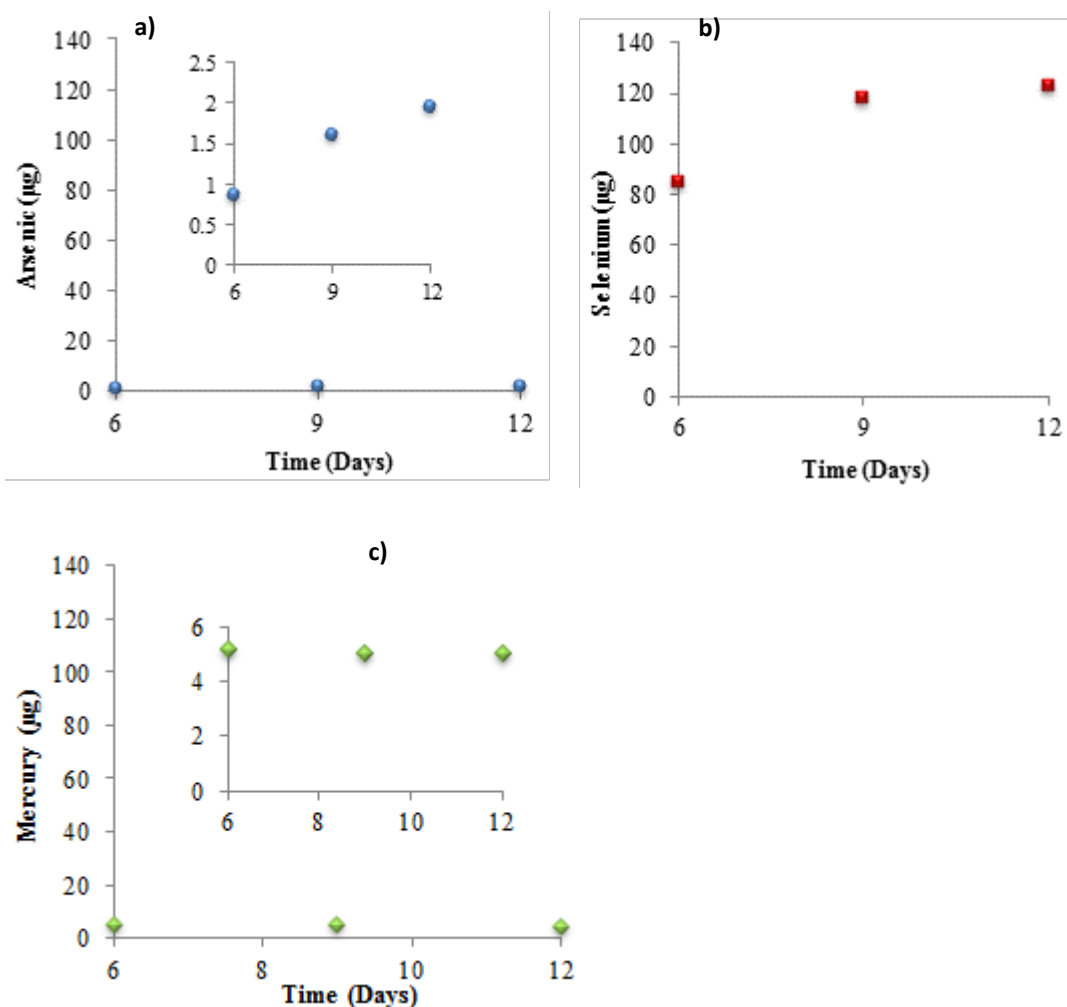


**Figure 72:** Preliminary study showing the uptake of a) arsenic and b) selenium and c) mercury by SCPEI-based DGT over 12 days. The inserts were added for better resolution.

#### 4.2.4.2 Performance of SCPEI-PCPEI resin mixture impregnated in agarose gel

The binding phase in DGT should ideally have high affinity towards the targeted analytes and high capacity to retain the bound analytes (Zhang and Davison, 1995). Conventionally, the DGT resin gel is prepared by impregnating the resin of choice in polyacrylamide mixed with a patented agarose-derived cross linker (DGT Research Ltd, UK) (Zhang and Davison, 1995). The advantage of incorporating resin in a gel is to ensure uniformity of the resin layer, inherently, improving the reproducibility between different DGT devices.

SCPEI-PCPEI mixture when impregnated in agarose gel shows reduced capacity for arsenic and selenium beyond day 9 (Figure 73). Initially, between day 3 and day 9 the mass of arsenic and selenium increased linearly, however, after day 9 the mass started to decline. The decline suggests that the analytes are moving out of the passive sampler. According to the principles

of passive sampling, when a passive sampler has reached maximum capacity it attains equilibrium with the surrounding medium. The trend in Figure 73 is therefore unusual.

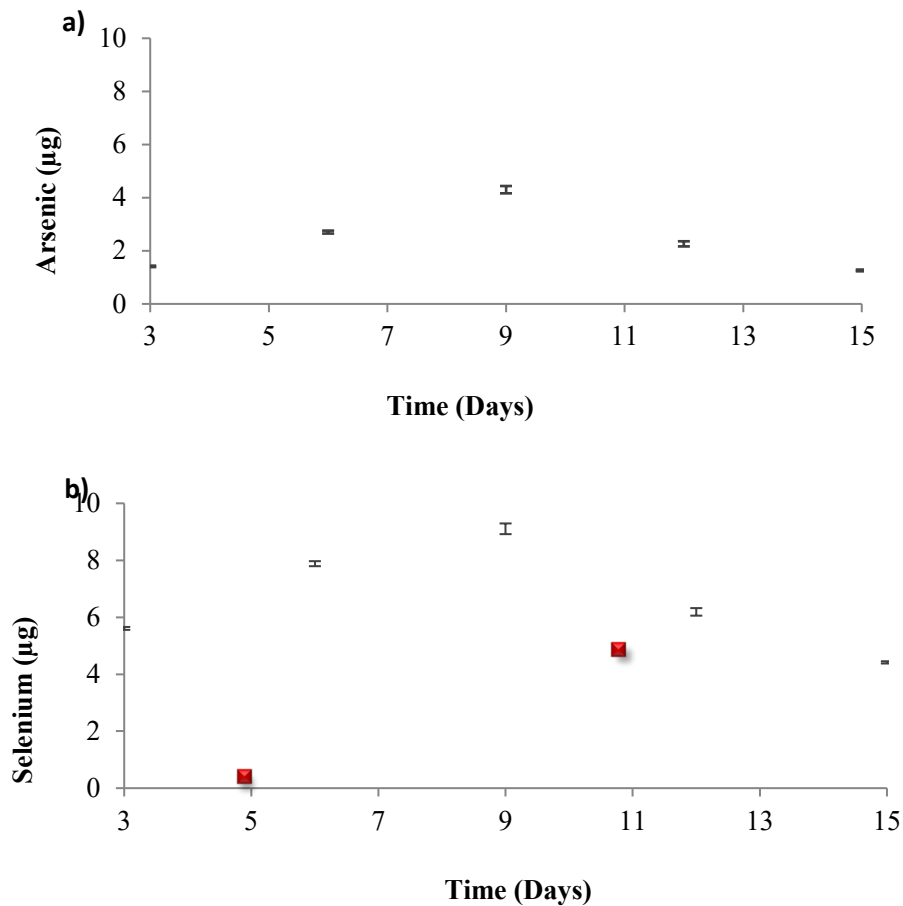


**Figure 73:** Accumulation of a) arsenic and b) selenium in SCPEI-PCPEI resin mixture embedded in agarose gel (n = 3).

Operation of DGT requires rapid adsorption to the binding layer in order to keep the analyte concentration at the binding surface as zero. This can only happen if the binding layer has high affinity and capacity for its target analytes. Zero concentration at the resin-diffusive gel interface helps develop and maintain a constant concentration gradient from the bulk solution and through the diffusive layer (Zhang and Davison, 1995a). This means that on day 9, the concentration at the resin-diffusive gel interface started increasing due to the reduced rate of analyte adsorption. This caused the concentration gradient to favour the bulk solution instead of the DGT resin, leading to the desorption of arsenic and selenium.

Mongin et al. (2013) further explained that during extended deployment periods, as more binding sites are occupied, the uptake deviates from linearity as the net flux decreases towards

equilibrium with the bulk solution. Since equilibrium was not attained, SCPEI-PCPEI resin was not just facing a capacity issue but reduced affinity for arsenic and selenium as well. The assumption is that the agarose obstructed some of the adsorption sites. Furthermore, when SCPEI-PCPEI resin is exposed to water, it physically swells up. This could be another mechanism by which it adsorbs arsenic and selenium. By incorporating in agarose gel, the swelling of SCPEI-PCPEI is restricted, thus reducing the extent of adsorption.

#### 4.2.4.3 The effect of SCPEI-PCPEI resin mass on DGT capacity

In order for DGT to function, the DGT binding phase has to demonstrate a linear mass accumulation over time (Hutchins et al., 2012). Increasing the resin mass from 0.4 to 0.8 g extended the linear region from 6 days to 15 for both arsenic and selenium (Figure 74). The uptake of selenium is generally higher in comparison to arsenic.

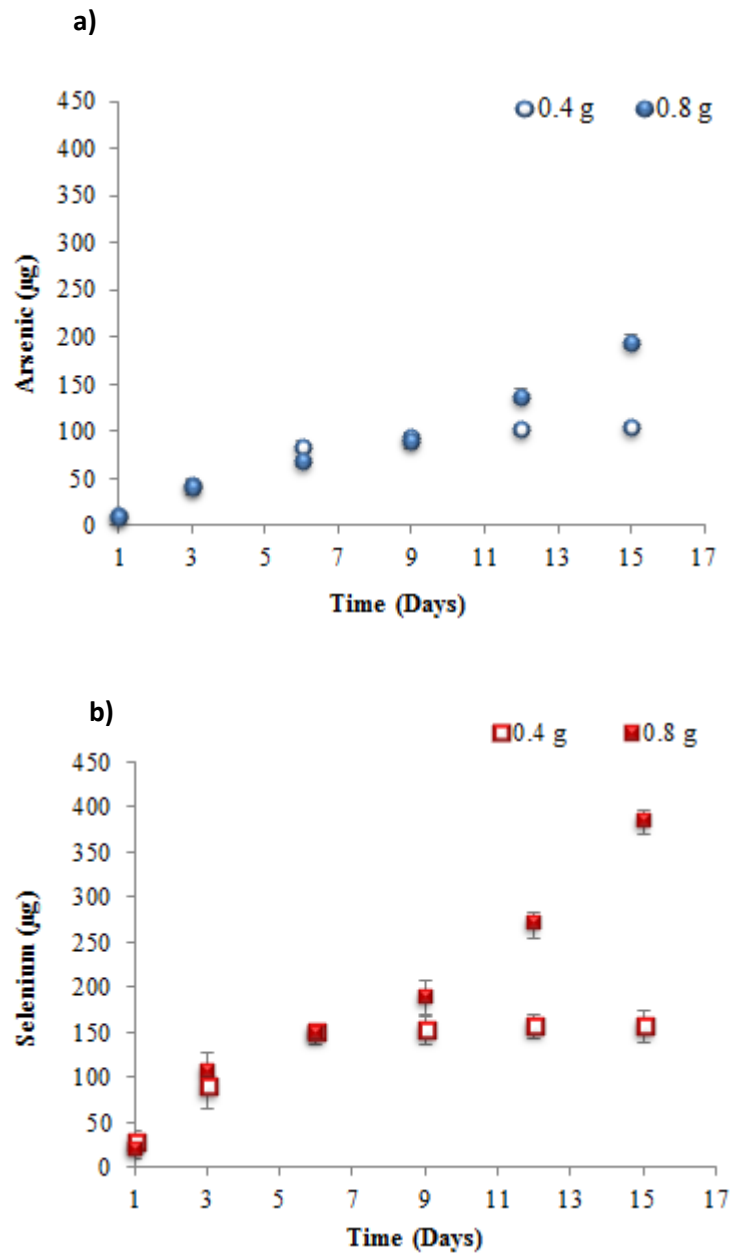


**Figure 74:** The influence of SCPEI-PCPEI resin mass on the accumulation of a) arsenic and b) selenium (n = 3).

#### 4.2.4.4: The role of the diffusive gel in SCPEI-PCPEI-based DGT

A low sampling rate is a key feature in DGT and all passive samplers because it guarantees longer deployment times and the subsequent determination of TWA concentrations (Namieśnik et al., 2005). The arrangement of the layers in DGT along with a diffusive gel of known thickness will reduce the sampling rate by ensuring that transport into DGT is exclusively by molecular diffusion (Davison and Zhang, 1994; Zhang and Davison, 1995b).

Results in Figure 75 show that the inclusion of a diffusive gel led to a slower uptake rate compared to DGT without a diffusive gel. In the absence of a diffusive gel, DGT approaches equilibrium much faster. It is also apparent that the inclusion or exclusion of the diffusive gel has no bearing on the capacity since the amount accumulated without a diffusive gel was the same as the amount obtained with a diffusive gel present. These results also highlight the reproducibility of the technique.

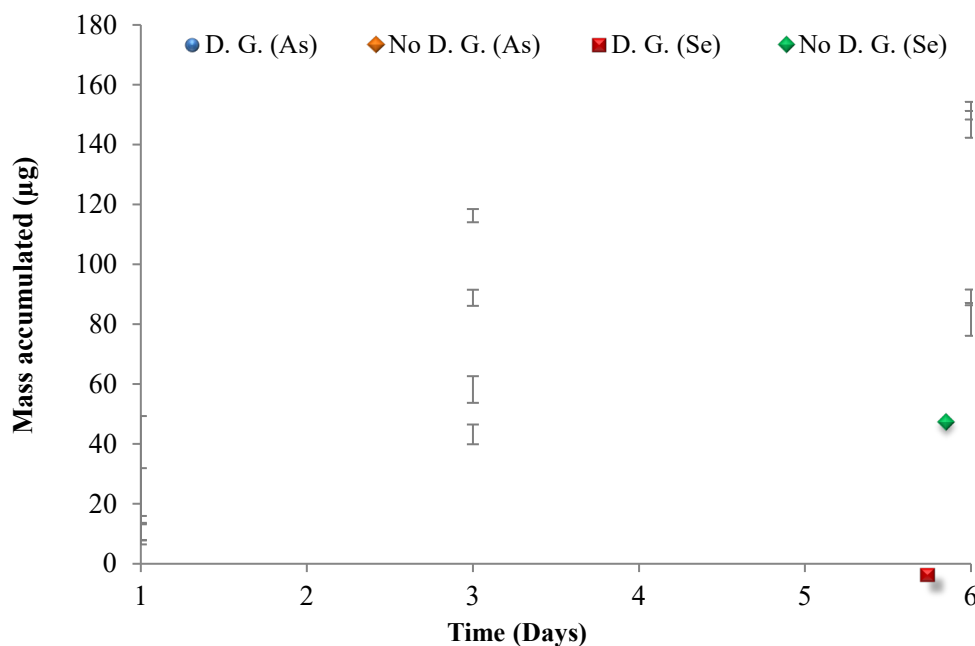


**Figure 75a:** The effect of the agarose diffusive gel (D. G.) on uptake of arsenic and selenium using 0.4 g of SCPEI-PCPEI resin (n = 3).

Arsenic and selenium generally exist as oxyanions in solution depending on the conditions. Wang et al. (2016) observed that at low ionic strength, the fixed negative charges on agarose are enough to cause weak repulsion of oxyanions. Even if this was the case, in the current DGT, the extent was not severe since both elements were able to cross the diffusive layer and accumulate within the SCPEI-PCPEI resin. Wang et al. (2016) also further explained that despite their claim that anions concentrations determined using DGT were comparable to those measured directly in natural fresh and sea water, thus validating agarose as a component of the diffusive gel.

#### 4.2.4.5 The diffusive gel thickness

It was important to evaluate the optimum thickness range as it would influence the ability of labile arsenic and selenium species to diffuse through the diffusive layer. This effect was evaluated using flux ( $\text{nmol cm}^{-2}$ ) as shown in Figure 75. When the diffusive gel is 0.12 cm, there is a noticeable decrease in the flux for arsenic and selenium. This is because with a diffusive gel as thick as 0.12 cm it takes longer for the analytes to diffuse. The optimum diffusive gel thickness range was between 0.069 and 0.08 cm.

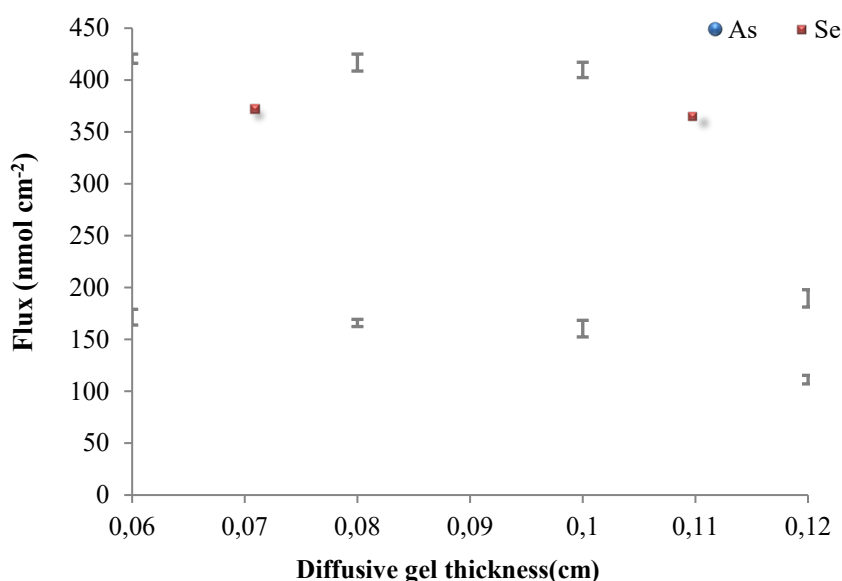


**Figure 75b:** The changes in flux as a result of increasing diffusive gel thickness ( $n = 3$ ).

#### 4.2.4.6 The effect of turbulence on DGT uptake

Turbulence addresses the molecular dynamic of the solution. DGT must be able to operate in fast moving water bodies such as a river, or in quiescent water at the bottom of a lake. With this in mind, a time series experiment was conducted to assess the uptake of arsenic and selenium over time. As expected, under stagnant conditions, the rate of mass accumulation was slower (Figure 76). Concerning arsenic, it would seem stagnant conditions encourage a slow and steady increase with time as evidenced by the linear curve. Solution agitation will result in more movement of analytes, which is why DGT approaches equilibrium by day 6. It should be noted that for this experiment 0.4 g total mass of SCPEI-PCPEI resin was used instead of 0.8 g, which could explain the lower capacity.

The trend observed for selenium in both stirred and stagnant solutions was the same: Selenium approaches equilibrium after the same number of days irrespective of the fluid dynamics. The only difference is the magnitude, with mass accumulated in stirred solutions

being higher. As previously discussed, the diffusion coefficient for selenium in agarose was higher compared to arsenic. The trend observed in Figure 76 further highlights this notion, despite little turbulence within the solution, selenium still moves faster through the diffusive gel, occupying majority of the adsorption sites. This is why arsenic approached equilibrium on day 6 but at a much lower mass. Furthermore, the DBL thickness was higher for selenium, in a stirred solution. Stagnant conditions are expected to increase the DBL thickness even further; however this did not retard movement of selenium into the passive sampler.

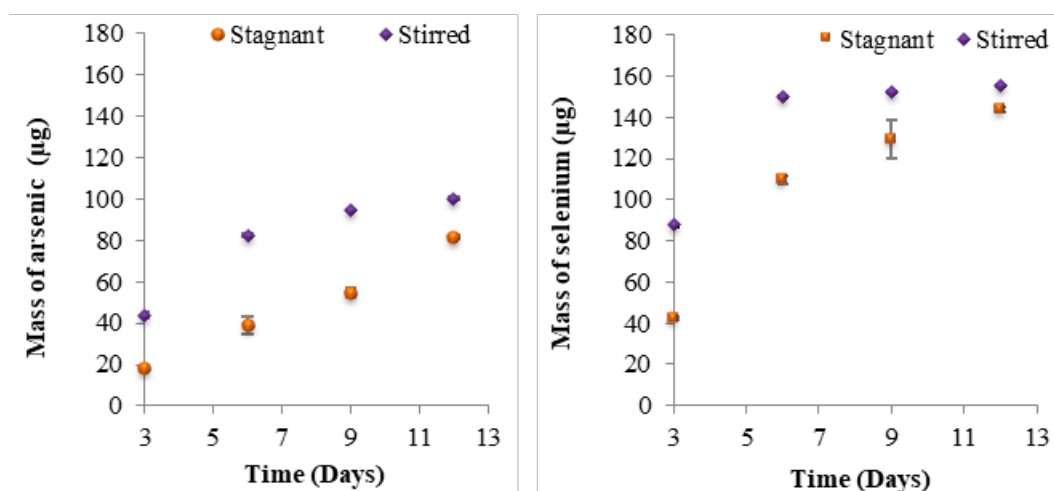


**Figure 76:** The effect of turbulence on mass uptake of a) arsenic and b) selenium (0.4 g of SCPEI-PCPEI; 60-rpm stirring rate; n = 3).

DGT directly measures a flux, which is dependent on the kinetics of the solution, enabling DGT to measure labile fractions in solution and not species that are kinetically inert (Zhang and Davison, 1995). In DGT deployments, the stirring rate not only affects the thickness of the DBL but it also affects flux. The flux measures the amount (nmol) of either arsenic or selenium per unit area ( $\text{cm}^{-2}$ ) of SCPEI-PCPEI DGT passive sampler. The flux was also used to further verify the effects of turbulence on uptake (Table 9). The flux was indeed higher in the stirred solutions. The flux was even higher for selenium. It is also apparent that between day 3 and day 6, there is a notable increase in flux, between day 6 and day 12, once the samplers have moving towards equilibrium, the movement into the sampler also slows down.

**Table 9:** Flux differences between stirred and stagnant solutions

Time (Days)	Flux for arsenic (nmol cm <sup>-2</sup> )		Flux for selenium (nmol cm <sup>-2</sup> )	
	Stirred	Stagnant	Stirred	Stagnant
3	0.19	0.08	0.35	0.17
6	0.35	0.16	0.60	0.44
9	0.40	0.23	0.61	0.52
12	0.43	0.35	0.63	0.58

#### 4.2.4.7 The effect of sample concentration on DGT uptake

Operation of DGT relies on the establishment of a concentration gradient between the aqueous solution and DGT. DGT devices were deployed in solutions of varying concentration (Figure 77). The flux was higher in the 1 mg L<sup>-1</sup> and 0.5 mg L<sup>-1</sup> solutions. When the concentration in the bulk solution is higher, there is a faster rate of diffusion into DGT. This is why DGT obtained a higher flux in the 1 mg L<sup>-1</sup> solution compared to 0.5 and 0.25 mg L<sup>-1</sup> solutions. The implication is that for environmental samples with trace concentrations, longer deployment times are required, to allow enough time for analyte molecules to move from the bulk into DGT.

Davison and Zhang (2012) also pointed out that the maximum rate at which an analytes can diffuse through the diffusive layer correlates to the concentration in solution. By increasing the concentration of an analyte the sampling device reaches equilibrium is faster (Mongin et al., 2013).

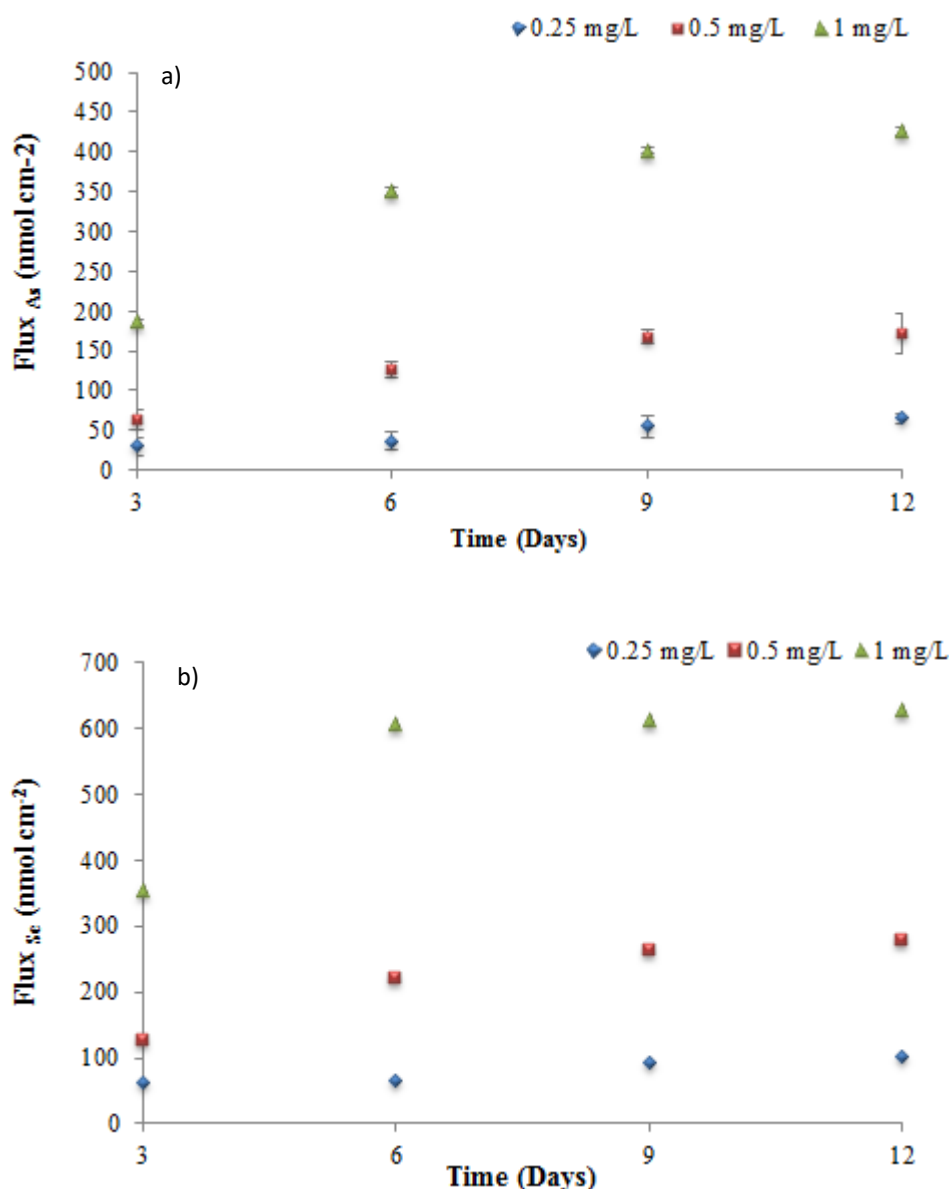


**Figure 77:** The effect of bulk solution concentration on flux of a) arsenic and b) selenium in SCPEI-PCPEI DGT (0.4 g SCPEI-PCPEI; n = 3).

#### 4.2.4.8 The effect of pH on DGT uptake

SCPEI-PCPEI-based DGT passive samplers were designed for application in AMD and natural water. At pH 3, arsenic and selenium are accumulated linearly for the 15 day deployment time (Figure 78). On the other hand mercury shows a linear uptake trend for the first 9 days, after which the passive sampler seems to be approaching equilibrium. On the other hand the plots for arsenic and selenium at pH 5 follow the uptake trend of a typical passive sampler; there is a distinct linear region between day 1 and day 9, there after the

passive sampler approaches the equilibrium mode. Upon closer examination, for arsenic and selenium, between day 1 and day 9 the slopes of the curves at pH 5 appear to be higher compared to the ones obtained at pH 3. This suggests faster accumulation for the first 9 days.

Figure 78 also shows that the capacity is not significantly affected by pH, with the disparity being lower with arsenic than selenium. The pH does however; seem to affect the rate at which arsenic and selenium are accumulated in SCPEI-PCPEI DGT. At pH 3, there is a slow and steady increase of arsenic and selenium in SCPEI-PCPEI DGT. According to Li et al. (2005) and Mongin et al. (2013) this is because at low pH the functional groups in the binding layer are acidic, due to strong competition with protons which reduce the binding strength. At pH 5 the uptake rate is faster (SCPEI-PCPEI DGT reaches equilibrium on day 9) and it can be assumed that this is due to partial protonation of the functional groups as a result of the reduced proton concentration. Partial protonation of arsenic and selenium means a more efficient anion exchange mechanism between  $\text{SO}_3^-$  and  $\text{SeO}_3^{2-}$ ; and  $\text{HAsO}_4^{2-}$  with  $\text{PO}_4^{2-}$  (Saad et al., 2013a; 2013b). SCPEI-PCPEI can operate effectively between pH 3 and 5. Although results for mercury were not obtained at pH 5, it can be assumed that this will not significantly affect operation in natural water.

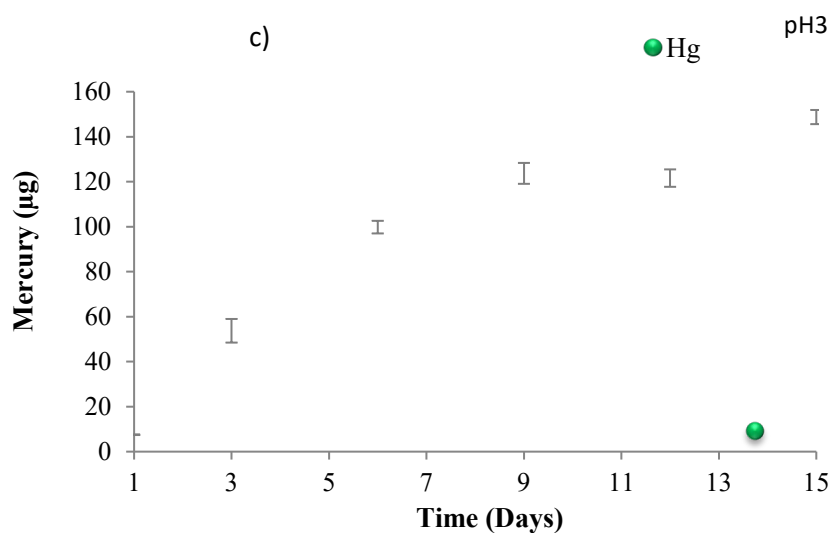
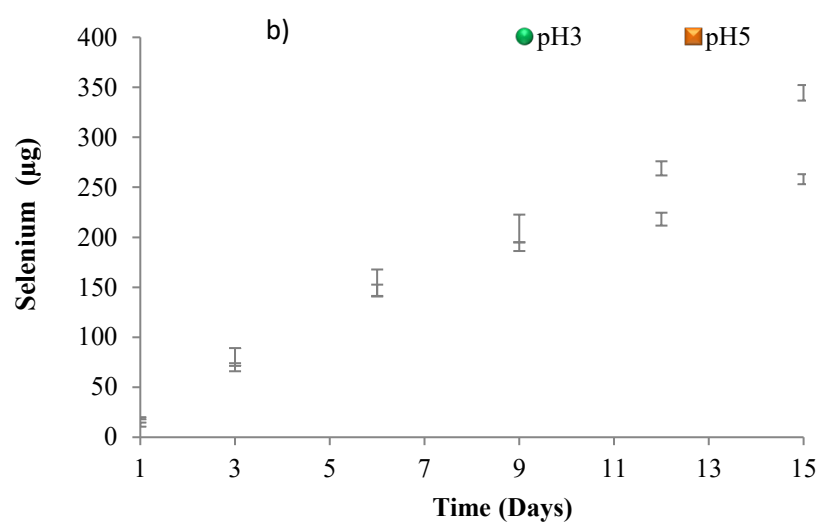
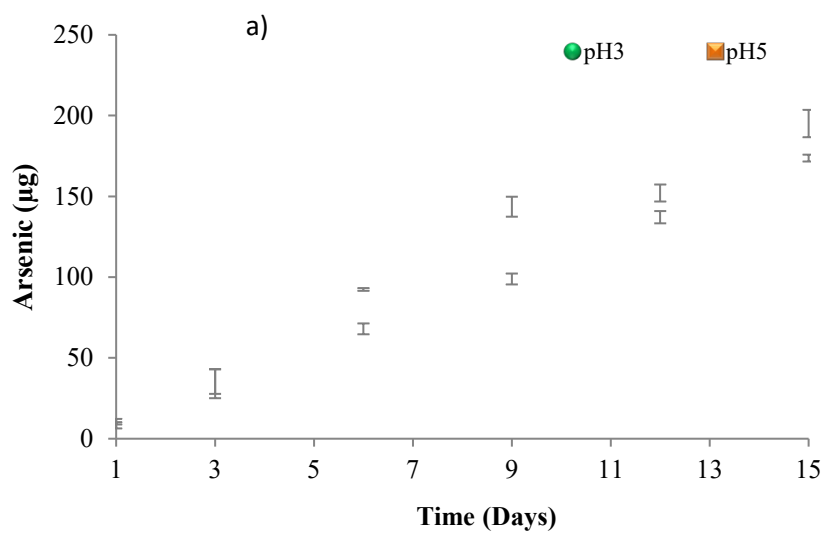


**Figure 78:** Influence of pH on the mass of a) arsenic and b) selenium c) the accumulation of mercury at pH 3 (0.8 g SCPEI-PCPEI; n = 3).

## 4.2.5 Calculation of the diffusion coefficient (D) and diffusive boundary layer (DBL)

### 4.2.5.1 The diffusion coefficient

The diffusion coefficients of arsenic and selenium were determined through a time series experiment (Figure 79). The curves from the time series experiment are linear, with selenium showing the highest mass accumulation compared to arsenic. The diffusion coefficients were calculated from the slopes of these curves and the relevant information is shown in Table 9.

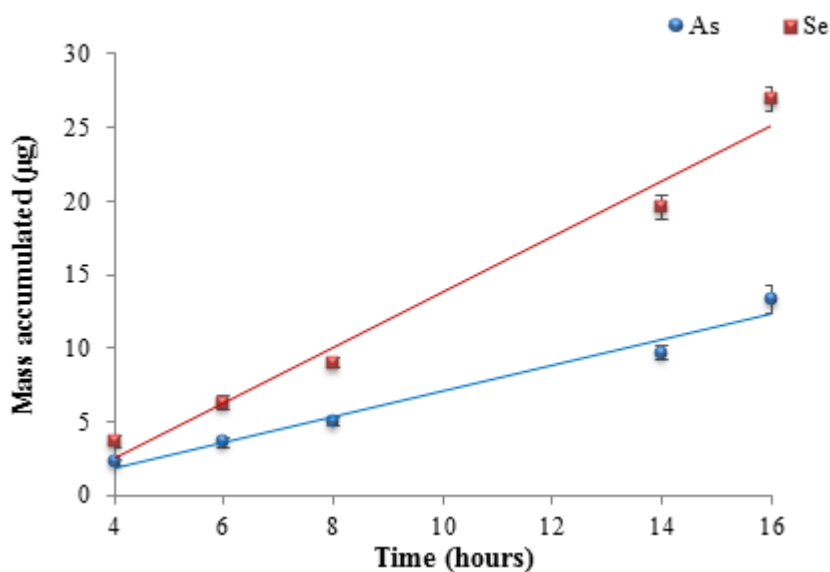


**Figure 79:** Time series experiment for the determination arsenic and selenium diffusion coefficients in spiked Milli-Q water (n = 3).

The diffusion coefficients of arsenic and selenium at pH 3 were calculated to be  $9.53 \times 10^{-5}$  and  $1.11 \times 10^{-4} \text{ cm}^2 \text{ s}^{-1}$ , respectively. The diffusion coefficients were measured at 22°C. The diffusion coefficient of selenium is much higher compared to arsenic. These values reflect the trend that has been observed thus far where the mass of selenium is generally higher than arsenic. Selenium is able to move at a faster rate from the bulk solution through the diffusive gel. This also supports the notion that selenium occupies the adsorption sites first, subsequently hindering arsenic to bind on adjacent sites.

These diffusion coefficients are a few orders of magnitude higher than values previously reported in agarose cross-linked polyacrylamide (Table 10). At pH 3 arsenic and selenium both exist as the uncharged species  $\text{H}_3\text{AsO}_3$  and  $\text{Se}(0)$ , respectively. It has been suggested by Li and Gregory (1974) that molecules with a large hydration layer of water molecules are retarded to a greater extent. The lack of charge could mean a smaller hydration layer as well as little repulsion from the negative agarose surface charges Wang et al. (2016).

**Table 10: Determination of the diffusion coefficient (*D*) from the slope of a linear plot of the mass against time (22°C)**

Equation of line	R <sup>2</sup>	Slope (µg hr <sup>-1</sup> )	Slope (µg s <sup>-1</sup> ) <sup>1</sup>	Δg (cm)	C <sub>soln</sub> (mg L <sup>-1</sup> )	C <sub>soln</sub> (µg cm <sup>-3</sup> )	A (cm <sup>2</sup> )	D (cm <sup>2</sup> s <sup>-1</sup> )
y = 0.8851 x - 1.7499	0.9757	0.8851	3186.36	0.083	0.88	884000	3.14	9.53 × 10 <sup>-5</sup>
y = 1.7003 x - 3.8364	0.9947	1.7003	6121.08	0.083	1.46	1463333	3.14	1.11 × 10 <sup>-4</sup>

**Table 11: Comparison of arsenic and selenium diffusion coefficients**

Method	Hydrogel	As (III)	As (V)	Se (IV)	Se (VI)	References
SCPEI-PCPEI DGT	Agarose	-	-	-	-	Current work
TiO <sub>2</sub> DGT	APA	10.5 × 10 <sup>-6</sup>	6.83 × 10 <sup>-6</sup>	8.91 × 10 <sup>-6</sup>	<i>bdl</i>	Bennett et al., 2010
Ferrihydrite DGT	APA	-	5.25 × 10 <sup>-6</sup>	-	5.83 × 10 <sup>-6</sup>	Luo et al., 2010
Ferrihydrite DGT	APA	1.01 × 10 <sup>-5</sup>	6.28 × 10 <sup>-6</sup>	-	-	Moreno-Jiménez et al., 2013
Ferrihydrite DGT	APA	5.3 × 10 <sup>-6</sup>	4.90 × 10 <sup>-6</sup>	-	-	Panther et al., 2008
Ferrihydrite DGT	APA	-	-	6.37 × 10 <sup>-6</sup>	6.28 × 10 <sup>-6</sup>	Peng et al., 2017
Diffusion in water (D <sub>water</sub> )	-	-	9.05 × 10 <sup>-6</sup>	-	9.46 × 10 <sup>-6</sup>	Li and Gregory, 1974

APA= agarose cross-linked polyacrylamide

*For SCPEI-PCPEI DGT diffusion coefficients are for total arsenic and selenium since no speciation studies were performed*

The pores in 1.5% agarose gels are described as having an open structure, yielding with pore sizes greater than 20 nm (Zhang and Davison, 1999) resulting in diffusion coefficients similar to those in water (Chramback, 1985; Attwood et al., 1981). This could be the other reason why arsenic and selenium entered the diffusion coefficient with ease.

The diffusion rate in SCPEI-PCPEI DGT is also influenced by the filter membrane. Wang et al. (2016) conducted experiments to evaluate the role of filter membrane on the diffusion of analytes. They found that filter membranes enhanced the diffusion rate, which could be a result of the larger pore size in the filter membrane compared to agarose. In their study, arsenic diffusion rates were improved with the addition of either cellulose nitrate or PES filter membrane (Wang et al. (2016). On the other hand Scally et al. (2006) showed that the diffusion coefficient in the filter membrane is not statistically different from that in the diffusive gel.

The time series method for determining D is often used because the measurement conditions are the same as ones encountered during DGT deployment (Wang et al., 2016; Price et al., 2013; Scally et al., 2006; Shiva et al., 2015). However, it would have been ideal to measure the diffusion coefficient using a diffusion cell for comparison purposes even though the use of diffusion cell is only recommended for quality control purposes (Shiva et al., 2015).

#### 4.2.5.2 The DBL

A plot of mass vs  $1/\Delta g$  (Figure 80) can be used to calculate the DBL. If this plot is non-linear, then it means a DBL is present and should be considered in calculations (Davison and Zhang, 1994; Warnken et al., 2006). The reciprocal plots of arsenic and selenium were linear. The correlation coefficient of arsenic was higher than selenium because arsenic showed better linearity. The equations obtained for these plots were:  $y = 0.0427x + 0.0216$  and  $y = 0.0063x + 0.0091$  for arsenic and selenium respectively. The DBL values were 0.51 cm for arsenic and 1.44 cm for selenium. On average, the thickness of the filter membrane and diffusive gel combined is 0.092 cm; the DBL values are much higher than this. According to Warnken et al. (2006) this means that the DBL should be considered in the calculation of  $C_{TWA}$

Warnken et al. (2006) studied the effects of stirring rate under laboratory settings on the DBL thickness. The DBL was 0.044 cm for solutions stirred at 60 rpm and 0.150 cm under stagnant solutions. The DBL values obtained in this study correlate with those obtained under stagnant conditions even though the solutions were also stirred at 60 rpm.

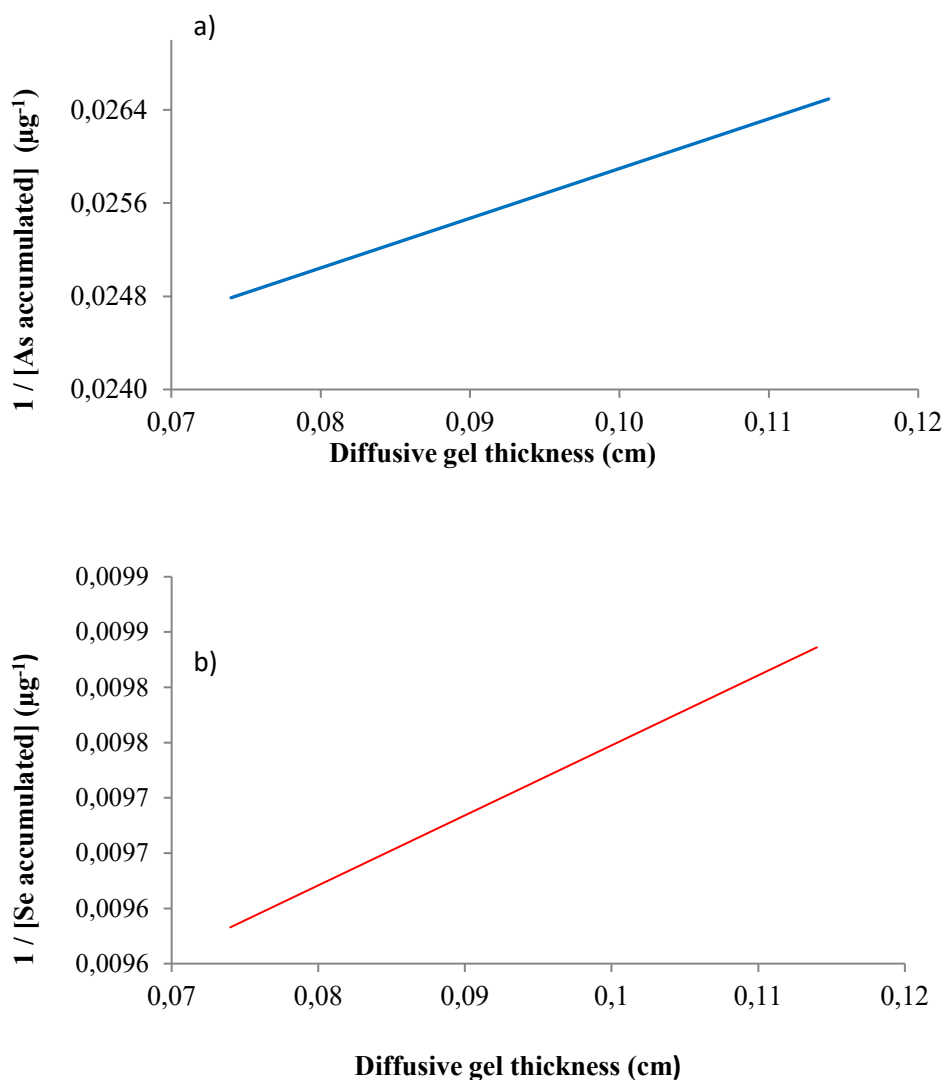


**Figure 80:** The reciprocal mass of a) arsenic and b) selenium accumulated by DGT ( $\mu\text{g}^{-1}$ ) with varying diffusive layer thickness.

#### 4.2.6 Determination of resin blanks and method detection limits

Resin blanks were important for the verification of SCPEI-PCPEI DGT technique. The resin blanks were  $0.33 \pm 0.002$  ( $17 \mu\text{g L}^{-1}$ ) and  $0.32 \pm 0.001 \mu\text{g}$  ( $16 \mu\text{g L}^{-1}$ ) for arsenic and selenium, respectively. The MDL values which are 3 times the standard deviation of the blanks were  $50 \mu\text{g L}^{-1}$  for arsenic and  $48 \mu\text{g L}^{-1}$  for selenium. The MDL values are very low which means SCPEI-PCPEI DGT is suitable for ultra-trace analysis.

#### **4.2.7 Literature comparison of other DGT**

The results of the comparison of the optimised parameters in the CPEI resin-based DGT to other DGTs in literature is shown in Table 12. The results indicate that most DGT passive samplers optimised with new resins were deployed only for few days with 7 days being maximum. Thus in the developed sampler, it could be deployed up to 14 days depending on the sample matrix with surface water the ideal sample matrix.

**Table 12:** Examples of how some resin gels were prepared and the maximum number of days the DGT passive samplers were deployed

Target analyte (s)	Composition of resin / binding gel	Maximum deployment period in the laboratory	Maximum deployment in the field	References
Arsenic and selenium	<b>1 g</b> titanium dioxide in <b>10 mL</b> of gel solution	24 hours	4 days	Bennett et al. (2010)
Nitrate	4 g anion exchange resin (SIR-100-HP) <b>11 mL</b> agarose	48 hours	20 hours	Cai et al. (2017)
Illicit drugs	<b>2 g</b> XAD18 in <b>10 mL</b> agarose gel	24 hours	7 days	Guo et al. (2017)
Mercury	<b>3 g</b> of: 1) 3-Mercaptopropyl functionalized SBA-15 2) 3-mercaptopropyl functionalized ethenylene bridged periodic mesoporous organosilica 3) Sumichelate Q10R 4) 3-mercaptopropyl functionalized silica gel 5) Chelex-100 resin Each resin was dissolved in <b>10 mL</b> of gel solution	24 hours	2 days	Gao et al. (2011)
Antibiotics	<b>1 g</b> of either XDA-1, LX-1180, XDA-600, LX-4027, D296, NKA-9, CAD-40 or XAD-18 resin in <b>10 mL</b> agarose	12 hours	8 hours	Xie et al. (2017)

#### 4.2.8 Application of optimised SCPEI-PCPEI-based DGT

Laboratory-based performance tests using standard solutions demonstrated the ability of SCPEI-PCPEI DGT to effectively operate under acidic and alkaline conditions. However, these solutions were not representative of the complex matrices normally found in the natural environment. In this section the performance of SCPEI-PCPEI-based DGT was evaluated in different environmental samples as well as field deployments.

##### 4.2.8.1 Uptake by DGT in lab-based experiments using water from Fleurhof Dam

###### Composition of Fleurhof dam water

The pH of Fleurhof dam water was 6.3 and the conductivity ( $0.50 \text{ mS cm}^{-1}$ ). The redox potential averaged most surface water at 324 mV. The anion and metal composition are shown in Table 13. The low conductivity obtained from Fleurhof dam correlates to the low concentration of dissolved anions and metals (Table 13). Compared to concentrations obtained from areas impacted with AMD, the concentrations of sulphate and iron were  $138.5$  and  $0.143 \text{ mg L}^{-1}$ , respectively. The chloride was  $19.69 \text{ mg L}^{-1}$ . Sodium and magnesium were the highest metal concentrations, at merely  $138.3$  and  $132.1 \text{ mg L}^{-1}$ , respectively. The general decrease in concentration could be attributed to the higher water pH in Fleurhof dam. Acidic water enhances the release of metals from surrounding rock and sediments.

**Table 13: Anion and metal composition of water sampled at Fleurhof dam.**

	Concentration (mg L <sup>-1</sup> )
F <sup>-</sup>	0.109
Cl <sup>-</sup>	19.69
NO <sub>3</sub> <sup>-</sup>	6.92
SO <sub>4</sub> <sup>2-</sup>	138.5
Al	<i>bdl</i>
Ca	29.55
K	47.97
Mg	132.1
Na	138.3
Co	<i>bdl</i>
Cr	<i>bdl</i>
Cu	<i>bdl</i>
Fe	0.143
Mn	0.532
Ni	<i>bdl</i>
Zn	<i>bdl</i>
As	0.022
Se	0.032

#### Accumulation of arsenic, selenium and mercury from Fleurhof dam water

Two applications using Fleurhof dam water were carried out in the lab. In the first application the water was spiked with arsenic, selenium and mercury to a final concentration of 0.5 mg L<sup>-1</sup>. In the second application, the water collected from Fleurhof dam was used without spiking. The amounts accumulated are compared to each other.

SCPEI-PCPEI DGT showed a linear uptake trend for the accumulation of arsenic, selenium and mercury, from spiked Fleurhof dam water (Figure 81a, c and e). By day 9 the accumulation rate had slowed down for arsenic and selenium. The maximum mass accumulated was 2.9 µg of arsenic and 7.1 µg of selenium. The mass of mercury was significantly lower at 0.06 µg.

In unspiked Fleurhof dam water the trend remained linear for arsenic and selenium (Figure 81b, d), however the maximum mass accumulated was significantly lower (0.04  $\mu\text{g}$  for arsenic and 0.012  $\mu\text{g}$  for selenium). The mass of Mercury decreased with deployment time (Figure 81)

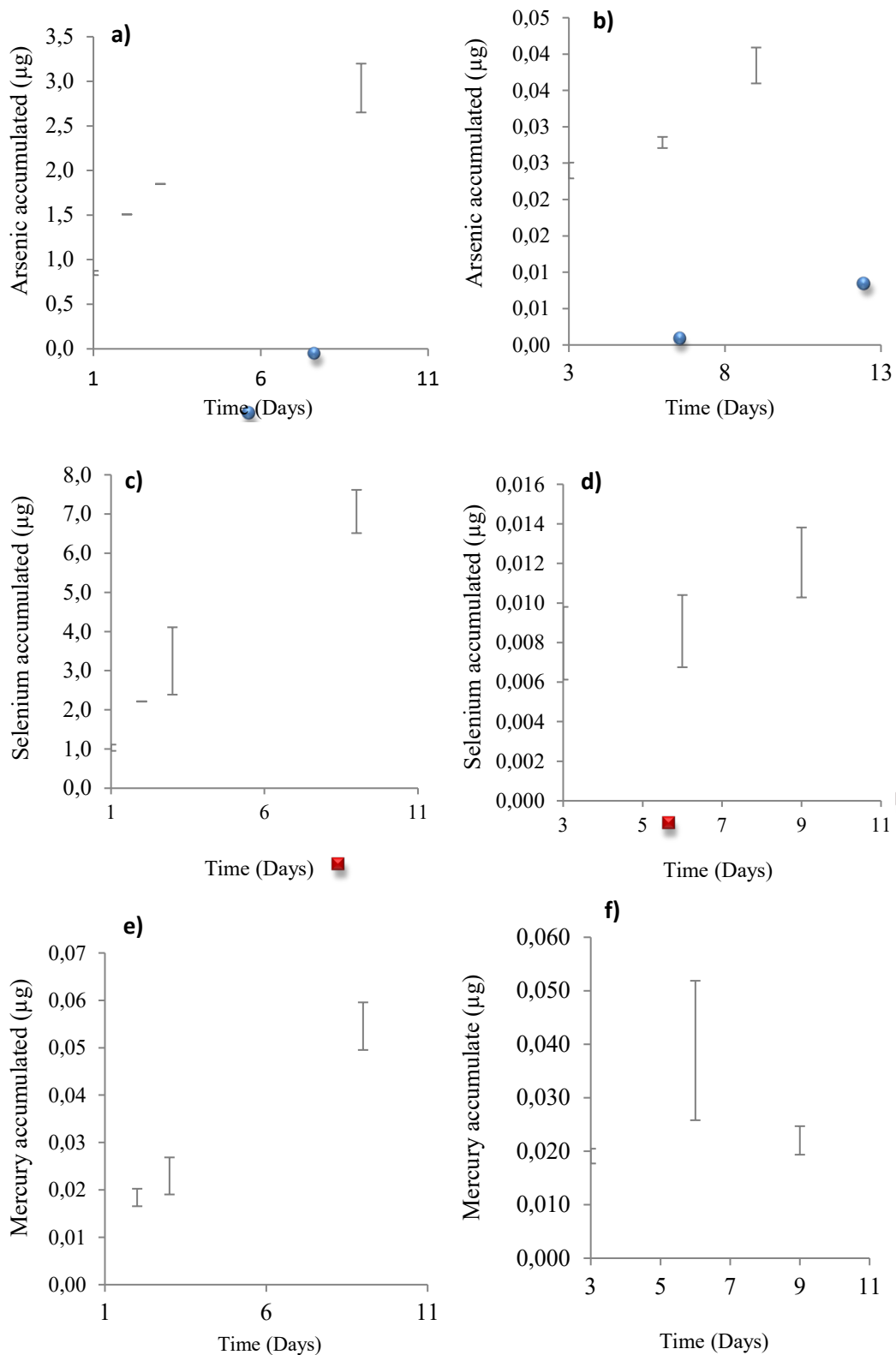


**Figure 81:** Uptake of a) and b) arsenic; c) and d) selenium; e) and f) mercury in spiked ( $0.5 \text{ mg L}^{-1}$ ) and unspiked Fleurhof dam water, respectively.

The concentration of arsenic, selenium and mercury in the spiked sample were sufficiently high to allow an effective concentration gradient to be established. In the unspiked sample

however, the overall concentrations were significantly low and this affected the diffusion rate into SCPEI-PCPEI DGT. The low concentrations do correspond with those found in natural water; arsenic is usually between 0.15 and 0.45  $\mu\text{g L}^{-1}$  (Smedley and Kinniburgh, 2002) and selenium 0.02  $\mu\text{g L}^{-1}$  (Fernández-Martínez and Chalet, 2009). The low concentrations did not however, deter SCPEI-PCPEI DGT from accumulating arsenic and selenium. Another observation is that in unspiked water SCPEI-PCPEI was not able to retain mercury, suggesting poor adsorption kinetics.

#### Uptake of major cations from Fleurhof dam water

The metals adsorbed from Fleurhof dam water were also determined (Figure 82). The concentration of sodium in SCPEI-PCPEI was elevated and seemed to increase with deployment time. The other metals did not show a specific trend. Iron was accumulated from day 6. In the previous application using AMD, the concentration of iron in DGT was elevated due to high concentration and not necessary due to selectivity.

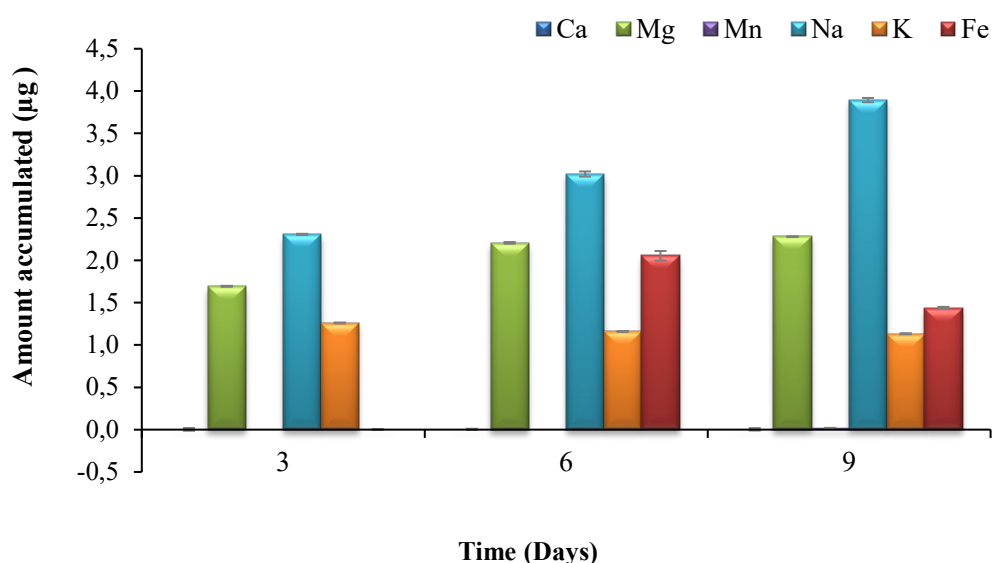


**Figure 82:** Accumulation of background metals by DGT in the lab-based experiments using Fleurhof dam water.

#### 4.2.8.2 Deployment in Fleurhof dam

##### Accumulation of arsenic, selenium and mercury in Fleurhof dam

SCPEI-PCPEI will prove as a valid technique if it is able to accumulate the target analytes both in the lab and in the field. Arsenic, selenium and mercury accumulated from field deployments in Fleurhof dam were significantly low, and this is because they are naturally

found in trace concentrations (Figure 83). Arsenic was accumulated linearly over the 12 day deployment period. This implies that some arsenic adsorption sites are still available. Most importantly, it suggests that SCPEI-PCPEI is selective enough towards labile trace arsenic in environmental water. The maximum amount accumulated was 0.045 µg. This correlates with the mass obtained from unspiked Fleurhof water in the laboratory-based experiment.

In the field, selenium was unsuccessfully accumulated in SCPEI-PCPEI DGT: On day 3 the mass of selenium was the highest but had declined by day 6, afterwards the amount of selenium in DGT remained constant. This suggests that with regards to selenium SCPEI-PCPEI is operating in the equilibrium mode: Previous experiments had shown that selenium diffuses into SCPEI-PCPEI DGT quickly. It is therefore possible that the maximum amount of selenium was accumulated in the first 3 days, occupying majority of the available sites. Secondly, the dynamic movement of selenium between the bulk solution and DGT, as well as poor retention by SCPEI-PCPEI resin meant that any significant concentration fluctuations in the vicinity of DGT will likely cause selenium to move out of the passive sampler. The same argument may hold true for mercury. The fact that SCPEI-PCPEI resin does not have a high capacity for mercury was apparent in the laboratory-based experiments using unspiked Fleurhof dam water, when the mass of mercury decreased with time

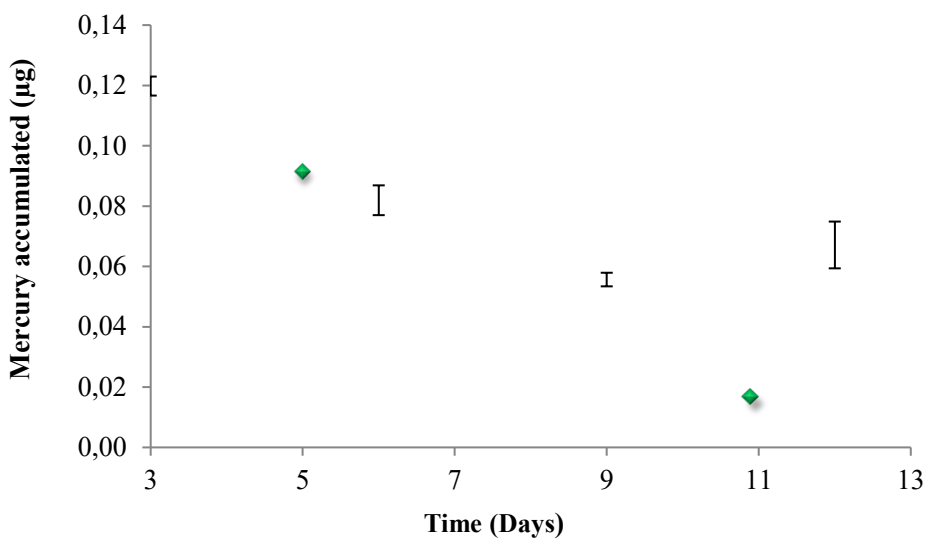
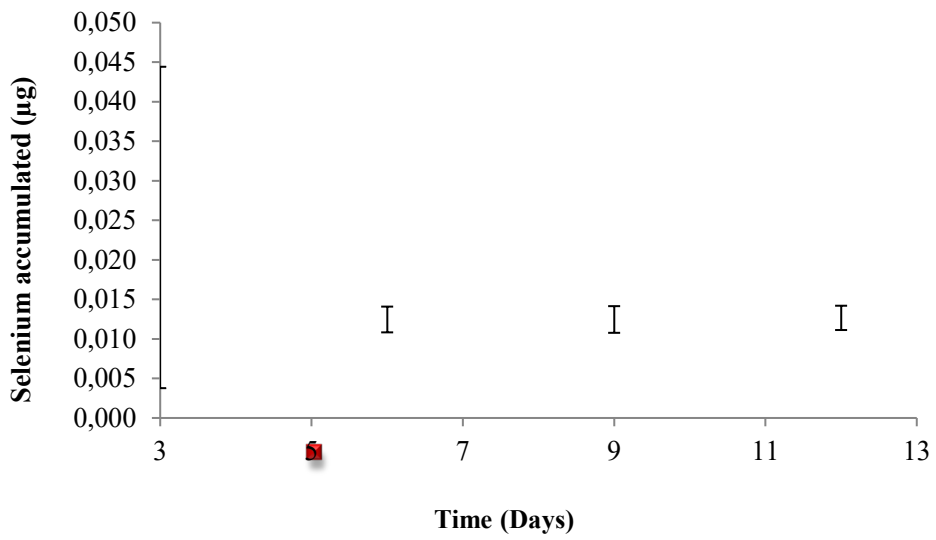
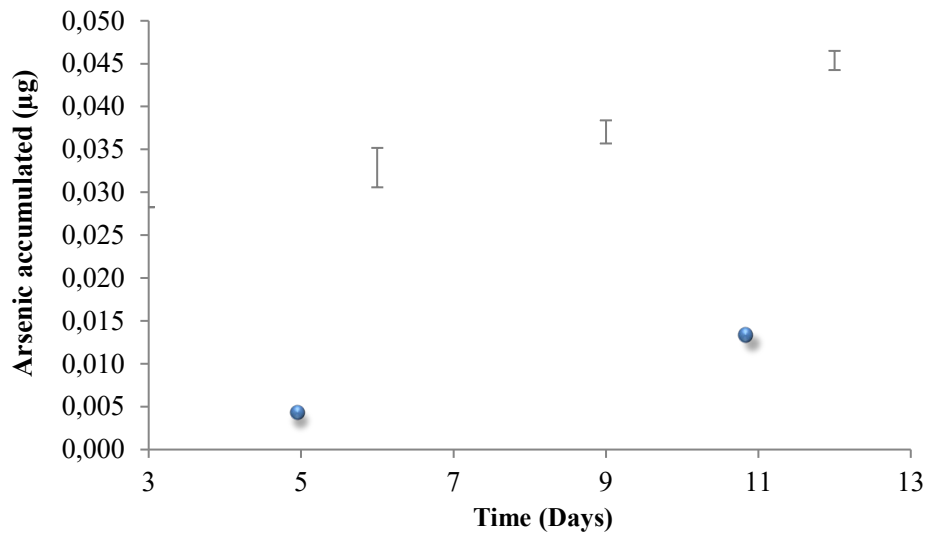


**Figure 83:** Accumulation of a) arsenic b) selenium c) mercury in Fleurhof dam

## Accumulation of major cations from Fleurhof dam

In the field SCPEI-PCPEI DGT accumulated relatively high amounts of iron compared to the other metals (Figure 84). Once again, there is no distinct trend in the accumulation of iron. In fact the other metals also do not show a specific uptake trend.

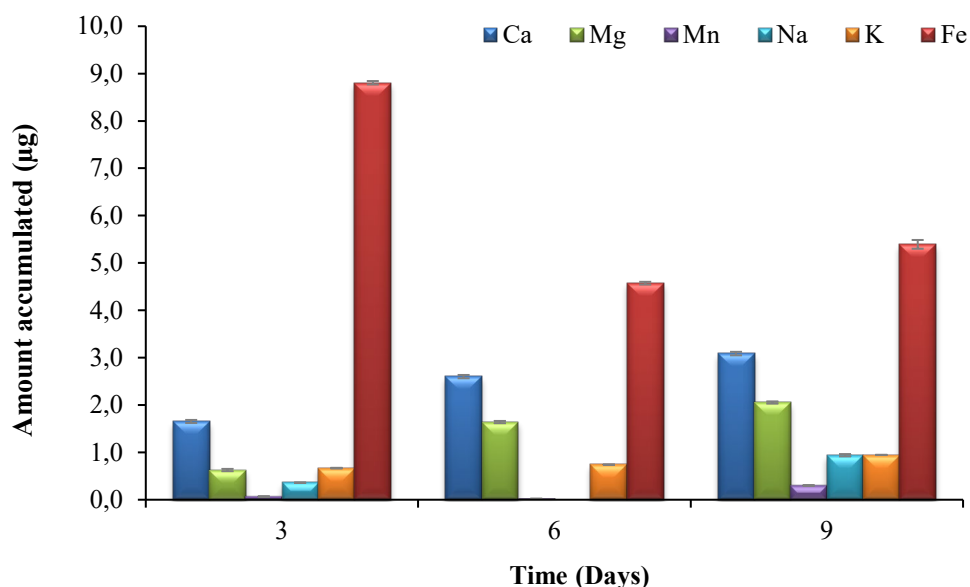


**Figure 84:** Metals accumulated in SCPEI-PCPEI DGT from Fleurhof dam

The mass of iron accumulated in the field deployments is higher compared to mass accumulated from the lab-based experiments (Figure 84). It is most likely that over time, the water collected from Fleurhof dam was subjected to changes in speciation leading to the precipitation of iron. The physiochemical properties of unspiked Fleurhof dam water were therefore measured for 17 days to check if any significant changes in conductivity or redox potential took place. The results are shown in Table 13.

The pH fluctuated over the 17 day period but was still within the required range. The redox potential also fluctuated significantly, the initial value was 291 mV, on day 3 this value had increased to 431 mV. After day 3 the redox potential seems to have stabilised. The temperature of the water samples was 16.1°C when they were collected. The temperatures in the laboratory were higher, and this could possibly have affected the redox potential. The conductivity did not vary much with time.

**Table 14:** Changes in the physiochemical properties of Fleurhof dam water with deployment time

	pH	mV	mS	ppt	(°C)
Day 0	6.38	291	0.36	0.16	16.1
Day 3	6.12	413	0.39	0.19	24.8
Day 6	6.04	281	0.43	0.21	23.0
Day 9	6.37	260	0.41	0.20	23.5
Day 12	6.25	379	0.40	0.20	24
Day 14	6.31	378	0.41	0.20	25.7
Day 17	6.19	381	0.39	0.19	21.5

#### 4.2.8.3 Arsenic, selenium and mercury uptake from dissolved efflorescent crust

##### Composition of dissolved efflorescent crust

The dissolved efflorescent crust formed a highly acidic solution with a pH value of 2.3. The measured conductivity was  $5.30 \text{ mS cm}^{-1}$ . In a study on efflorescent crusts, Camden-Smith et al. (2013) also obtained EC values ranging between  $5.7$  and  $6.4 \text{ mS cm}^{-1}$  for crust solutions with a high quantity of observable insoluble mass. Indeed after dissolution, the crust solution was very cloudy and precipitated significantly within a few hours of preparation. Conversely, for solutions that were completely dissolved, Camden-Smith et al. (2013) obtained conductivity values as high as  $10 \text{ mS cm}^{-1}$ .

The composition of the dissolved efflorescent crust (Table 15) shows elevated concentrations of sulphate, chloride, iron, nitrate, aluminium and manganese. Concentrations of major cations calcium, potassium, lithium, magnesium and sodium, as well as the transition metals cadmium, cobalt, chromium, copper, nickel and zinc were relatively lower compared to the rest of the constituents. Arsenic and selenium were below the detection limit.

High sulphate and iron concentrations are consistent with AMD samples because they are by-products of sulphide mineral oxidation. Alternatively, the high nitrate concentration suggests the source of the efflorescent crust was close to an industrial site since high nitrate levels found in surface and ground water, are usually associated with factors such as the use of fertilizers and treated municipal waste water (Nolan and Hitt, 2006; Thorburn et al., 2003). The concentration of chloride ions, together with the other metals present in the crust will depend on the composition of the sulphide mineral being oxidised as well as the chemical reactions that took place in the original water source (Camden-Smith et al., 2013; Cheng et al., 2009).

Camden-Smith et al. (2013) studied the composition of efflorescent crusts (Table 14b) and found that crusts classified as white with bright green had the highest

**Table 15a:** Anion and metal analysis of the dissolved efflorescent crusts

Element	Cl <sup>-</sup>	NO <sub>3</sub> <sup>-</sup>	SO <sub>4</sub> <sup>2-</sup>	Al	Ca	K	Li	Mg	Na	Cd	Co	Cr	Cu	Fe	Mn	Ni	Zn	As	Se
Con (mg/L)	908.3	297.3	5623	214.5	7.78	0.29	0.35	4.51	13.53	0.09	6.94	0.70	1.49	474.4	79.00	14.05	4.89	<i>bdl</i>	<i>bdl</i>

*bdl* = below the detection limit

**Table 15b:** Mole percentages of metals found in efflorescent crusts (Camden-Smith et al., 2013)

Colour of crust	Al	Ca	Cr	Co	Cu	Fe	K	Mg	Mn	Na	Ni	Tl	Zn
Yellow white	56.9			0.6	0.3		0.6	39.1	1.0		0.9		0.7
Beige	51.4			0.4	0.3	0.3	0.5	43.9	1.2	0.7	0.7		0.6
Green-yellow	38.7			0.5	0.9	29.8	2.0	26.6	0.6		0.6		0.4
Pink yellow	50.4		0.1	0.5	0.7	6.6	0.6	38.7	1.0		0.8		0.6
Orange-brown	43.6	2.0		0.4	0.5	7.5	1.4	41.7	0.8		0.6	1.0	0.4
<b>White with bright green</b>	14.6	0.1	0.1	0.2	0.3	71.9	0.5	11.4	0.3		0.2	0.3	0.1

**Bold** = colour of crust used in current study

iron content. Efflorescent crusts have different colours depending on their mineralogy (Camden-Smith et al., 2013; Naicker et al., 2003). The crust in the current study had a white-greenish colour based on the classification used by Camden-Smith et al. (2013). When comparing the general composition of the two white-greenish crusts it is apparent that they shared similar mineralogy trends: The crust studied by Camden-Smith et al. (2013) had elevated iron and aluminium concentrations. The crust in this study also had high concentrations of iron and aluminium.

#### DGT deployment in the dissolved crust

A linear uptake trend is an indication that DGT has successfully accumulated analytes at a constant and definable rate, within the constraints of the kinetic regime. The dissolved efflorescent crust was spiked with arsenic, selenium and mercury ( $1 \text{ mg L}^{-1}$ ), however, only arsenic could be determined from this study. The accumulation of labile arsenic fractions from the spiked dissolved efflorescent crust solution followed a linear regression between day 3 and day 15 (Figure 85). Nonetheless, after day 15, the curve began to slightly deviate from a linear trend, an indication that the SCPEI-PCPEI resin was becoming saturated.

The amount accumulated represents the labile and bioavailable fraction of arsenic in the dissolved crust solution. This amount is relatively low considering the dissolved crust solution was spiked with arsenic, selenium and mercury at  $1 \text{ mg L}^{-1}$  concentration levels for each. However, the measured concentration was  $0.34 \pm 0.01 \text{ mg L}^{-1}$  for arsenic and the concentrations of the other elements were below the detection limit. The large discrepancy between the spiked and measured arsenic could be attributed to the high proportion of precipitate arising from the dissolved efflorescent crust.

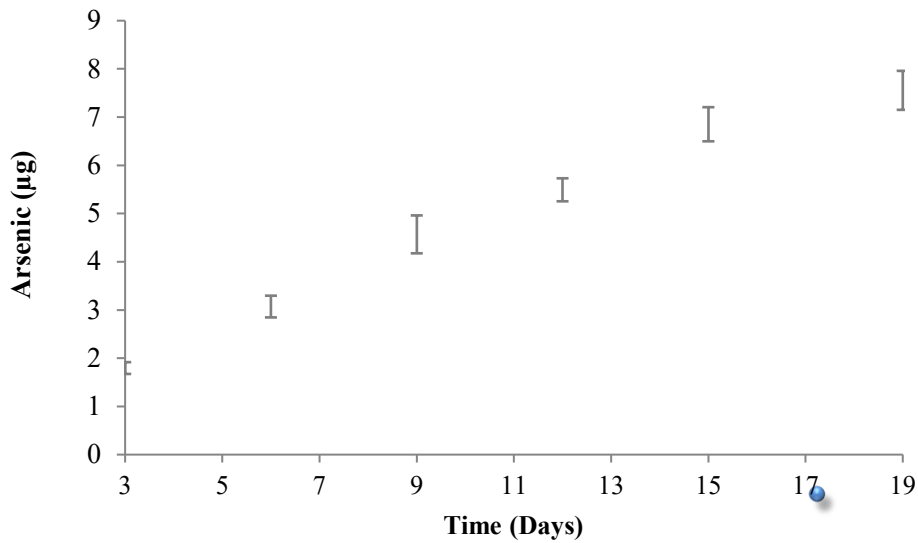


**Figure 85:** Time series experiment in the dissolved crust spiked with arsenic ( $1 \text{ mg L}^{-1}$ ) using 0.8 g of SCPEI-PCPEI resin ( $n = 3$ ).

SCPEI-PCPEI resin targets arsenic and selenium through an anion replacement mechanism based on the premise that they are ionic in solution (Saad et al., 2013a; 2013b). Mercury is adsorbed via a complexation mechanism. Based on their respective Pourbaix diagrams at pH 2.9, under redox potential of surface water arsenic is expected to exist as  $\text{H}_3\text{AsO}_3^0$  (arsenite) or  $\text{H}_2\text{AsO}_4^-$  (arsenate oxyanion), conversely, selenium predominates as elemental selenium  $\text{Se}(0)$ . The mercury species that predominates is either  $\text{Hg}(l)$  or  $\text{HgCl}_2$ . This information was validated using PHREEQC (results are shown in the Appendix). According to PHREEQC, at pH 2.9, 100% of arsenite exists as  $\text{H}_3\text{AsO}_3^0$  and 89% of arsenate as  $\text{H}_2\text{AsO}_4^-$ , with the uncharged arsenite species predominating. On the other hand, selenide ( $\text{H}_2\text{Se}$ ) was the main selenium species in the efflorescent crust at approximately 86% followed by selenite ( $\text{HSeO}_3^-$ ). Selenite was much lower compared to selenide. Majority of mercury was elemental mercury, the proportion of inorganic mercury was very low and the predominating species was ( $\text{HgCl}_2$ ) at 71%.

The speciation information stated above shows that at pH 2.9, majority of arsenic and selenium do not exist in their oxyanion forms. This suggests that the anion replacement mechanism was most probably limited. The proportion that is charged is found in much lower concentrations. With regards to arsenic, this is the fraction that is likely to be pre-concentrated by SCPEI-PCPEI via the anion replacement mechanism. More so considering that no phosphate anions were detected in the dissolved crust solution as these could have limited arsenic adsorption in SCPEI-PCPEI. Regarding the selenium oxyanion, the anion replacement mechanism was restricted by the extremely high sulphate concentration and the extremely

low selenium oxyanion concentration: even if selenium was able to replace a single sulphonyl anion, due to the high sulphate concentration it would be replaced right back. Additionally, the likelihood of mercury being adsorbed by SCPEI-PCPEI is low considering that majority of mercury was  $\text{HgCl}_2$ . The high concentration of chloride in the dissolved crust meant that complexation would favour chloride in solution instead of the sulphonyl group in within the SCPEI-PCPEI resin.

#### Uptake of major cations by SCPEI-PCPEI DGT

The success of DGT is also dependent on the selectivity of the resin. Analysis of the desorbed SCPEI-PCPEI resin after deployment shows that cations can also be accumulated by SCPEI-PCPEI DGT (Figure 86). Iron, aluminium and magnesium showed the highest uptake. Regarding iron and aluminium, this was expected since their concentration in the dissolved crust was high (Table 5.7 a). The mass of magnesium accumulated was unexpectedly higher than manganese and yet manganese had a much higher concentration in the dissolved crust solution. Uptake by a passive sampler is expected to follow the trend shown in figure 2.6. In figure 5.20 only aluminium shows linearity between day 6 and day 19. The rest of the metals do not show a specific trend in uptake with increasing deployment time. The mass of iron accumulated shows linearity between day 3 and day 9, afterwards no specific trend is observed according to uptake by passive samplers. This could be due to saturation of the resin capacity.

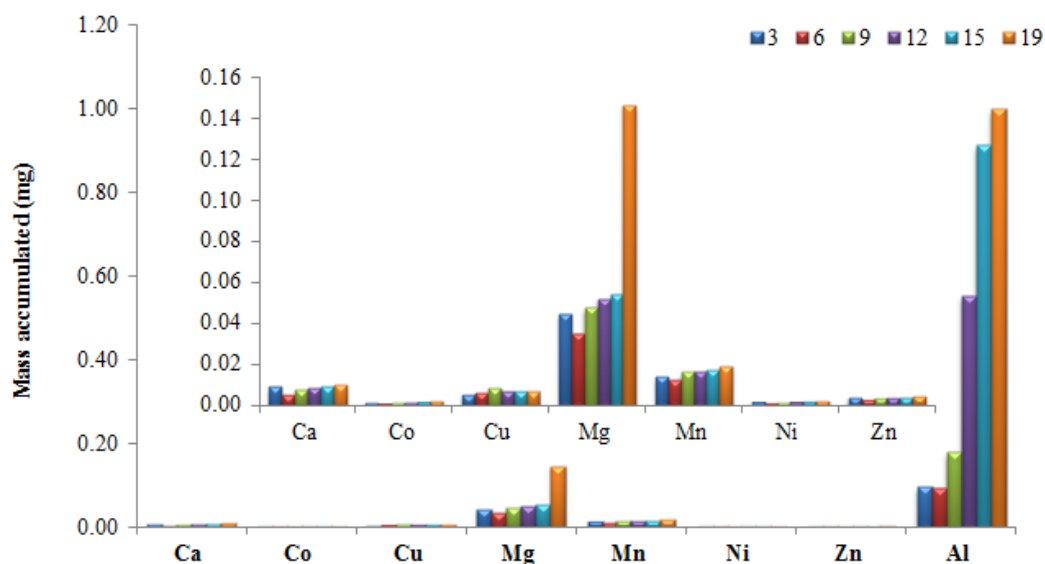


**Figure 86a:** The mass of the major cations accumulated from the dissolved crust

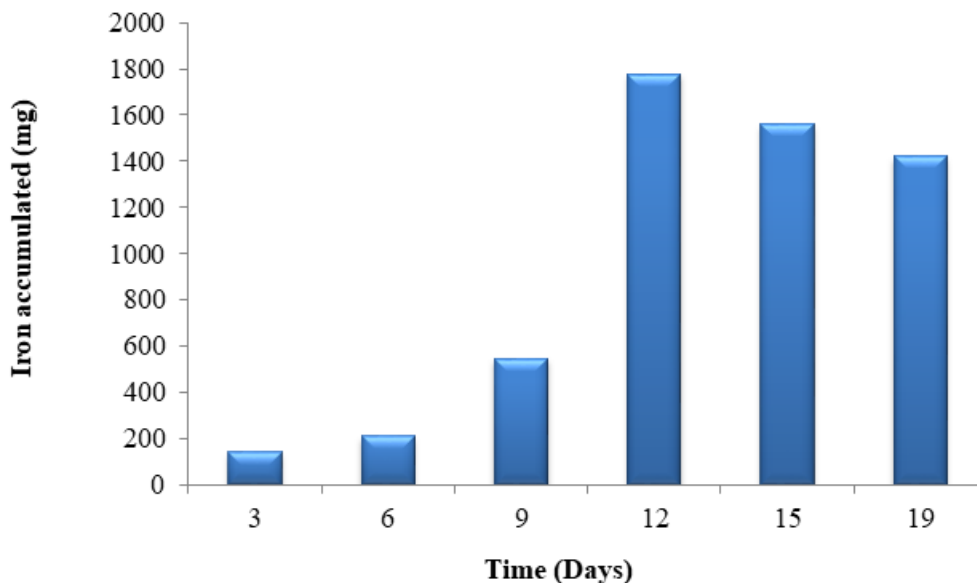


**Figure 86b:** Iron accumulated from the dissolved crust

PEI, the major constituent in CPEI, has a large number of primary and secondary amine groups (Spell, 1969), which are effective at adsorbing metals, either through complexation or either electrostatic interactions (Pang et al., 2011a; Pang et al., 2011b). The lack of specific binding sites for metals other than the amine groups in PEI means that competition for binding sites amongst the metal ions is very high. For example, in a study by Saad et al. (2011) CPEI was able to remove chromium, zinc, iron, nickel, manganese and lead from water. Wang and Li (2015) used a PEI-functionalised ion imprinted hydrogel for the selective removal of Cu (II) from water; however, the adsorbent also targeted lead, cadmium and nickel from solution. The lack of selectivity would also explain why SCPEI-PCPEI DGT does not follow the typical trend followed by passive samplers (Figure 86).

According to PHREEQC, the majority of iron exists as  $\text{Fe}^{2+}$  and  $\text{FeSO}_4$ , while the predominant aluminium species are  $\text{AlSO}_4^+$ ;  $\text{Al}(\text{SO}_4)^{2-}$  and  $\text{Al}^{3+}$ . Magnesium, which was the third highest metal adsorbed by SCPEI-PCPEI DGT existed mainly as  $\text{Mg}^{2+}$  and  $\text{MgSO}_4$ . Manganese also predominated as  $\text{Mn}^{2+}$  and  $\text{MnSO}_4$ . The only difference between magnesium and manganese was that the concentration of free magnesium ion in solution was higher compared to manganese; hence, the higher uptake. Uptake of iron and aluminium was enhanced due to their high concentrations in solution.

#### 4.2.8.4 Uptake in laboratory-based experiments using AMD drainage water

The sampled AMD drainage water was highly acidic at pH 2.4 and had a high conductivity ( $10.5 \text{ mS cm}^{-1}$ ) which can be attributed to the higher concentration of dissolved metals and anions, in particular sulphate anions, compared to the efflorescent crust. The redox potential (366 mV) corresponds with redox potentials of most surface water (Zhang et al., 2017).

#### Composition of AMD

The composition of the AMD drainage water was determined using ICP-OES (Table 16). The trend as observed in Table 16 shows elevated sulphate ( $4319 \text{ mg L}^{-1}$ ) and iron ( $3793 \text{ mg L}^{-1}$ ) concentrations. The concentrations of aluminium ( $570 \text{ mg L}^{-1}$ ), magnesium ( $395 \text{ mg L}^{-1}$ ), calcium ( $376 \text{ mg L}^{-1}$ ) and manganese ( $97.5 \text{ mg L}^{-1}$ ) were relatively high, so were the concentrations of the trace metals cobalt ( $34.94 \text{ mg L}^{-1}$ ), nickel ( $32.32 \text{ mg L}^{-1}$ ).

**Table 16:** Anion and metal composition in AMD water

	Concentration ( $\text{mg L}^{-1}$ )
Cl <sup>-</sup>	42.47
SO <sub>4</sub> <sup>2-</sup>	4319
Al	570
Ca	376
Co	34.94
Cr	1.91
Cu	17.38
Fe	3793
Mg	395
Mn	97.5
Ni	32.32
Zn	<i>bdl</i>
As	0.554
Se	<i>bdl</i>

## Accumulation in AMD drainage water

The AMD drainage water sample was spiked with arsenic, selenium and mercury ( $0.5 \text{ mg L}^{-1}$ ). SCPEI-PCPEI DGT devices were deployed for 5 days. Figure 86a) shows that by day 5, fouling from iron colloid particles had formed. The high iron content also caused changes within the passive sampler interior: the SCPEI-PCPEI resin changed colour and iron colloids had formed on the resin (Figure 86b). After 5 days, a thin layer had formed on top the AMD water (Figure 86c).

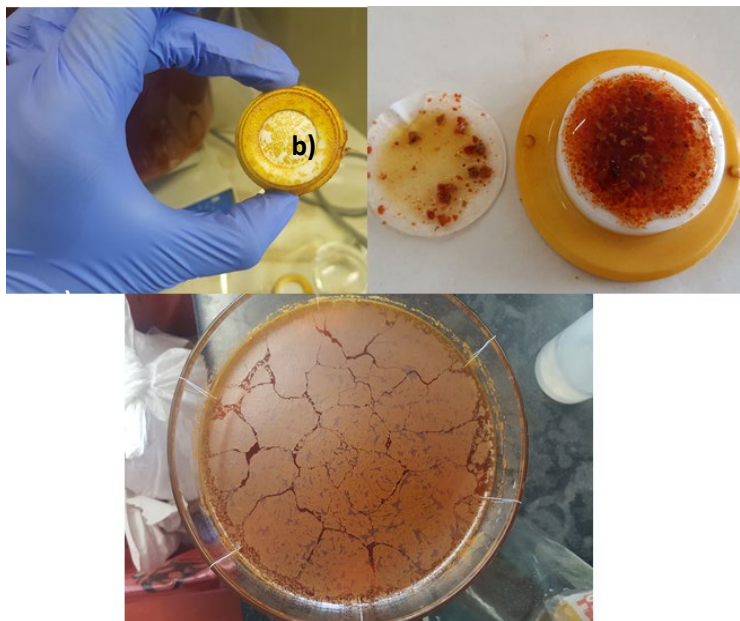


**Figure 87:** Fouling on SCPEI-PCPEI DGT after 5 day deployment in AMD drainage water b) passive sampler interior shows the colour change that took place on the resin and the formation of iron colloids c) The formation of a thin layer on top of the AMD drainage water after 5 days.

Figure 87 shows the accumulation of arsenic in AMD drainage water. A linear uptake trend is observed. Linearity is more precise between day 2 and day 5. On day 5 there is no indication that maximum capacity for arsenic has been attained. This means developed passive sampler can still further be deployed for more days in AMD for arsenic uptake.

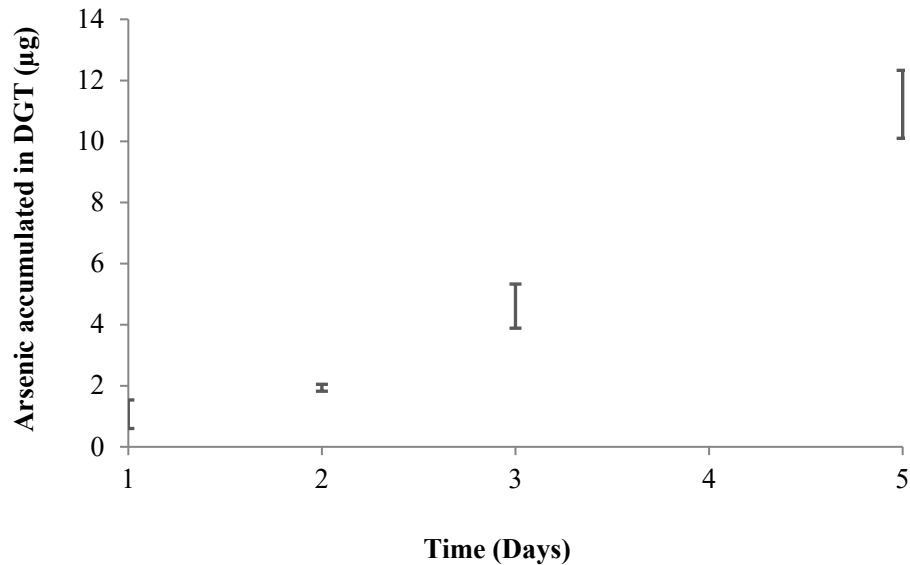


**Figure 88:** The accumulation of arsenic by DGT in water collected from AMD affected site spiked with arsenic ( $0.5 \text{ mg L}^{-1}$ ). ( $n=3$ ,  $\text{RSD} < 10\%$ ).

As seen with the dissolved efflorescent crust, the amount of selenium and mercury could not be determined. The measured concentration in AMD after spiking arsenic was  $0.64 \text{ mg L}^{-1}$ . This was the total available arsenic in solution. Selenium and mercury were below the detection limit. The species of arsenic, selenium and mercury available in solution were similar to those found in the dissolved efflorescent crust, because of similarities in pH and background components. Majority of arsenic was uncharged arsenite ( $\text{H}_3\text{AsO}_3$ ); the concentration of arsenate specie ( $\text{H}_2\text{AsO}_4^-$ ) was extremely low. This explains why low levels of arsenic were accumulated in the DGT passive sampler.

Selenium was overwhelmed by the high concentration of sulphate which is why it was not retained within the passive sampler. Similarly, mercury could not accumulate in the passive sampler because inorganic mercury although present, complexed with chloride ions, according to PHREEQC modelling.

#### Matrix effects and major cations

It has already been established that SCPEI-PCPEI DGT will simultaneously accumulate cations from solution. Metal ions accumulated from the AMD solution are shown in figure 88. Figure 88 shows high accumulation for iron, aluminium, calcium and magnesium, respectively. This is according to their concentrations in the AMD solution. These results further confirm non-specific

binding with regards to metal ions: The mass of iron increases with increasing deployment time. However no linear uptake is seen even for iron. The other metals do not show any distinct trend. This could be attributed to limited capacity of the sorbent so that within few hours of deployment, sampler capacity is exceeded as these metals are in high concentration in AMD.

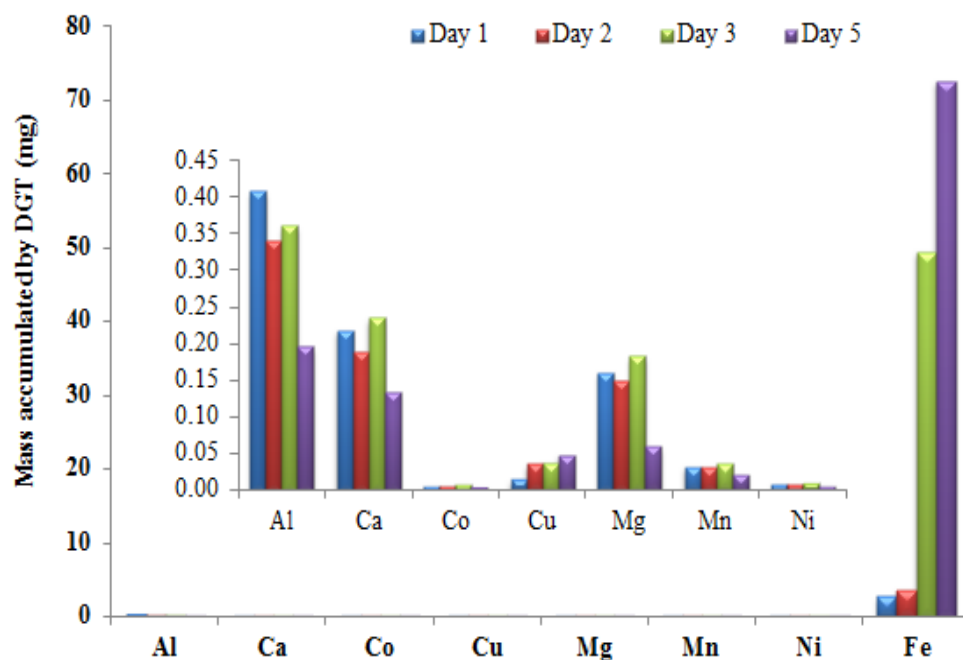


**Figure 89:** Metals accumulated from AMD water

Figure 86b shows the SCPEI-PCPEI DGT resin after deployment for 5 days. The resin had changed colour and iron colloids had started to form. During deployment, metals slowly occupied the binding sites, however, because the concentration of iron was so high, it occupied majority of the sites. This probably increased competition for binding sites with other metals, particularly aluminium, which is why aluminium slowly decreased with deployment time and the other metals do not show a distinct uptake pattern. Ultimately, iron continued to move into the interior of the passive sampler, the binding sites were occupied until none was available. This led to the formation of iron colloid particles within the resin layer. This could possibly explain why some metals showed a non-specific uptake trend (Figure 88).

### **4.3 Comparison between PIM and DGT samplers**

The developed polymer inclusion membrane was found to be more versatile than diffusive gradient in thin films passive sampler. The PIM sampler was found to withstand harsh AMD environmental conditions and was still able to perform and extract as much metals as possible. It also litter suffered biofouling as the releasing of protons to the donor side kept the pH low enough to prevent any bacteria growth. It was also found to have a much higher capacity. The DGT-based sampler suffered heavy biofouling in AMD and its capacity was easily exceeded due to high concentration of other metals like iron, copper and aluminium. The DGT-based sampler could only perform better in dam water with little other metals.

## CHAPTER FIVE: CONCLUSIONS AND RECOMMENDATIONS

### 5.1 Conclusions

The current study was aimed at the development, optimisation and application of a DGT passive sampler for arsenic, selenium and mercury. Further, development, optimisation and application of PIM sampler for metal uptake of copper, nickel, cobalt and iron was investigated.

Successful construction of the DGT sample holders was demonstrated. The new cap design provided a proper seal ensuring that only the filter membrane is exposed to the bulk solution. The sample holders were also durable, and easy to maintain, therefore ideal for long term use. CPEI was successfully functionalised to form SCPEI and PCPEI. A resin mixture of SCPEI-PCPEI showed enhanced selectivity in the laboratory-based experiments towards arsenic and selenium. A total resin mass of 0.8 g was able to extend the linear uptake regime up to day 15 in the laboratory-based experiments. The uptake of selenium was generally higher compared to arsenic and this can be attributed to the higher diffusion coefficient of selenium. The diffusion coefficients for both analytes were a few orders of magnitude higher compared to those obtained in agarose cross-linked polyacrylamide, as found in commercial DGT.

SCPEI-PCPEI-based DGT showed abilities to operate under stagnant conditions and low solution concentrations. The diffusion rate into the passive sampler was however reduced, demonstrated by the flux. The uptake abilities of SCPEI-PCPEI DGT were also not affected by pH. The only difference is that at pH 5, the rate of mass accumulation was faster compared to pH 3. This was expected since at pH 5, the functional groups on SCPEI-PCPEI resin are partially charged, so are arsenic and selenium, whereas at pH 3 the functional groups are fully protonated. Deployment of SCPEI-PCPEI DGT in dissolved efflorescent crust and AMD water showed a reduced mass accumulation compared to the laboratory-based experiments. This can simply be a consequence of the complex matrix in the dissolved crust and AMD water. The high concentration of iron meant that occupied majority to the binding sites leading to the formation of colloid particles within the passive sampler. This meant that SCPEI-PCPEI-based DGT is not ideal for application in AMD since there is not enough selectivity. The passive sampler was also able to accumulate major cations in solution, however, even this was not successful because there was no distinct uptake trend resulting from the lack of selectivity in the CPEI backbone as well as the colloid particles that behaved as secondary binding sites.

Application using Fleurhof dam water was successful in that it provided a better understanding into the behaviour of selenium and mercury. Analysis of Fleurhof dam water shows significantly reduced concentrations compared to the AMD samples. This was expected. In the spiked water samples SCPEI-PCPEI DGT was able to accumulate all three elements linearly. In the unspiked sample however, the concentrations are in trace levels, therefore the sampling capabilities of SCPEI-PCPEI resin are truly tested. SCPEI-PCPEI failed to accumulate mercury. Even in the field deployments a similar trend is observed. Alternatively, selenium was accumulated in the unspiked water sample, however in the field, the mass of selenium decreased with time. It can therefore be concluded that SCPEI-PCPEI-based DGT was successfully developed, optimised and applied for arsenic. The capacity and retention abilities for selenium and mercury were limited, and this was demonstrated by application with water at trace concentrations.

A PIM passive sampler has been successfully designed, optimised and field-tested in studying the uptake of metals in surface and AMD waters. The sampler holders made out of PTFE and screwed together proved to be very rugged and able to withstand harsh environmental conditions. The use of solid PIM barrier in the new sampler proved to be very stable with insignificant leaching of the membrane liquid phase. In addition, since that barrier has a permanent acidic surface from  $H^+$  involved in driving the process and from D2EHPA used as carrier ensured bactericidal properties in the sampler. This prevented biofouling of the membrane and could be reused especially in surface water. The uptake of targets was linear from 5-12 days in deionised water, surface water and AMD. Thus, the developed PIM sampler is very versatile and rugged as it was able to tolerate harsh environment from AMD at pH 3 with high amounts of metal ions and anions. It was also able to uptake a lot of other metal ions. The PIM passive sampler was also able to relate the observed physical-chemical changes in the water during deployment to the uptake kinetics. This is very important as it can be used to study the transport and fate of the target metals in an aquatic system after outside perturbation.

## **5.2 Recommendations**

The study on DGT-based sampler paved the way for more sorbents to be explored which would be relevant in assessing the specific trace elements affecting South African fresh water systems. As long as the basic principles in passive sampler design and assembly are honoured, adaptations may be carried out to accommodate the sorbent type, as was seen in this study. From this study, the following recommendations are suggested for DGT-based sampler:

- Explore various sorbents that would be robust and selective enough to withstand conditions in AMD. Here sorbents with very high capacity and that are selective is needed.
- Because of the dynamics of AMD, field calibration of the passive sampler is recommended as this water quickly changes its chemistry once stationed in the laboratory.

The study on PIM-based sampler was found that the sampler is very versatile and rugged. The following are recommended;

- Using the optimised PIM to quantify the bioavailable fractions of the target metals in both surface and AMD. In the study, sampling rates have been calculated as first trial but detailed determination of sampling rates is needed and using these to determine the amount of bioavailable fractions in the waters.
- The passive sampler demonstrated that it could take many other metals along with target metals. Thus, it is proper to check whether some of these are linearly taken in the sampler and what is the maximum deployment time for them before equilibrium is reached.
- Seasonal changes leads to the perturbation of the aquatic systems and this affects metal transport and behaviour. Thus, deployment of the passive sampler in various seasons to study the transport and fate of metals in mining polluted water system within South Africa could be of interest. In summer, surface water in these areas has high evaporation rate and the water chemistry is dramatically affected as seen from the preliminary study.
- Building pilot plant versions of the PIM sampler so that it can be used for passive remediation of polluted waters. This means designing and machining an upscaled version of the lab-based version say moving from 5.5 ml to 2500 ml.

## REFERENCES

1. Akbarzadeh, A., Rezaei-Sadabady, R., Davaran, S., Joo, San. W. Zarghami, N., Hanifehpour, Y.S., Mohammad, K., Mohammad and Kazem, N.K. (2013). Liposome: classification, preparation, and applications, *Nanoscale Research Letters*, vol. 8, no. 1, pp. 102.
2. Allan, I. J. Knutsson, J. Guigues, N. Mills, G.A. Fouillac, A-M. Greenwood, R. (2008). Chemcatcher and DGT passive sampling devices for regulatory monitoring of trace metals in surface water, *Journal of Environmental Monitoring*, vol. 10, no. 7, pp. 821-829.
3. Bennett, W.W., Teasdale, P.R., Panther, J.G., Welsh, D.T., Zhao, H. and Jolley, D.F. (2012). Investigating arsenic speciation and mobilization in sediments with DGT and DET: A mesocosm evaluation of oxic-anoxic transitions. *Environmental Science & Technology*, 46(7), pp.3981-3989.
4. Brown, R.H., Harvey, R.P., Purnell, C.J. and Saunders, K.J. (1984). A diffusive sampler evaluation protocol. *The American Industrial Hygiene Association Journal*, 45(2), pp.67-75.
5. Bryan, G. W. and Langston, W. J. (1992). Bioavailability, accumulation and effects of heavy metals in sediments with special reference to United Kingdom estuaries: a review, *Environmental Pollution*, vol. 76, no. 2, pp. 89-131.
6. Clarisse, O. and Hintelmann, H. (2006). Measurements of dissolved methylmercury in natural waters using diffusive gradients in thin film (DGT). *Journal of Environmental Monitoring*, vol. 8, no. 12, pp. 1242-1247.
7. Clarisse, O. Dimock, B. Hintelmann, H. and Best, E.P.H. (2011). Predicting net mercury methylation in sediments using diffusive gradient in thin films measurements. *Environmental Science and Technology*, vol. 45, no. 4, pp. 1506-1512.
8. Clarisse, O. Foucher, D. and Hintelmann, H. (2009). Methylmercury speciation in the dissolved phase of a stratified lake using the diffusive gradient in thin film technique. *Environmental Pollution*, vol. 157, no. 3, pp. 987-993.
9. Dabrin, A., Ghestem, J.P., Uher, E., Gonzalez, J.L., Allan, I.J., Schintu, M., Montero, N., Balaam, J., Peinerud, E., Miege, C., Coquery, M. (2016). Metal measurement in aquatic environments by passive sampling methods: Lessons learning from an in situ intercomparison exercise. *Analytica Chimica Acta*, 208, 299-308
10. Davison, W. And Zhang, H. (1994). In situ speciation measurements of trace components in natural waters using thin-film gels, *Nature*, vol. 367, no. 6463, pp. 546-548.
11. Davison, W., Grime, G.W., Morgan, J.A.W. and Clarke, K. (1991). Distribution of dissolved iron in sediment pore waters at submillimetre resolution. *Nature*, 352, pp.323-325.

12. Davison, W., Zhang, H. and Grime, G.W. (1994). Performance characteristics of gel probes used for measuring the chemistry of pore waters. *Environmental Science & Technology*, 28(9), pp.1623-1632.
13. Dawson, D. C. and Ballatori, N. (1995). In: Toxicology of metals: biochemical aspects, Goyer R. A. and Cherian M. G. ed. *Membrane transporters as sites of action and routes of entry for toxic metals*, Springer-Verlag, pp. 53-76.
14. De Oliveira, R.L.F., Pedrobom, J.H., Menegario, A.A., Domingos, R.N., Py Junior, D.A., Kiang, C.H. (2013). Determination of in situ speciation of manganese in treated acid mine drainage water by using multiple diffusive gradients in thin films devices. *Analytica Chimica Acta*, 799, 23-28
15. Diviš, P. Leermaker, M. Dočekalová, H. Gao, Y. (2005). Mercury depth profiles in river and marine sediments measured by the diffusive gradients in thin films technique with two different specific resins, *Analytical and Bioanalytical Chemistry*, vol. 382, no. 7, pp. 1715-1719.
16. Djane, N., Ndung'u, K., Malcus, F., Gohansson, G., Mathiasson, L. (1997). Supported liquid membrane enrichment using an organophosphorus extractant for analytical trace metal determinations in river waters. *J. Fresenius Anal. Chem.* 358, 822.
17. Dočekalová, H. and Diviš, P. (2005). Application of diffusive gradient in thin films technique (DGT) to measurement of mercury in aquatic systems, *Talanta*, vol. 65, no. 5, pp. 1174-1178.
18. Foulkes, E.C. (2000). Transport of toxic heavy metals across cell membranes, *Proceedings of the Society for Experimental Biology and Medicine*, vol. 223 no. 3, pp. 234-240.
19. Gavrilescu, M. (2004). Removal of Heavy Metals from the Environment by Biosorption, *Engineering in Life Sciences*, vol. 4, no. 3, pp. 219-232.
20. Gorny, J., Lesven, L., Billon, G., Dumoulin, D., Noiriel, C., Pirovano, C. and Madé, B. (2015). Determination of total arsenic using a novel Zn-ferrite binding gel for DGT techniques: Application to the redox speciation of arsenic in river sediments. *Talanta*, 144, pp.890-898.
21. Herrick, W. G. Nguyen, T. V. Sleiman, M. McRae, S. Emrick, T. S. Peyton, S. R. (2013). PEG-phosphorylcholine hydrogels as tunable and versatile platforms for mechanobiology, *Biomacromolecules*, vol. 14, no. 7, pp. 2294-2304.
22. Horowitz, A. J. (1997). Some Thoughts on Problems Associated With Various Sampling Media Used for Environmental Monitoring, *Analyst*, vol. 122, pp. 1193-1200.
23. Iwasaki, Y. and Ishihara, K. (2005). Phosphorylcholine-containing polymers for biomedical applications. *Analytical and bioanalytical chemistry*, vol. 381, no. 3, pp. 534-546.
24. Karp, G. (2009). Cell and molecular biology: Concepts and experiments. 6<sup>th</sup> ed: Wiley, 48, 123.

25. Kocar, B.D., Herbel, M.J., Tufano, K.J. and Fendorf, S. (2006). Contrasting effects of dissimilatory iron (III) and arsenic (V) reduction on arsenic retention and transport. *Environmental Science & Technology*, 40(21), pp.6715-6721.
26. Lee, A. G. (2005). How lipids and proteins interact in a membrane: a molecular approach, *Molecular bioSystems*, vol. 1, no. 3, pp. 203-212.
27. Li, W. Zhao, H. Teasdale, P.R. John, R. Zhang, S. (2002). Application of a cellulose phosphate ion exchange membrane as a binding phase in the diffusive gradients in thin films technique for measurement of trace metals, *Analytica Chimica Acta*, vol. 464, no. 2, pp. 331-339.
28. Mengistu, H., Roeyset, O., Tessema, A., Abiye, T.A. and Demlie, M.B. (2012). Diffusive gradient in thin-films (DGT) as risk assessment and management tools in the Central Witwatersrand Goldfield, South Africa. *Water SA*, 38(1), pp.15-22.
29. Mountouris, A. Voutsas, E., and Tassios, D. (2002). Bioconcentration of heavy metals in aquatic environments: the importance of bioavailability, *Marine Pollution Bulletin*, vol. 44, no. 10, pp. 1136-1141.
30. Namieśnik, J. Zabiegała, B. Kot-Wasik, A. Partyka, M. and Wasik, A. (2005). Passive sampling and/or extraction techniques in environmental analysis: a review, *Analytical and Bioanalytical Chemistry*, vol. 381, no. 2, pp. 279-301.
31. Namieśnik, J., Zabiegała, B., Kot-Wasik, A., Partyka, M. and Wasik, A. (2005). Passive sampling and/or extraction techniques in environmental analysis: a review. *Analytical and Bioanalytical Chemistry*, 381(2), pp.279-301.
32. Pesavento, M., Alberti, G., Biesuz, R. (2009). Analytical methods for determination of free metal ion concentration, labile species fraction and metal complexation capacity of environmental waters: A review. *Analytica Chimica Acta*, 631, 129-141
33. Pham, A.L.T., Johnson, C., Manley, D. and Hsu-Kim, H. (2015). Influence of Sulfide Nanoparticles on Dissolved Mercury and Zinc Quantification by Diffusive Gradient in Thin-Film Passive Samplers. *Environmental Science & Technology*, 49(21), pp.12897-12903.
34. Pozo, K., Harner, T., Lee, S.C., Sinha, R.K., Sengupta, B., Loewen, M., Geethalakshmi, V., Kannan, K. and Volpi, V. (2011). Assessing seasonal and spatial trends of persistent organic pollutants (POPs) in Indian agricultural regions using PUF disk passive air samplers. *Environmental Pollution*, 159(2), pp.646-653.
35. Price, H.L., Teasdale, P.R., Jolley, D.F., An evaluation of ferrihydrite and Metsorb DGT techniques for measuring oxyanion species (As, Se, V, P): Effective capacity, competition and diffusion coefficients. *Analytica Chimica Acta*, 803, 56-65

36. Rascio, N., Navari-Izzo, F. (2011). Heavy metal hyperaccumulating plants: how and why do they do it? And what makes them so interesting? *Plant Science*, vol. 180, no. 2, pp. 169-181.
37. Reeder, R. J. Schoonen, M. A. A. Lanzirotti, A. (2006). Metal Speciation and Its Role in Bioaccessibility and Bioavailability, *Reviews in Mineralogy and Geochemistry*, vol. 64, no. 1, pp. 59-113.
38. Reeder, R.J., Schoonen, M.A. and Lanzirotti, A. (2006). Metal speciation and its role in bioaccessibility and bioavailability. *Reviews in Mineralogy and Geochemistry*, 64(1), pp.59-113.
39. Saad, D.M., Cukrowska, E.M. and Tutu, H. (2011). Development and application of cross-linked polyethylenimine for trace metal and metalloid removal from mining and industrial wastewaters. *Toxicological & Environmental Chemistry*, 93(5), pp.914-924.
40. Saad, D.M., Cukrowska, E.M. and Tutu, H. (2012). Phosphonated cross-linked polyethylenimine for selective removal of uranium ions from aqueous solutions. *Water Science and Technology*, 66(1), pp.122-129.
41. Saad, D.M., Cukrowska, E.M. and Tutu, H. (2012). Sulfonated cross-linked polyethylenimine for selective removal of mercury from aqueous solutions. *Toxicological & Environmental Chemistry*, 94(10), pp.1916-1929.
42. Saad, D.M., Cukrowska, E.M. and Tutu, H. (2013). Functionalisation of cross-linked polyethylenimine for the removal of As from mining wastewater. *Water SA*, 39(2), pp.257-264.
43. Saad, D.M., Cukrowska, E.M. and Tutu, H., 2013. Modified cross-linked polyethylenimine for the removal of selenite from mining wastewaters. *Toxicological & Environmental Chemistry*, 95(3), pp.409-421.
44. Saad, D.M., Cukrowska, E.M. and Tutu, H. (2013). Selective removal of mercury from aqueous solutions using thiolated cross-linked polyethylenimine. *Applied Water Science*, 3(2), pp.527-534.
45. Semple, K. T. Doick, K. J. Jones, K. C. Burauel, P. Craven, A. and Harms, H. (2004). Peer reviewed: defining bioavailability and bioaccessibility of contaminated soil and sediment is complicated, *Environmental Science & Technology*, vol. 38, no. 12, pp. 228A-231A.
46. Shaw, M., Negri, A., Fabricius, K. and Mueller, J.F. (2009). Predicting water toxicity: pairing passive sampling with bioassays on the Great Barrier Reef. *Aquatic Toxicology*, 95(2), pp.108-116.
47. Søndergaard, J., Bach, L. and Gustavson, K. (2014). Measuring bioavailable metals using diffusive gradients in thin films (DGT) and transplanted seaweed (*Fucus vesiculosus*), blue

- mussels (*Mytilus edulis*) and sea snails (*Littorina saxatilis*) suspended from monitoring buoys near a former lead-zinc mine in West Greenland. *Marine Pollution Bulletin*, 78(1), pp.102-109.
48. Tafurt-Cardona, M., Eismann, C.E., Suarez, C.A., Menegario, A.A., Luko, K.S., Junior, E.S. (2015). In situ selective determination of methylmercury in river water by diffusive gradient in thin films technique using baker yeast (*Saccharomyces cerevisiae*) immobilized in agarose gel as binding phase. *Analytica Chimica Acta*, 887, 38-44
49. Tufano, K.J., Reyes, C., Saltikov, C.W. and Fendorf, S. (2008). Reductive processes controlling arsenic retention: revealing the relative importance of iron and arsenic reduction. *Environmental Science & Technology*, 42(22), pp.8283-8289.
50. Turner, G.S.C., Mills, G.A., Teasdale, P.R., Burnett, J.L., Amos, S., Fones, G.R. (2012). Evaluation of DGT techniques for measuring inorganic uranium species in natural waters: Interferences, deployment time and speciation. *Analytica Chimica Acta*, 739, 37-46
51. Turner, G.S.C., Mills, G.A., Teasdale, P.R., Burnett, J.L., Amos, S., Fones, G.R. (2015). Evaluation of diffusive gradients in thin films using a Dphnix resin for monitoring dissolved uranium in natural waters. *Analytica Chimica Acta*, 854, 78-85
52. Ullrich, M. Hanuš, J. Dohnal, J. Štěpánek, F. (2013). Encapsulation stability and temperature-dependent release kinetics from hydrogel-immobilised liposomes. *Journal of colloid and interface science*, vol. 394, pp. 380-385.
53. Vrana, B. Allan, I. J. Greenwood, R. Mills, G. A. Dominiak, E. Svensson, K. Knutsson, J. and Morrison, G. (2005). Passive sampling techniques for monitoring pollutants in water. *Trends in Analytical Chemistry*, vol. 24, no. 10, pp. 845-868.
54. Vrana, B., Allan, I.J., Greenwood, R., Mills, G.A., Dominiak, E., Svensson, K., Knutsson, J. and Morrison, G. (2005). Passive sampling techniques for monitoring pollutants in water. *TrAC Trends in Analytical Chemistry*, 24(10), pp.845-868.
55. Zhang, H. and Davison, W. (1995). Performance Characteristics of Diffusion Gradients in Thin Films for the in Situ Measurement of Trace Metals in Aqueous Solution. *Analytical Chemistry*, vol. 67, no. 19, pp. 3391-3400.
56. Zhang, H., Davison, W., Miller, S. and Tych, W. (1995). In situ high resolution measurements of fluxes of Ni, Cu, Fe, and Mn and concentrations of Zn and Cd in porewaters by DGT. *Geochimica et Cosmochimica Acta*, 59(20), pp.4181-4192.
57. Zhou, Y. Stotesbury, T. Dimock, B., Vreugdenhil, A. Hintelmann, H. (2013). Novel silica sol-gel passive sampler for mercury monitoring in aqueous systems. *Chemosphere*, vol. 90, no. 2, pp. 323-328.